The Influence of Local Hydrodynamics on Fish Movement in Fluvial Infrastructure

by

Kaylin Jones

A dissertation submitted in partial fulfillment
of the requirements for the degree of
Doctor of Philosophy
(Environmental Engineering)
in the University of Michigan
2024

Doctoral Committee:

Associate Professor Aline Cotel, Chair
Assistant Professor Karen Alofs
Professor Valeriy Ivanov
Lecturer IV Lissa MacVean

Kaylin Jones

kaylinj@umich.edu

ORCID iD: 0000-0002-8930-5454

Dedication

To Kyle—for always encouraging me to stay confident in and positive about my PhD journey.

Acknowledgements

cats Larry, Casper, Mrs. Banana, and Sonora, thank you for the companionship and cuddles. Meow.

And finally, to my future husband Kyle Pettibone, you always believed in me and made me feel confident in myself that I could do this. Without your partnership, my time in graduate school would not have been the positive experience it was, and throughout the last five years, finding you is my only accomplishment greater than this dissertation.

Table of Contents

List of Tables

List of Figures

xiii

List of Appendices

Abstract

River systems across the developed world have been dammed for a variety of reasons, including power generation, recreation, and flood control. While providing benefits, there are a wide array of negative environmental effects associated with this infrastructure, including disconnecting migratory fish habitat, rendering certain fluvial populations unable to complete their life cycle. To reduce this impact, it is necessary to pass fishes across dams. However, it is not desirable to pass all fishes; in the case of invasive species, dams act as beneficial barriers to prevent wider proliferation in watersheds. Thus, conservation goals require increasing passage rates for some fishes while reducing passage rates of others. This dissertation focuses on ways to leverage the local hydrodynamics associated with fish passage infrastructure to achieve passage goals.

Fishes primarily pass dams using fishways, adjacent structures designed specifically for this purpose. Many of these designs impart intense turbulence into the flow, and the turbulent fluctuations can prevent fishes from successfully passing; for fishes that can pass, heightened stress has negative impacts at times such as loss of fertility or increased mortality rates. Altering these flows to be more amenable to successful passage is therefore of interest. *Chapter 2* of this dissertation provides a framework for applying turbulence theory to fishway design for estimation and remediation of strain rate and eddy size, two flow metrics shown to be harmful to early-life stage fishes. This framework offers a simple way to consider the turbulent hydraulic conditions prior to construction of new, or retrofit of existing, fishways.

Another challenge to habitat restoration efforts is a deficiency in meaningful

environmental turbulence data, due to a lack of instrumentation able to directly measure turbulence metrics in-situ. *Chapter 3* details and provides proof-of-concept for a novel field instrument utilizing Particle Image Velocimetry (PIV) to address this instrumentation gap.

Fishway efficiency largely depends on the turbulence present; to assess a common fishway design, *Chapter 4* maps the hydrodynamics within Denil fishways, the detailed flows in which have never been quantified experimentally. Using a physical model of a Denil fishway and PIV, flow patterns at several slopes and flowrates are measured to examine how the flow changes with different design grades. This study found there are two primary flow phenomena that hinder passage: with increasing slope, low-speed refuges are lost, and areas of heightened vorticity with high potential to destabilize fishes develop directly in the swimming path.

Detailing environmental hydrodynamics may be additionally used to block passage and improve trapping of invasive species. *Chapter 5* explores improving sea lamprey (an invasive parasitic fish in the Laurentian Great Lakes) trap entrance rates through mapping the hydrodynamics surrounding and within two common trap types, mesh face and solid face. These flows were measured in flumes in both a controlled hydraulics laboratory and at Hammond Bay Biological Station (HBBS). These measurements are paired with sea lamprey observation conducted at HBBS in response to these flows, to develop an understanding of both what turbulent conditions are experienced at these traps, and how sea lampreys respond to them. This study found the solid face trap to be attractive at close range, but performed poorly due to presenting hydraulic obstacles to sea lampreys attempting entrance. The mesh face trap at high flows was the most successful design with the highest entry rates.

Chapter 1 Introduction

Dams have become widespread worldwide as a means of providing hydropower, recreation, flood control, and many other benefits to the communities surrounding them (Silva et al., 2018). Dams can also aid in environmental efforts through preventing invasive species from accessing entire watersheds (Miehls et al., 2020; Vélez-Espino et al., 2011). Unfortunately, the severe extent to which this infrastructure alters the landscape can negatively affect ecosystem health, including disconnecting habitat for native migratory fishes (Castro-Santos & Haro, 2010). Many current fish conservation efforts therefore focus on balancing the presence of dams with the health of fluvial populations through passing desirable fishes across dams; turbulence within the flow can be taken advantage of to advance fish passage.

This dissertation examines the connections between turbulent hydrodynamics and fish passage as a means of optimizing fish passage metrics, whether that is increasing passage for native fishes or preventing passage of invasives. To leverage turbulence in this way, two intertwined bodies of work must be considered—characterizing turbulence fishes encounter, and characterizing their response to these flow patterns. These fields are here investigated theoretically, experimentally, and through the development of instrumentation and methodology. This work expands current knowledge on environmental hydrodynamics and fish behavior, and offers new tools to future researchers, natural resource managers, and conservationists.

1.1 Mechanics of Turbulence

Turbulence has various definitions, all of which stem from one of two general approaches: statistical or physical. The former is based on analyzing unsteadiness of flow

statistics, and provides a quantitative view of various flow features such as velocity fluctuations

at a point; however, this approach makes direct analysis of multi-dimensional flow

characteristics such as vortices difficult. Many of the flow features that have been shown to

affect fishes are these multi-dimensional structures, and therefore, this dissertation adopts a

physical approach to turbulence, defining a turbulent flow as one that is eddy-dominated

(Davies, 1972; Tritico, 2009). Eddy structure in a flow is dictated by Reynolds number (Re), the

ratio of kinetic forces to viscous forces. Re is defined in Equation 1.1:

$$Re = \frac{UL}{v}$$
(Equation 1.1)

Where U is velocity, L is length scale, and v is kinematic viscosity. As eddies are turbulent

features significant to fishes (Tritico & Cotel, 2010), their influence over several key attributes of

turbulent flows is briefly discussed below.

Eddies are responsible for the dominant mass and momentum transport in turbulent

flows—eddies each have an associated mass and angular momentum, defined in Equations 1.2

and 1.3 respectively (Tritico, 2009; Tritico & Cotel, 2010):

$$m_e = \frac{\pi \rho_w L_e d_e^2}{4}$$
(Equation 1.2)

$$\Pi_e = \frac{\pi \rho_w \omega_e d_e^5}{64}$$
(Equation 1.3)

Where ρ_w is water density, L_e is eddy length, ω_e is eddy angular velocity, and d_e is eddy diameter.

The presence of eddies in flow is reflected by vorticity. Vorticity is defined as the curl of

the velocity vector field, and can be thought of as the strength and orientation of swirling motion

in a flow. Energy transfer within the flow is also theorized to happen through eddies by a process

known as the energy cascade, described by Kolmogorov (1941). The energy cascade theorem

states that energy is initially contained within the largest eddies of a turbulent flow, the size of

which are constrained by geometric boundaries (e.g. pipe size or river depth). This energy is inviscidly passed to eddies of increasingly smaller diameters, until a smallest size in the inertial range is reached. At this point, viscosity dominates, and energy dissipates into the surrounding fluid.

Phenomena in turbulent flow is not only dictated by eddies, but also by fluctuations in velocity. The velocity fluctuations in turbulent flows can be described through turbulent kinetic energy (TKE), which is denoted k and defined in Equation 1.4:

$$k = \frac{1}{2}\left(\overline{u'^2} + \overline{v'^2} + \overline{w'^2}\right)$$
(Equation 1.4)

Where u', v', and w' are turbulent velocity fluctuations from the mean in the x-, y-, and z-directions respectively. TKE provides a means to understand the unsteady nature of flows, and quantifies the additional kinetic energy contained within a flow due to its turbulent fluctuations.

Both the unsteadiness of turbulent flows and the eddies within them impart velocity differentials into the flow field. Velocity differentials result in shearing of parcels of fluid in the flow. The shear stress in the flow resulting from this is defined in Equation 1.5:

$$\tau = \mu \frac{dU}{dy}$$
(Equation 1.5)

Where τ is shear stress, μ is dynamic viscosity, and $\frac{dU}{dy}$ is spatial velocity gradient, referring to the rate of change of velocity with respect to distance. Presence of this stress induces deformation of the fluid parcel (see Figure 2.1); the ratio of deformation to parcel size is known as strain, and the rate at which it occurs is strain rate.

The above aspects of turbulent fluid mechanics are used in this dissertation to characterize the flows fishes encounter, and to understand the behavioral responses observed.

1.2 Turbulence and Fishes

The study of turbulence impacts on fish behavior is a relatively new field, its popularity significantly increasing after the work by Pavlov et al (2000). Since then, turbulence has been shown to have far-reaching effects on fishes, including altering swimming ability (Cada & Odeh, 2001; Cotel & Webb, 2015; Liao, 2007; Liao et al., 2003a; Odeh et al., 2002; Silva et al., 2012; Tritico, 2009; Tritico & Cotel, 2010), changing survival rates across all life stages (Baiandina & Khanaychenko, 2018; Liao, 2007; Megrey & Hinckley, 2001; Navarro et al., 2019; Neitzel et al., 2004; Prada et al., 2018, 2019; Rehmann et al., 2003), influencing habitat choice (Cotel et al., 2006; Hockley et al., 2014; Lupandin, 2005; Trinci et al., 2020; Tritico, 2009; Wang & Chanson, 2018), and affecting feeding behavior (Dower et al., 1997; Higham et al., 2015; Hilder et al., 2017; Marrasé et al., 1990; Rothschild & Osborn, 1988). These effects result from interactions between fish and the various characteristics of turbulent flows discussed above in *1.1 Mechanics of Turbulence*, including eddies.

Eddies of all diameters exist in turbulent flows, and accordingly fishes must interact with a wide range of eddy sizes when subjected to these conditions (Cada & Odeh, 2001). The relative size of an eddy to a fish determines the effect the fish will feel during these interactions (Cotel & Webb, 2015; Lupandin, 2005; Nikora et al., 2003; Tritico, 2009), and eddies can therefore be divided into three different categories: small-scale (diameter significantly smaller than fish length), mid-scale (diameter on the same order of magnitude as fish length), and large-scale (diameter significantly larger than fish length). Large-scale eddies have not been shown to have any significant impact on fishes, since their large size makes them effectively rectilinear to the fish and they therefore have the same impact as a large-scale current. Thus, only effects by small-scale and mid-scale eddies are investigated in this body of work.

Small-scale eddies largely affect early-life stage fishes (Cada & Odeh, 2001; K. Jones et al., 2022; K. Jones & Cotel, 2023; Rehmann et al., 2003). They occur at high frequency and have high velocity differentials across their small diameters. High velocity differential causes high strain rate, and their high frequency means this heightened strain rate is widespread in the flow. The tough integument of most adult fishes means their mature bodies can withstand this, but vulnerable larvae and some juveniles cannot; this flow characteristic results in increased mortality of young fishes, potentially altering fish populations and overall assemblage.

Mid-scale eddies have the most significant impact on fish swimming ability. Posture, swimming speed, tail-beat frequency, and tail-beat amplitude are all affected by their presence (K. Jones et al., 2022; Tritico, 2009). This is the only eddy size capable of inducing spills, where the fish loses control and/or station in the flow. During a spill, a fish may undergo a rotational and/or translational displacement, which then requires additional effort for the fish to reorient correctly. Interaction with mid-scale eddies can also alter a fish's trajectory, as they are either pushed off their intended path or required to compensate for the increased effort needed and change path. These effects are due to the momentum and vorticity in the flow that fishes must endure when encountering these eddies.

Generally, when mid-scale eddies are unpredictable or too strong for the fish to navigate, it makes swimming more difficult and increases stress levels. However, certain turbulent conditions have been shown to positively affect swimming when fishes are able to properly take advantage of the eddy structure within the flow. Liao et al (2003a) found that when vortices were periodically shed behind a cylinder, fish were able to alter their swimming pattern to a mode known as the Kármán gait (Liao et al., 2003b), allowing them to exploit the velocity induced by eddies and reduce their muscle activity. Therefore, turbulence in the flow can affect swimming in

both positive and negative ways depending on its structure, and can act as either a deterrent or an attractant to fishes.

1.3 Fluid Mechanics and Fish Passage

Fish passage at dams is largely achieved through fishways, infrastructure adjacent to dams that allows fishes to gradually overcome the hydraulic head. These are typically designed around target species—in North America, salmonids (Ackerman et al., 2019; Autier & Heindel, 2021; P. E. Jones et al., 2020). Salmonids are strong swimmers and can overcome hydrodynamic conditions other species cannot (P. E. Jones et al., 2020); when fishways are designed to enable the strongest swimmer to move through, many other migratory species are neglected and their habitat remains fractured.

The hydraulics within fishways are known to be stressful conditions for passing fishes. Heightened stress can have undesirable consequences, including loss of reproductive capability, immunosuppression, and death (Shahabi et al., 2021). The flow within fishways is fast and highly turbulent, these characteristics being the main cause of stress and obstacle to passage (Duguay et al., 2017; K. Jones & Cotel, 2023). To improve passage outcomes, the turbulent conditions should therefore be altered. Doing so strategically can be used to direct fishes towards certain desirable paths, such as into fishways or, in the case of invasive species, traps. Generally, fish response to turbulence encountered can be leveraged to encourage swimming behaviors surrounding dam passage that align with conservation goals.

1.4 Summary of Dissertation

Turbulence as it relates to fishes and the goal of optimized fish passage is addressed in this dissertation in several ways. *Chapter 2* develops a theoretical, accessible framework for

future or retrofit fishway designs meant to provide guidance on considering certain turbulent flow characteristics and how they may affect early-life stage fishes prior to construction. This chapter has been previously published in the Journal of Great Lakes Research[1]. *Chapter 3* details a novel instrument that brings Particle Image Velocimetry, a laboratory flow measurement method, to the field to enable better environmental turbulence measurements. This chapter has been previously published in the Journal of Ecohydraulics[2]. *Chapter 4* experimentally measures turbulence in Denil fishways, a common fishway type, under updated slope recommendations. This chapter provides an understanding of what the hydrodynamics will be and how they will impact fishes under the new design suggestions. *Chapter 5* experimentally quantifies the hydrodynamics of traps for sea lampreys, an invasive species in the Laurentian Great Lakes. These measurements are paired with observations of sea lamprey behavior to understand how these fish respond to the turbulence they encounter near these traps, and how this turbulence may be altered to improve trapping rates moving forward. Through these four chapters, this dissertation enriches the scientific body of knowledge necessary to optimize fluvial fish infrastructure, and offers instruments and methodologies for other researchers to build upon to expand the impact of this work further.

[1] Jones, K., & Cotel, A. J. (2023). A hydrodynamics-based framework to evaluate the impact of fishways on drifting lake sturgeon larvae. Journal of Great Lakes Research, 49(1), 332–338. https://doi.org/10.1016/j.jglr.2022.11.006

[2] Jones, K., & Cotel, A. J. (2023). Low-cost field particle image velocimetry for quantifying environmental turbulence. Journal of Ecohydraulics. https://doi.org/10.1080/24705357.2023.2248986

1.5 References

Ackerman, N. K., Pyper, B. J., David, M. M., Wyatt, G. J., Cramer, D. P., & Shibahara, T. M. (2019). Passage Effectiveness at a Pool-and-Weir Fishway Designed to Accommodate Pacific Lampreys. North American Journal of Fisheries Management, 39(3), 426–440. https://doi.org/10.1002/nafm.10281

Autier, V., & Heindel, J. A. (2021). Technical Fishway Limitations and Common Misconceptions. Fisheries and Aquaculture Journal, 12(5).

Baiandina, I. S., & Khanaychenko, A. N. (2018). Water turbulence effect on egg survival and characteristics of hatched larvae of the Black Sea turbot Scophthalmus maeoticus (Pallas, 1814). Marine Biological Journal, 3(4), Article 4. https://doi.org/10.21072/mbj.2018.03.4.11

Cada, G. F., & Odeh, M. (2001). Turbulence at Hydroelectric Power Plants and its Potential Effects on Fish. (DOE/BP-26531-1). Bonneville Power Administration, Portland, OR (US). https://doi.org/10.2172/781814

Castro-Santos, T., & Haro, A. (2010). Fish Guidance and Passage at Barriers. In Fish Locomotion (pp. 62–89). https://doi.org/10.1201/b10190-4

Cotel, A. J., & Webb, P. W. (2015). Living in a Turbulent World—A New Conceptual Framework for the Interactions of Fish and Eddies. Integrative and Comparative Biology, 55(4), 662–672. https://doi.org/10.1093/icb/icv085

Cotel, A. J., Webb, P. W., & Tritico, H. (2006). Do Brown Trout Choose Locations with Reduced Turbulence? Transactions of the American Fisheries Society, 135(3), 610–619. https://doi.org/10.1577/T04-196.1

Davies, J. T. (1972). CHAPTER 1—VELOCITIES AND STRESSES IN TURBULENT FLOWS. In J. T. Davies (Ed.), Turbulence Phenomena (pp. 1–78). Academic Press. https://doi.org/10.1016/B978-0-12-206070-0.50006-7

Dower, J. F., Miller, T. J., & Leggett, W. C. (1997). The Role of Microscale Turbulence in the Feeding Ecology of Larval Fish. In J. H. S. Blaxter & A. J. Southward (Eds.), Advances in Marine Biology (Vol. 31, pp. 169–220). Academic Press. https://doi.org/10.1016/S0065-2881(08)60223-0

Duguay, J. M., Lacey, R. W. J., & Gaucher, J. (2017). A case study of a pool and weir fishway modeled with OpenFOAM and FLOW-3D. ECOLOGICAL ENGINEERING, 103. https://doi.org/10.1016/j.ecoleng.2017.01.042

Higham, T. E., Stewart, W. J., & Wainwright, P. C. (2015). Turbulence, Temperature, and Turbidity: The Ecomechanics of Predator–Prey Interactions in Fishes. Integrative and Comparative Biology, 55(1), 6–20. https://doi.org/10.1093/icb/icv052

Hilder, P. E., Cobcroft, J. M., & Battaglene, S. C. (2017). Factors affecting the feeding response of larval southern bluefin tuna, Thunnus maccoyii (Castelnau, 1872). Aquaculture Research, 48(6), 2752–2766. https://doi.org/10.1111/are.13108

Hockley, F. A., Wilson, C. a. M. E., Brew, A., & Cable, J. (2014). Fish responses to flow velocity and turbulence in relation to size, sex and parasite load. Journal of The Royal Society Interface, 11(91), 20130814. https://doi.org/10.1098/rsif.2013.0814

Jones, K., & Cotel, A. J. (2023). A hydrodynamics-based framework to evaluate the impact of fishways on drifting lake sturgeon larvae. Journal of Great Lakes Research, 49(1), 332–338. https://doi.org/10.1016/j.jglr.2022.11.006

Jones, K., Cotel, A. J., & Webb, P. W. (2022). Stability and turbulence. In Reference Module in Life Sciences. Elsevier. https://doi.org/10.1016/B978-0-323-90801-6.00018-5

Jones, P. E., Svendsen, J. C., Borger, L., Consuegra, S., Jones, J. A. H., & Leaniz, C. G. de. (2020). One size does not fit all: Inter- and intraspecific variation in the swimming performance of contrasting freshwater fish. Conservation Physiology, 8(1), 1dl–1dl. https://doi.org/10.1093/conphys/coaa126

Kolmogorov, A. (1941). The Local Structure of Turbulence in Incompressible Viscous Fluid for Very Large Reynolds' Numbers. Akademiia Nauk SSSR Doklady, 30, 301–305. https://doi.org/10.1098/rspa.1991.0075

Liao, J. C. (2007). A review of fish swimming mechanics and behaviour in altered flows. Philosophical Transactions of the Royal Society B: Biological Sciences, 362(1487), 1973–1993. https://doi.org/10.1098/rstb.2007.2082

Liao, J. C., Beal, D. N., Lauder, G. V., & Triantafyllou, M. S. (2003a). Fish Exploiting Vortices Decrease Muscle Activity. Science, 302(5650), 1566–1569. https://doi.org/10.1126/science.1088295

Liao, J. C., Beal, D. N., Lauder, G. V., & Triantafyllou, M. S. (2003b). The Kármán gait: Novel body kinematics of rainbow trout swimming in a vortex street. Journal of Experimental Biology, 206(6), 1059–1073. https://doi.org/10.1242/jeb.00209

Lupandin, A. I. (2005). Effect of Flow Turbulence on Swimming Speed of Fish. Biology Bulletin, 32(5), 461–466. https://doi.org/10.1007/s10525-005-0125-z

Marrasé, C., Costello, J. H., Granata, T., & Strickler, J. R. (1990). Grazing in a turbulent environment: Energy dissipation, encounter rates, and efficacy of feeding currents in Centropages hamatus. Proceedings of the National Academy of Sciences, 87(5), 1653–1657. https://doi.org/10.1073/pnas.87.5.1653

Megrey, B. A., & Hinckley, S. (2001). Effect of turbulence on feeding of larval fishes: A sensitivity analysis using an individual-based model. ICES Journal of Marine Science, 58(5), 1015–1029. https://doi.org/10.1006/jmsc.2001.1104

Miehls, S., Sullivan, P., Twohey, M., Barber, J., & McDonald, R. (2020). The future of barriers and trapping methods in the sea lamprey (Petromyzon marinus) control program in the Laurentian Great Lakes. Reviews in Fish Biology and Fisheries, 30(1), 1–24. https://doi.org/10.1007/s11160-019-09587-7

Navarro, A., Boys, C. A., Robinson, W., Baumgartner, L. J., Miller, B., Deng, Z. D., & Finlayson, C. M. (2019). Tolerable ranges of fluid shear for early life-stage fishes: Implications for safe fish passage at hydropower and irrigation infrastructure. Marine and Freshwater Research, 70(11), 1503–1512. https://doi.org/10.1071/MF18131

Neitzel, D. A., Dauble, D. D., Čada, G. F., Richmond, M. C., Guensch, G. R., Mueller, R. P., Abernethy, C. S., & Amidan, B. (2004). Survival Estimates for Juvenile Fish Subjected to a Laboratory-Generated Shear Environment. Transactions of the American Fisheries Society, 133(2), 447–454. https://doi.org/10.1577/02-021

Nikora, V. I., Aberle, J., Biggs, B. J. F., Jowett, I. G., & Sykes, J. R. E. (2003). Effects of fish size, time-to-fatigue and turbulence on swimming performance: A case study of Galaxias maculatus. Journal of Fish Biology, 63(6), 1365–1382. https://doi.org/10.1111/j.1095-8649.2003.00241.x

Odeh, M., Noreika, J., Haro, A., Maynard, A., Castro-Santos, T., & Cada, G. (2002). Evaluation of the Effects of Turbulence on the Behavior of Migratory Fish. Report for Bonneville Power Administration.

Pavlov, D., Lupandin, A. I., & Skorobogatov, M. A. (2000). The effects of flow turbulence on the behavior and distribution of fish. Journal of Ichthyology, 20, 232–261.

Prada, A. F., George, A. E., Stahlschmidt, B. H., Chapman, D. C., & Tinoco, R. O. (2018). Survival and drifting patterns of grass carp eggs and larvae in response to interactions with flow and sediment in a laboratory flume. PLOS ONE, 13(12), e0208326. https://doi.org/10.1371/journal.pone.0208326

Prada, A. F., George, A. E., Stahlschmidt, B. H., Jackson, P. R., Chapman, D. C., & Tinoco, R. O. (2019). Influence of turbulence and in-stream structures on the transport and survival of grass carp eggs and larvae at various developmental stages. Aquatic Sciences, 82(1), 16. https://doi.org/10.1007/s00027-019-0689-1

Rehmann, C. R., Stoeckel, J. A., & Schneider, D. W. (2003). Effect of turbulence on the mortality of zebra mussel veligers. Canadian Journal of Zoology, 81(6), 1063–1069. https://doi.org/10.1139/z03-090

Rothschild, B. J., & Osborn, T. R. (1988). Small-scale turbulence and plankton contact rates. Journal of Plankton Research, 10(3), 465–474. https://doi.org/10.1093/plankt/10.3.465

Shahabi, M., Ghomeshi, M., Ahadiyan, J., Mohammadian, T., & Katopodis, C. (2021). Do fishways stress fish? Assessment of physiological and hydraulic parameters of rainbow trout navigating a novel W-weir fishway. Ecological Engineering, 169, 106330. https://doi.org/10.1016/j.ecoleng.2021.106330

Silva, A. T., Katopodis, C., Santos, J. M., Ferreira, M. T., & Pinheiro, A. N. (2012). Cyprinid swimming behaviour in response to turbulent flow. Ecological Engineering, 44, 314–328. https://doi.org/10.1016/j.ecoleng.2012.04.015

Silva, A. T., Lucas, M. C., Castro-Santos, T., Katopodis, C., Baumgartner, L. J., Thiem, J. D., Aarestrup, K., Pompeu, P. S., O'Brien, G. C., Braun, D. C., Burnett, N. J., Zhu, D. Z., Fjeldstad, H.-P., Forseth, T., Rajaratnam, N., Williams, J. G., & Cooke, S. J. (2018). The future of fish passage science, engineering, and practice. Fish and Fisheries, 19(2), 340–362. https://doi.org/10.1111/faf.12258

Trinci, G., Harvey, G. L., Henshaw, A. J., Bertoldi, W., & Hölker, F. (2020). Turbulence, instream wood and fish: Ecohydraulic interactions under field conditions. Ecohydrology, 13(5), e2211. https://doi.org/10.1002/eco.2211

Tritico, H. M. (2009). The Effects of Turbulence on Habitat Selection and Swimming Kinematics of Fishes [Thesis]. http://deepblue.lib.umich.edu/handle/2027.42/62393

Tritico, H. M., & Cotel, A. J. (2010). The effects of turbulent eddies on the stability and critical swimming speed of creek chub (Semotilus atromaculatus). Journal of Experimental Biology, 213(13), 2284–2293. https://doi.org/10.1242/jeb.041806

Vélez-Espino, L. A., McLaughlin, R. L., Jones, M. L., & Pratt, T. C. (2011). Demographic analysis of trade-offs with deliberate fragmentation of streams: Control of invasive species versus protection of native species. Biological Conservation, 144(3), 1068–1080. https://doi.org/10.1016/j.biocon.2010.12.026

Wang, H., & Chanson, H. (2018). On upstream fish passage in standard box culverts: Interactions between fish and turbulence. Journal of Ecohydraulics, 3(1), 18–29. https://doi.org/10.1080/24705357.2018.1440183

Chapter 2 A Hydrodynamics-Based Framework to Evaluate the Impact of Fishways on Drifting Lake Sturgeon Larvae

2.1 Introduction

In recent decades in the North American Great Lakes region, lake sturgeon (*Acipenser fulvescens*)—referred to as "sturgeon" throughout this paper—have been a target for conservation due to their declining populations and threatened status (Baril et al., 2018; Bruch et al., 2016; COSEWIC, 2017; Haxton et al., 2014; Krieger, 2017). Overfishing, pollution, dam construction, shrinking food sources, loss of spawning habitat, and effects from invasive species have all contributed to this species' degradation (Bruch et al., 2016; COSEWIC, 2017; Gillespie et al., 2020; Haxton et al., 2014; Pratt et al., 2020; Priegel et al., 1974). The conservation efforts undertaken to help rehabilitate sturgeon include monitoring and improving habitat and water quality, population restoration through stocking, transfer, and increased spawning habitat, and minimizing human activities that directly reduce sturgeon populations such as fishing (Bruch et al., 2016; Priegel et al., 1974).

A challenge for sturgeon population restoration is the species' spawning success. Much work has focused on creating and maintaining suitable spawning habitat (Baril et al., 2018; Bennion and Manny, 2014; Dammerman et al., 2019), with little efforts focused on improving

the viability of the resultant eggs and larvae. Since survival rates of early life sturgeon significantly affect population success (Caroffino et al., 2010; Holland and Sylvester, 1983; Krieger, 2017), there remains a need to aid in successful completion of the journey undertaken by early life stage sturgeon. This study examines a portion of this journey, focusing on conditions leading to fatality during downstream larval drift through fishways.

2.2 Background

2.2.1 Spawning and Downstream Drift

Improving spawning conditions of sturgeon presents a conservation challenge. Male sturgeon often do not reach sexual maturity until 8-16 years of age, while female sturgeon often are not sexually mature until 24-26 years of age (COSEWIC, 2017; Priegel et al., 1974). Additionally, male sturgeon are able to spawn every 2-7 years, and female sturgeon every 4-9 years (COSEWIC, 2017). Together, the long time period required for sturgeon to sexually mature and the long time period between spawning events for mature fish means that any disturbances to successful spawning and survival of the resultant early-life fish have a significant impact on the population's growth (Dammerman et al., 2019; Forsythe et al., 2013).

An important factor in the spawning cycle and population survival is the downstream migration of recently-hatched sturgeon. Sturgeon spawn in gravel riverbeds (Baril et al., 2018), releasing eggs that adhere themselves to the substrate at the base of the river. After these eggs hatch into larvae, they mature for several days before entering the water column and subsequently undergoing downstream drift (Dammerman et al., 2019). This downstream drift is generally considered to be "passive", i.e. the larvae follow the flow of the river (COSEWIC, 2017; Duong et al., 2011; Krieger, 2017); however, there is growing evidence that there is an "active" piece to the drift, where larvae are able to choose when to leave the protection of the

substrate and enter and exit the water column during their downstream journey (COSEWIC, 2017; Krieger, 2017). Despite this active element, once the larvae enter the water column, a larva's downstream path follows river flow patterns.

Because downstream movement during drift is passive, the path taken can be inferred from the spawning location. In the St. Clair-Detroit River system, sturgeon egg counts were taken from 2005-2014 to increase general knowledge on the species' spawning choices and to inform conservation efforts surrounding sturgeon spawning in the area (Prichard et al., 2017). They found sturgeon eggs almost exclusively at artificial spawning reefs, with egg counts increasing over time. This longitudinal study implies that given the choice, sturgeon will show a strong preference for spawning in locations with ideal spawning characteristics. These include: mean velocity of 0.4-1.3 m/s, mean river depth between 0.5-7 m in large rivers (defined as having greater than 100 m^3/s mean annual flow), mean river depth between 0.4-2 m in small rivers (defined as having less than 100 m^3/s mean annual flow), average substrate sizes between 16-256 mm, and certain water temperatures, the ideal range of which depends on latitude of the sturgeon population (increasing latitude leads to decreasing ideal temperature) (Baril et al., 2018; Bennion and Manny, 2014). Sturgeon are predicted to spawn in areas of river systems as close to these ideals as possible. Spawning location and drift path can therefore be predicted based on locations of ideal habitat within sturgeon ranges; however, each of these currently known ideal ranges per habitat parameter is very large, all spanning orders of magnitude. While these studies begin to give general guidance on how sturgeon spawning habitat location may be predicted, these large ranges speak to further work needing to be done to better understand these ideal spawning habitat characteristics.

With greater knowledge of spawning characteristics and therefore expected spawning

location, a larva's drift path can be better predicted as well. While it is unknown exactly how far downstream larvae will drift, a study examining the St. Clair River found this drift to occur on average for 2-6 km (Krieger, 2017). Again, this wide range speaks to other factors influencing the larval drift path, and the need for further study of this process; based on the above work, however, if spawning sites are within 6 km upstream of a dam, that dam may have an impact on drifting sturgeon larvae.

2.2.2 Dam Impacts

Sturgeon use river habitats for many aspects of their life history, including spawning (Baril et al., 2018; Bennion and Manny, 2014; Bruch et al., 2016; Prichard et al., 2017; Priegel et al., 1974). Due to the widespread damming of rivers in lake sturgeon ranges, the likelihood of sturgeon spawning in a dammed river is high. When an adult passes and spawns upstream of a dam, the resultant larvae may need to travel downstream past that dam during their drift process. Larvae are able to pass downstream in one of three locations: the dam's turbines, spillways, or fish passageways (Alves et al., 2019; Pompeu et al., 2011). This travel is known to cause larval mortality through barotrauma, collision with hard infrastructure, or the turbulent flow patterns and the resultant fluid shear the larva encounters (Alves et al., 2019; Boys et al., 2016; Navarro et al., 2019). Which cause is more significant in the fatality depends on many factors, including geometry of the infrastructure, hydraulic conditions, and fish age (Navarro et al., 2019). This study focuses on turbulent shear's contribution to larval mortality. Shear here refers to shear stress, defined as the stress imposed on fluid by a velocity differential, specifically,

$$\tau = \mu \frac{dU}{dy} \qquad \text{(Equation 2.1)}$$

Where τ is shear stress, μ is dynamic viscosity, and dU/dy is the spatial velocity gradient. A velocity gradient across a fluid parcel induces deformation of that parcel, as demonstrated in

Figure 2.1. This resultant deformation is termed strain, and the rate at which this deformation occurs labelled as strain rate. When a larva is present in a deforming fluid parcel, its underdeveloped body structure may be unable to handle the strain, resulting in injury or death. Specifically, higher shear and therefore high strain rates in flow are associated with increased injury and fatality, and a strain rate threshold exists where 100% mortality occurs (Navarro et al., 2019; Neitzel et al., 2004; Rehmann et al., 2003). Various studies have examined the relationship between strain rate and resultant injury and fatality across a variety of fish species. Details on this relationship are given in Table 2.1.

Shear-related injuries are highly prevalent in turbulent flow due to the breakdown of the eddy structure within the flow (Rehmann et al., 2003). The energy cascade theory states that eddies within the flow break down into smaller eddies before eventually a smallest size in the inertial range is reached, the energy then converted into heat (Kolmogorov, 1941). Eddies have high velocity differentials across them, creating shear stress in the flow at all physical size scales.

Figure 2.2 demonstrates this velocity differential and how it is distributed around an aquatic animal swimming within the eddy. Research suggests that aquatic animals are most affected by turbulent flow structure when the eddies are on the same length scale as the organism (Cotel and Webb, 2015; Odeh et al., 2002; Rehmann et al., 2003). Additionally, if at some point within this breakdown process the eddy sizes are similar to or smaller than larval size, larvae may experience increased mortality rates (Rehmann et al., 2003).

When applying this to drift past dams, the path larvae take is important. There are three possible passage methods (spillways, turbines, or fishways), and due to the highly variable hydraulic conditions across each passage method, each must be considered individually. Work has been done studying the impact of turbine and spillway conditions on early-life stage fishes
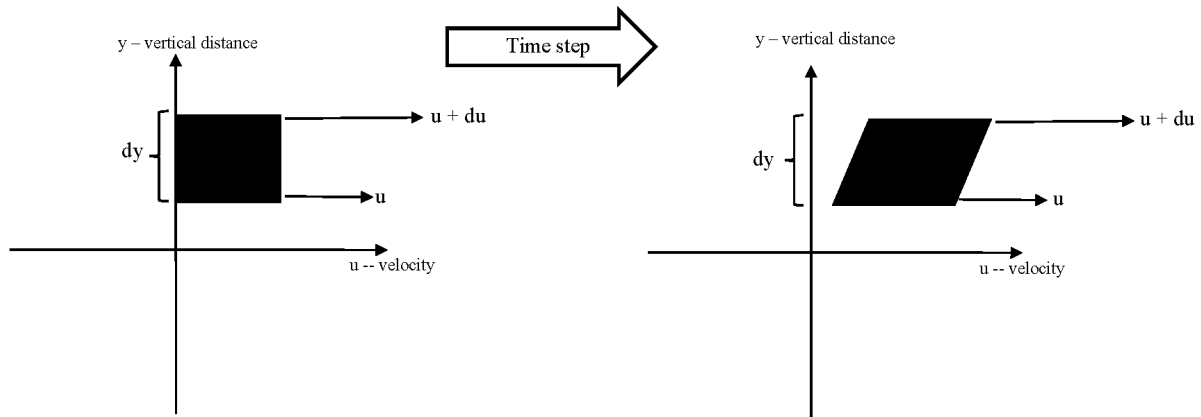
Figure 2.1: Strain induced by shear stress, u -- velocity, y -- vertical distance

Table 2.1: Strain rate effects on various early-life fishes

Strain Rate (1/s)	Effects
0 - 500	• 10% mortality increase observed in murray cod (*Maccullochella peelii*) larvae 9 days post-hatch (Navarro et al., 2019)
500 - 1000	• 10% mortality increase observed in murray cod larvae 29 days post hatch, golden perch (*Macquaria ambigua*) 18 days post-hatch, silver perch (*Bidyanus bidyanus*) 13 days post-hatch, and juvenile chinook salmon (*Oncorhynchus tshawytscha*) • 10% increase in injuries for juvenile chinook salmon, rainbow trout (*Oncorhynchus mykiss*), and steelhead trout (*Oncorhynchus mykiss*) (Navarro et al., 2019; Neitzel et al., 2004)
1000 - 1500	• 100% mortality of juvenile american shad (*Alosa sapidissima*) within 48 hours of exposure (Neitzel et al., 2004)
1500 - 2000	• 75% mortality increase observed in murray cod 9 days post-hatch and silver perch 13 days post-hatch • 10% mortality increase observed in silver perch 19 days post-hatch (Navarro et al., 2019)
2000 - 2500	• 75% mortality increase observed in golden perch 26 days post-hatch (Navarro et al., 2019)
2500 - 3000	• 75% mortality increase observed in murray cod 29 days post-hatch (Navarro et al., 2019)
3000 - 3500	• 75% mortality increase observed in silver perch 19 days post-hatch (Navarro et al., 2019)

(Cada et al., 2006; Cada, 1990; Duncan and Carlson, 2011; Ploskey et al., 2008; Richmond et al., 2007); similar work on the impact of fishways is lacking. Knowing the range of eddy sizes and the strain rates that larvae would experience during drift past dams in all three passage methods can inform retrofitting measures to adjust the relevant method's geometry or flow conditions, reducing this strain rate to tolerable values and lending to the reduction of larval mortality due to turbulence. Here we begin examining these parameters within fish passageways.

This study applies well-known dimensional arguments to fishways, a novel application, in order to estimate the smallest eddy size and strain rate larvae experience within them. This understanding can provide an initial diagnosis of which fishways may require further study and retrofitting measures, resulting in more efficient allocation of conservation effort. Further, this estimation can be performed on future fishways, helping to adjust designs prior to construction to potentially mitigate this mortality rate.

2.3 Turbulence and Strain Rate Analysis

2.3.1 Energy Cascade and Eddy Size Estimation

Kolmogorov's energy cascade theory (Kolmogorov, 1941) states that energy is transferred from the coarse scales of the flow (e.g. large eddies constrained by geometry, in this case, physical dimensions of the fishway) to finer scales of the flow until, eventually, a smallest eddy size in the inertial range is reached. According to the theory, this energy transfer is inviscid, and at that smallest scale, it is dissipated into thermal energy. This scale is the Kolmogorov scale. Because of typical flow conditions in fishways, there is a chance that the smallest eddy size could be on the same order of magnitude as or smaller than fish larvae moving through such infrastructure. Since the size of this smallest eddy relative to larva size affects mortality rate (Rehmann et al., 2003), determining this size is important when examining how larvae may be
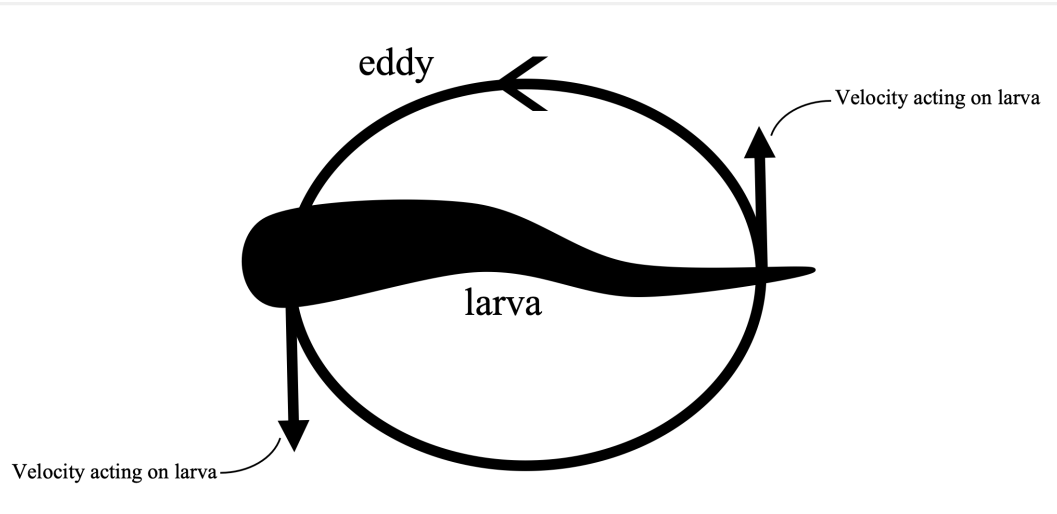
Figure 2.2: Larva and eddy velocity distribution interaction
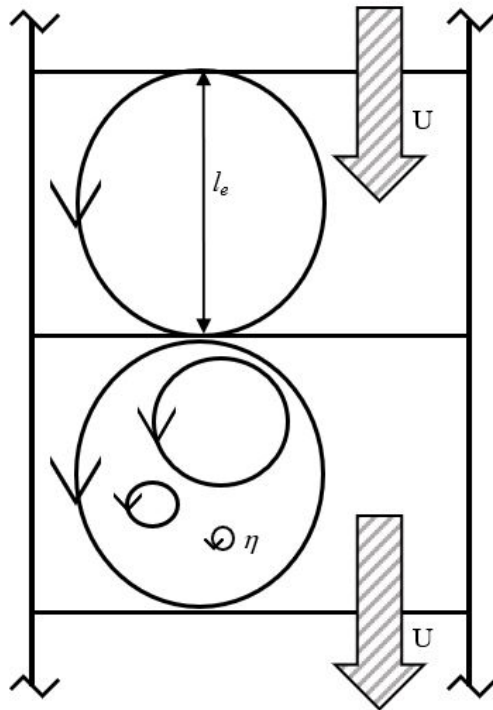
Figure 2.3: Top view of pool-and-weir fishway with several relevant physical parameters

affected by flow within fishways. Figure 2.3 depicts an aerial view of a portion of a pool-and-weir fishway, and illustrates several relevant physical parameters to this calculation.

At the Kolmogorov scale, viscosity dissipating all kinetic energy to thermal energy means the Reynolds number of this eddy must be approximately 1. That is,

$$Re_\eta = \frac{\eta U_\eta}{v} \approx 1 \qquad \text{(Equation 2.2)}$$

Where η is the smallest eddy diameter, U_η is the relevant velocity scale of the smallest eddy, and v is the kinematic viscosity of the water. Taking the smallest fishway pool dimension and hence largest eddy diameter to be l_e, the Reynolds number of the macroscale flow, based on the largest eddies, can be expressed as

$$Re = \frac{l_e U}{v} \qquad \text{(Equation 2.3)}$$

Where U is the relevant macroscale flow velocity through the fishway, typically the average velocity in the region of interest. The theory's assumption of an inviscid energy transfer means the rate of energy transfer must be constant between all eddy sizes. Kinetic energy per unit mass of an eddy of intermediate size d can be approximated as U_d^2, and the time required to transfer energy of this eddy size to the next size down can be approximated by the rotation rate of that particular eddy (Kolmogorov, 1941). The transfer time is therefore d/U_d, giving an energy transfer rate of U_d^3/d. Since this remains constant across all eddy sizes, we have the following relationship between the smallest and largest eddies:

$$\frac{U_\eta^3}{\eta} = \frac{U^3}{l_e} \qquad \text{(Equation 2.4)}$$

Equation 2.4 therefore shows

$$\frac{\eta}{l_e} = \frac{U_\eta^3}{U^3} \qquad \text{(Equation 2.5)}$$

From Equations 2.2 and 2.3,

$$U^3 = \frac{Re^3 v^3}{l_e^{\ 3}} \qquad\qquad \text{(Equation 2.6)}$$

$$U_\eta^{\ 3} \approx \frac{v^3}{\eta^3} \qquad\qquad \text{(Equation 2.7)}$$

Combining these results with Equation 2.5,

$$\frac{\eta^4}{l_e^{\ 4}} \approx Re^{-3} \qquad\qquad \text{(Equation 2.8)}$$

We therefore obtain the following expression to estimate smallest eddy size:

$$\frac{\eta}{l_e} \approx Re^{\frac{-3}{4}} \qquad\qquad \text{(Equation 2.9)}$$

Thus, if the macroscale Reynolds number and largest eddy size of the flow are known, the smallest eddy size can be estimated (Kolmogorov, 1941). In fishways, the largest eddy is determined by the fishway pool dimensions, and the Reynolds number determined by the fishway dimensions, flow rate, and the water's kinematic viscosity.

2.3.2 Strain Rate Estimation

Since eddies lend to larval mortality due to the strain they impose on the larvae, estimating strain rate and not only eddy size in the flow is important. This is commonly estimated using Kolmogorov's theory as follows.

Strain is directly proportional to vorticity and therefore inversely proportional to eddy rotation period. Labeling the rotation period of the smallest eddy as t_η, this can be approximated as

$$t_\eta \approx \frac{\eta}{U_\eta} \qquad\qquad \text{(Equation 2.10)}$$

Giving the strain within that eddy S_η as

$$S_\eta \approx \frac{U_\eta}{\eta} \qquad\qquad \text{(Equation 2.11)}$$

21

Using the result from Equation 2.7, this gives

$$S_\eta \approx \frac{\nu}{\eta^2} \qquad \text{(Equation 2.12)}$$

And using Equation 2.9, strain within fishways can be related to water's kinematic viscosity, Reynolds number, and geometry by

$$S_\eta \approx \frac{\nu Re^{\frac{3}{2}}}{l_e^2} \qquad \text{(Equation 2.13)}$$

It is useful to non-dimensionalize this parameter for easy comparison across different scenarios. Dividing both sides of Equation 2.13 by Re and rearranging the equation, the dimensionless strain relation is thus

$$\frac{S_\eta l_e}{U} \approx Re^{1/2} \qquad \text{(Equation 2.14)}$$

Equations 2.9 and 2.14 may be directly applied to fishways of interest, giving an estimate of the smallest eddy size and turbulent strain rates within the structures. These estimates can be compared to values tolerable to sturgeon larvae, providing a simple diagnostic to determine if these fishways might be hazardous, and if further measurement and investigation should take place. A case study is presented below as an example of this application.

2.4 Vianney-Legendre Fishway Case Study

The above analysis is here applied to the Vianney-Legendre Fishway (VLF) to illustrate its usefulness, and to analyze VLF's potential impacts on drifting sturgeon larvae.

VLF is a fishway on the Richelieu River, enabling fish passage across the Saint-Ours dam in Québec, in which sturgeon have been observed passing through and spawning upstream of (Marriner et al., 2016; Thiem et al., 2011, 2016). VLF is a vertical slot fishway that is 48.5 m long consisting of 18 pools—12 regular pools, 2 turning pools, an entrance and an exit pool, and 2 additional pools directly downstream of the structure. Focusing on the regular pools as they

make up the majority of the structure, each of these is 3.5 m long, 3 m wide, and contain a 7.5 cm elevation drop. The vertical slots in this fishway are 0.609 m wide. An image and schematic of this fishway are given in Figure 2.4 (Marriner et al., 2016).

In VLF, flow through the slot has the highest velocities and turbulence due to forming a turbulent jet (Marriner et al., 2016). This analysis is therefore applied to VLF's slots to capture the most turbulent conditions a travelling larvae would experience. VLF's velocity through each slot can be conservatively approximated as 1.72 m/s (Thiem et al., 2011), and a median water depth approximated as 2.2 m (Marriner et al., 2016). Velocity and water depth are subject to change based on flow condition, but as this analysis provides an estimate of expected strain rates and eddy sizes, median and expected input values are sufficient.

(a)   (b)
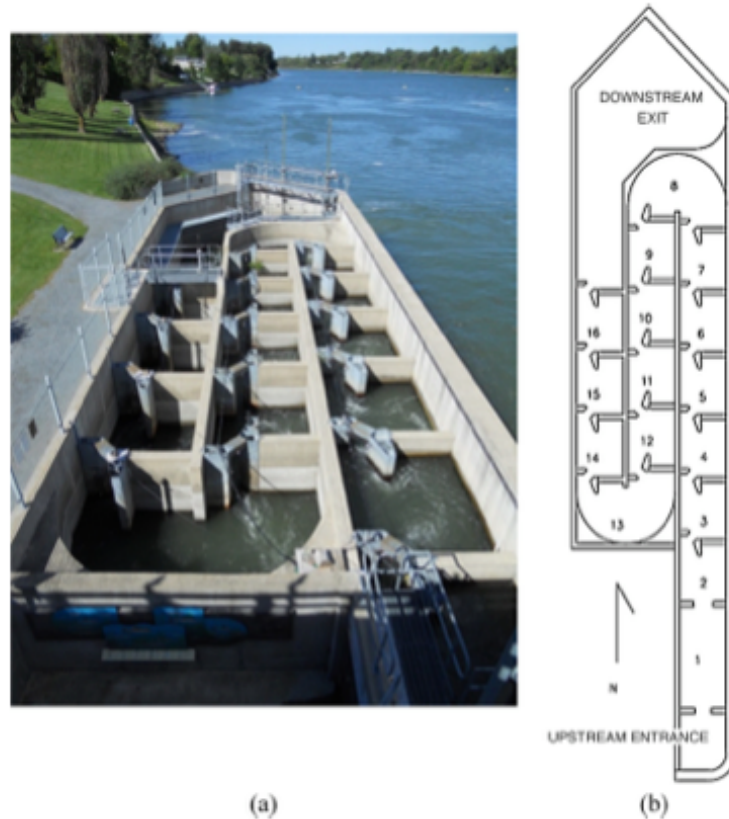
Figure 2.4: Picture (a) and diagram (b) of Vianney-Legendre Fishway (Marriner et al., 2016)

Since sturgeon are able to move upstream of this fishway, and have been observed spawning upstream of the fishway (Thiem et al., 2011, 2016), it can be expected that their larvae may need to drift past it. To determine if this fishway poses a hazard to these larvae and thus the sturgeon population in the area, the above eddy size and strain rate analysis is applied to VLF, based on its vertical slots, as follows.

2.4.1 Smallest Eddy Size

Smallest eddy size η_{VLF} can be estimated from Equation 2.9 as $\eta_{VLF} \approx 0.02$ mm. As this is smaller than sturgeon larvae at drift stage, the eddy structure itself might contribute to an increase in larval mortality (Rehmann et al., 2003), but since it is orders of magnitude smaller, it also may not (Cotel and Webb, 2015); it is therefore important to estimate turbulent strain rate within VLF as another diagnostic value for determining potential harm to larvae.

2.4.2 Strain Rate

Strain rate S_{VLF} can be estimated using Equation 2.14 as $S_{VLF} \approx 2353$ s^{-1}. To determine if this strain rate is hazardous, tolerable strain levels for sturgeon larvae must be considered. This work for sturgeon is currently lacking; this knowledge does, however, exist for other species, and can set a general guideline for how sturgeon larvae may react.

From Table 2.1, this strain rate would pose a significant hazard to a range of species. These hazards include a species-dependent increase in mortality between 10%-75%, total fatality for some fish species, and injuries including fin damage, yolk sac rupture, large bruises, spinal fractures, visible bleeding, eye damage, and gill damage for other fish that were able to survive these strain rate levels (Navarro et al., 2019; Neitzel et al., 2004). These effects are all caused by a fish's body and tissue being unable to withstand the flow it is subjected to. As sturgeon larvae

are not yet armored like their adult counterparts, it is likely their tissue would be unable to handle such conditions and would experience effects similar to those studied fish species. Therefore, this strain rate possibly poses a threat to sturgeon larvae; future work examining sturgeon larvae's tolerance towards heightened strain rate does need to be performed to confirm this conclusion.

2.4.3 Case Study Conclusion

The turbulent strain rate and eddy size analysis suggest that the current VLF geometry may be hazardous to sturgeon larvae should they pass downstream by use of the fishway. If there is concern about sturgeon populations in this area, VLF is a good candidate based on this method for further observations, measurements, studies, and potential retrofit designs to be considered for expanding conservation efforts.

2.5 Discussion

To assist in lake sturgeon conservation efforts, dam infrastructure must be taken into consideration. For a sturgeon group that is targeted for remediation, if spawning is either known to or expected to occur within 6 km upstream of a dam, the respective dam's impact on larval drift should be considered. The method presented in this study is meant as a diagnostic framework to aid in more effectively directing conservation efforts to problematic fishways when there is little available hydrodynamic data. At sites of concern (as defined by the method presented here), field observations and measurements can refine the estimates provided by this framework and offer a more complete understanding of the hydraulic conditions present.

The framework may be applied to existing or future fishways. For existing infrastructure, if the estimates indicate it may be detrimental to nearby sturgeon populations, hydrodynamic

data within the actual fishway should be collected—the framework given here helps determine which fishways would be strategic candidates for this field work. Alternatively, this method can offer an assessment of a future fishway's potential impact to sturgeon in the area, and can be used to alter the design prior to construction to reduce its harm.

2.6 Conclusions

Improving survival rates for lake sturgeon larvae is imperative to conservation efforts, as early life stage survival has a significant impact on adult sturgeon population retention (Holland and Sylvester, 1983). Many factors contribute to survival or mortality rates during this life stage, and all deserve attention. This paper focuses on larvae mortality caused by strain rate and flow structure within fishways that larvae encounter while drifting downstream past dams to nursery habitat.

The smallest eddy size expected within the flow can be estimated based on Kolmogorov's theory using Equation 2.9, and is dependent on fishway geometry and the macroscale flow's Reynolds number. This eddy size within fishways can be on the same order of magnitude as or smaller than sturgeon larval size, potentially creating a hazardous flow environment to sturgeon larvae. Additionally, strain rate can be estimated by Equation 2.14, and is dependent on fishway geometry, macroscale Reynolds number of the flow, and relevant macroscale velocity. Within a typical fishway, these strain rate values easily meet and surpass values that have been shown to be harmful to a variety of species during their early life (see Table 2.1), and it is expected that sturgeon may be similarly affected. Altering geometry or Reynolds number of the fishway can be done in such a way to reduce strain rates imposed on larvae and increase the smallest eddy size in the flow, overall creating a flow environment more conducive for successful larval drift.

To increase efficiency of this framework, more research should be done on the threshold of strain rate values sturgeon larvae can tolerate, and on methods to reasonably adjust flow through fishways while maintaining the original dam objective of power generation. Additionally, development of ways to simply estimate these same diagnostic metrics (smallest eddy size and strain rate) within turbines or spillways—the other means of drift past dams—will expand this work to gain a wider understanding of hydraulic conditions during all possible larval pathways past dams. Doing so will enable the entirety of larval drift past dams to be considered in lake sturgeon conservation, advancing success of such efforts.

2.7 References

Alves, D.C., Vasconcelos, L.P., da Câmara, L.F., Hahn, L., Agostinho, A.A. (2019). Protocol for the assessment of mortality and injuries in fish larvae associated with their downstream passage through hydropower dams. Reviews in Fish Biology and Fisheries, 29, 501–512. https://doi.org/10.1007/s11160-019-09564-0

Baril, A.-M., Buszkiewicz, J.T., Biron, P.M., Phelps, Q.E., Grant, J.W.A. (2018). Lake sturgeon (Acipenser fulvescens) spawning habitat: a quantitative review. Canadian Journal of Fisheries and Aquatic Sciences,. 75, 925+. https://doi.org/10.1139/cjfas-2017-0100

Bennion, D.H., Manny, B.A. (2014). A model to locate potential areas for lake sturgeon spawning habitat construction in the St. Clair–Detroit River System. Journal of Great Lakes Research, Conservation and Management of Fisheries and Aquatic Communities in Great Lakes Connecting Channels 40, 43–51. https://doi.org/10.1016/j.jglr.2014.02.002

Boys, C.A., Robinson, W., Miller, B., Pflugrath, B., Baumgartner, L.J., Navarro, A., Brown, R., Deng, Z. (2016). How low can they go when going with the flow? Tolerance of egg and larval fishes to rapid decompression. Biology Open 5, 786–793. https://doi.org/10.1242/bio.017491

Bruch, R.M., Haxton, T.J., Koenigs, R., Welsh, A., Kerr, S.J. (2016). Status of Lake Sturgeon (Acipenser fulvescens Rafinesque 1817) in North America. Journal of Applied Ichthyology, 32, 162–190. https://doi.org/10.1111/jai.13240

Cada, G.F., Loar, J., Garrison, L., Fisher, R., Neitzel, D. (2006). Efforts to Reduce Mortality to Hydroelectric Turbine-Passed Fish: Locating and Quantifying Damaging Shear Stresses. Environmental Management, 37, 898–906. https://doi.org/10.1007/s00267-005-0061-1

Cada, G.F. (1990). A Review of Studies Relating to the Effects of Propeller-Type Turbine Passage on Fish Early Life Stages. North American Journal of Fisheries Management 10, 418–426. https://doi.org/10.1577/1548-8675(1990)010<0418:AROSRT>2.3.CO;2

Caroffino, D.C., Sutton, T.M., Elliott, R.F., Donofrio, M.C. (2010). Early Life Stage Mortality Rates of Lake Sturgeon in the Peshtigo River, Wisconsin. North American Journal of Fisheries Management, 30, 295–304. https://doi.org/10.1577/M09-082.1

COSEWIC (2017). COSEWIC assessment and status report on the lake sturgeon, Acipenser fulvescens, western Hudson Bay populations, Saskatchewan-Nelson River populations, southern Hudson Bay-James Bay populations, Great Lakes-Upper St. Lawrence populations, in Canada. Committee on the Status of Endangered Wildlife in Canada, Ottawa.

Cotel, A.J., Webb, P.W. (2015). Living in a Turbulent World—A New Conceptual Framework for the Interactions of Fish and Eddies. Integrative and Comparative Biology, 55, 662–672. https://doi.org/10.1093/icb/icv085

Dammerman, K.J., Webb, M.A.H., Scribner, K.T. (2019). Riverine characteristics and adult demography influence female lake sturgeon (Acipenser fulvescens) spawning behavior, reproductive success, and ovarian quality. Canadian Journal of Fisheries and Aquatic Sciences, 76, 1147+. https://doi.org/10.1139/cjfas-2018-0141

Duncan, J.P., Carlson, T.J. (2011). Characterization of Fish Passage Conditions through a Francis Turbine, Spillway, and Regulating Outlet at Detroit Dam, Oregon, Using Sensor Fish, 2009 (No. PNNL-20365). Pacific Northwest National Lab. (PNNL), Richland, WA (United States). https://doi.org/10.2172/1013934

Duong, T.Y., Scribner, K.T., Crossman, J.A., Forsythe, P.S., Baker, E.A., Kanefsky, J., Homola, J.J., Davis, C. (2011). Relative larval loss among females during dispersal of Lake Sturgeon (Acipenser fulvescens). Environmental Biology of Fishes, 91, 459. https://doi.org/10.1007/s10641-011-9804-4

Forsythe, P.S., Scribner, K.T., Crossman, J.A., Ragavendran, A., Baker, E.A. (2013). Experimental Assessment of the Magnitude and Sources of Lake Sturgeon Egg Mortality. Transactions of the American Fisheries Society, 142, 1005–1011. https://doi.org/10.1080/00028487.2013.790847

Gillespie, M.A., McDougall, C.A., Nelson, P.A., Sutton, T., MacDonell, D.S. (2020). Observations regarding Lake Sturgeon spawning below a hydroelectric generating station on a large river based on egg deposition studies. River Research and Applications, 36, 2024–2042. https://doi.org/10.1002/rra.3731

Haxton, T., Whelan, G., Bruch, R. (2014). Historical biomass and sustainable harvest of Great Lakes lake sturgeon (Acipenser fulvescens Rafinesque, 1817). Journal of Applied Ichthyology, 30, 1371–1378. https://doi.org/10.1111/jai.12569

Holland, L.E., Sylvester, J.R. (1983). Distribution of Larval Fishes Related to Potential Navigation Impacts on the Upper Mississippi River, Pool 7. Transactions of the American Fisheries Society, 112, 293–301. https://doi.org/10.1577/1548-8659

Kolmogorov, A. (1941). The Local Structure of Turbulence in Incompressible Viscous Fluid for Very Large Reynolds' Numbers. Akademiia Nauk SSSR Doklady, 30, 301–305. https://doi.org/10.1098/rspa.1991.0075

Krieger, J. (2017). Habitat Utilization and Early Life History Characteristics of Larval, Young-of-Year, and Juvenile Lake Sturgeon (Acipenser fulvescens) in the Great Lakes Connecting Channels [Thesis]. https://deepblue.lib.umich.edu/handle/2027.42/137019

Marriner, B.A., Baki, A.B.M., Zhu, D.Z., Cooke, S.J., Katopodis, C. (2016). The hydraulics of a vertical slot fishway: A case study on the multi-species Vianney-Legendre fishway in Quebec, Canada. Ecological Engineering, 90, 190–202. https://doi.org/10.1016/j.ecoleng.2016.01.032

Navarro, A., Boys, C.A., Robinson, W., Baumgartner, L.J., Miller, B., Deng, Z.D., Finlayson, C.M. (2019). Tolerable ranges of fluid shear for early life-stage fishes: implications for safe fish passage at hydropower and irrigation infrastructure. Marine and Freshwater Research, 70, 1503–1512. https://doi.org/10.1071/MF18131

Neitzel, D.A., Dauble, D.D., Cada, G.F., Richmond, M.C., Guensch, G.R., Mueller, R.P., Abernethy, C.S., Amidan, B. (2004). Survival Estimates for Juvenile Fish Subjected to a Laboratory-Generated Shear Environment. Transactions of the America Fisheries Society, 133, 447–454. https://doi.org/10.1577/02-021

Odeh, M., Noreika, J.F., Haro, A. (2002). Evaluation of the Effects of Turbulence on the Behavior of Migratory Fish, Final Report 2002. (No. DOE/BP-00000022-1). Bonneville Power Administration (BPA), Portland, OR (United States). https://doi.org/10.2172/961896

Ploskey, G.R., Weiland, M.A., Hughes, J.S., Zimmerman, S.A., Durham, R.E., Fischer, E.S., Kim, J., Townsend, R.L., Skalski, J.R., Buchanan, R.A., McComas, R.L. (2008). Survival of Juvenile Chinook Salmon Passing the Bonneville Dam Spillway in 2007 (No. PNNL-18113). Pacific Northwest National Lab. (PNNL), Richland, WA (United States). https://doi.org/10.2172/946673

Pompeu, P.S., Nogueira, L.B., Godinho, H.P., Martinez, C.B. (2011). Downstream passage of fish larvae and eggs through a small-sized reservoir, Mucuri river, Brazil. Zoologia, 28, 739. https://doi.org/10.1590/S1984-46702011000600006

Pratt, T.C., Morrison, B.J., Quinlan, H.R., Elliott, R.F., Grunder, S.A., Chiotti, J.A., Young, B.A. (2020). Implications of the sea lamprey control program for lake sturgeon conservation and rehabilitation efforts. Journal of Great Lakes Research, 47, 421-429. https://doi.org/10.1016/j.jglr.2020.06.014

Prichard, C.G., Craig, J.M., Roseman, E.F., Fischer, J.L., Manny, B.A., Kennedy, G.W. (2017). Egg Deposition by Lithophilic-Spawning Fishes in the Detroit and Saint Clair Rivers, 2005-14 (Scientific Investigations Report), Scientific Investigations Report. U.S. Geological Survey.

Priegel, G.R., Wirth, T.L., Threinen, C.W., Hickey, S. (1974). The Lake Sturgeon: Its Life History, Ecology and Management. Wisconsin Department of Natural Resources, Madison, WI.

Rehmann, C. R., Stoeckel, J. A., & Schneider, D. W. (2003). Effect of turbulence on the mortality of zebra mussel veligers. Canadian Journal of Zoology, 81(6), 1063–1069. https://doi.org/10.1139/z03-090

Richmond, M.C., Carlson, T.J., Serkowski, J.A., Cook, C.B., Duncan, J.P., Perkins, W.A. (2007). Characterizing the Fish Passage Environment at The Dalles Dam Spillway: 2001-2004 (No. PNNL-16521). Pacific Northwest National Lab. (PNNL), Richland, WA (United States). Environmental Molecular Sciences Lab. (EMSL). https://doi.org/10.2172/926967

Thiem, J., Binder, T., Dawson, J., Dumont, P., Hatin, D., Katopodis, C., Zhu, D., Cooke, S. (2011). Behaviour and passage success of upriver-migrating lake sturgeon Acipenser fulvescens in a vertical slot fishway on the Richelieu River, Quebec, Canadian Endangered Species Research, 15, 1–11. https://doi.org/10.3354/esr00360

Thiem, J.D., Dawson, J.W., Hatin, D., Danylchuk, A.J., Dumont, P., Gleiss, A.C., Wilson, R.P., Cooke, S.J. (2016). Swimming activity and energetic costs of adult lake sturgeon during fishway passage. Journal of Experimental Biology, 219, 2534–2544. https://doi.org/10.1242/jeb.140087

Chapter 3 Low-cost Field Particle Image Velocimetry for Quantifying Environmental Turbulence

3.1 Introduction

Turbulence is inherent in environmental flows, and has many impacts on its surroundings including significant effects on aquatic life such as fish. Some of these effects are: both improved (Liao 2007; Liao et al. 2003) and diminished (Cotel & Webb 2015; Odeh et al. 2002; Silva et al. 2012; Tritico & Cotel 2010) swimming efficiency, changes in egg survival rates (Baiandina & Khanaychenko 2018; Prada et al. 2018, 2019), habitat selection (Cotel et al. 2006; Hockley et al. 2014; Trinci et al. 2020; Tritico 2009; Wang & Chanson 2018), altered feeding habits (Dower et al. 1997; Higham et al. 2015; Hilder et al. 2017; Marrase et al. 1990; Megrey & Hinckley 2001; Pekcan-Hekim et al. 2016; Rothschild & Osborn 1988), increased disorientation (Cotel & Webb 2015; Odeh et al. 2002; Tritico & Cotel 2010), injury (Liao 2007; Navarro et al. 2019; Neitzel et al. 2004; Odeh et al. 2002), and death (Megrey & Hinckley 2001; Navarro et al. 2019; Neitzel et al. 2004; Odeh et al. 2002; Prada et al. 2018, 2019; Rehmann et al. 2003). Because of its importance, ways of improving understanding of environmental turbulence are being widely pursued.

Turbulence has been defined in a variety of ways, depending on one's perspective and the

31

data used to quantify such flows. Because of our instrument's application, we here utilize a physical approach, defining turbulent flows as flows composed of a continuum of eddies (Tritico 2009). Because of the significance of turbulent eddies to fish (Cotel & Webb 2015; Liao 2007; Liao et al. 2003; Trinci et al. 2020; Tritico & Cotel 2010; Webb & Cotel 2010), enhanced field measurement techniques capable of capturing these multi-dimensional flow structures are needed. A method being newly adapted to field use is Particle Image Velocimetry (PIV), a technique using a laser, camera, and particles in the flow to quantify two-dimensional flow patterns. Previous efforts to bring PIV to the field have been successful, although each design faces its own challenges. This chapter proposes a new design to overcome these challenges while maintaining robust, reliable measurement.

3.2 Background

3.2.1 Environmental Turbulence

Environmental turbulence in aquatic environments has wide-reaching effects, e.g. significantly impacting fish and other aquatic life, influencing erosion, contributing to plant life changes, and affecting pollutant mixing. Here, impacts on fish populations and habitat are focused on, with the physical parameters of vorticity, eddy dynamics including size and circulation, and turbulent kinetic energy (TKE) used to characterize the flow.

Vorticity is defined as the curl of the local spatial variation of a velocity field (Wu et al. 2015). Generally, it can be thought of as the strength of the swirling motion of a flow. This metric has been shown to affect fish swimming, with increasing vorticity in the flow leading to a reduction in swimming capability and speed (Tritico & Cotel 2010; Zha et al. 2019), and altering swimming kinematics including tail-beat frequency of fishes (Tritico 2009). Vorticity also affects the trajectory of fish swimming, with a study finding that fish would linger in areas with lower

vorticity (Zha et al. 2019). Beyond fish swimming, vorticity also enhances turbulent mixing (Dimotakis 2005), having a direct impact on fish habitat, e.g. affecting transport of food particles and therefore feeding behaviors, altering macrobenthos distribution, and changing vegetation growth locations.

Eddies are parameterized here using eddy diameter and circulation. Eddy diameter plays a significant role in flow effects on fish, as swimming capability is largely affected by eddies on the same order of magnitude of size as the fish (Cada & Odeh 2001; Cotel & Webb 2015; Lupandin 2005; Nikora et al. 2003; Tritico & Cotel 2010). Therefore, with respect to fish conservation and understanding the environment's impact on fish populations, being aware of the distribution of eddy sizes within the flow is important. Further, eddy diameter's impact on fish is affected by the circulation contained within that eddy. Circulation can be thought of as the 'strength' of an eddy, and is defined as the surface integral of vorticity (Wu et al. 2015). In this paper, eddy diameter is determined through calculating circulation along concentric circles centered on a local maxima of vorticity magnitude, and the eddy diameter is the diameter of the circle with the greatest circulation, following Drucker and Lauder (1999). Besides its connection to eddy diameter, circulation itself is an important parameter to evaluate fish performance; high circulation has been shown to have a significant impact on aquatic animals (Tritico 2009), affecting their swimming form and stability.

TKE is a flow parameter that considers turbulent fluctuations in the flow's velocity, and therefore gives a general measure of turbulence within the flow. It is denoted k and defined as $k = \frac{1}{2}(\overline{(u')^2} + \overline{(v')^2} + \overline{(w')^2})$, where u', v', and w' indicate turbulent velocity fluctuations in the x-, y-, and z- directions respectively. This measure has high impacts on fish swimming ability and behavior, including their energy expenditure and swimming location (Li et al. 2021; Silva et

al. 2012; Trinci et al. 2020). Its importance to fish habitat makes it a parameter of interest with respect to fish conservation efforts.

3.2.2 Field PIV Systems

PIV is a non-intrusive flow measurement technique, consisting of four steps: seeding, illumination, recording, and evaluation (Raffel et al. 2018). In brief summary, PIV measurement is done through dispersing small, neutrally-buoyant, reflective particles throughout the flow of interest. These particles are termed 'seeds'. This seeded flow is then illuminated using a thin laser sheet to illuminate a plane. Multiple images are captured at a given frame rate using a camera placed perpendicularly to the laser sheet. Consecutive images are paired, and the pairs are evaluated through cross correlation, enabling tracking of particle movement and therefore flow pattern and velocity (Raffel et al. 2018; Thielicke & Stamhuis 2014). Figure 3.1 shows a general PIV setup. Currently, PIV is largely used in laboratory settings, although past successful efforts have been made to utilize this tool in field settings (Jin 2019; Katija & Dabiri 2008; Morgan 2013; Tritico et al. 2007). Several of these past systems are described here.
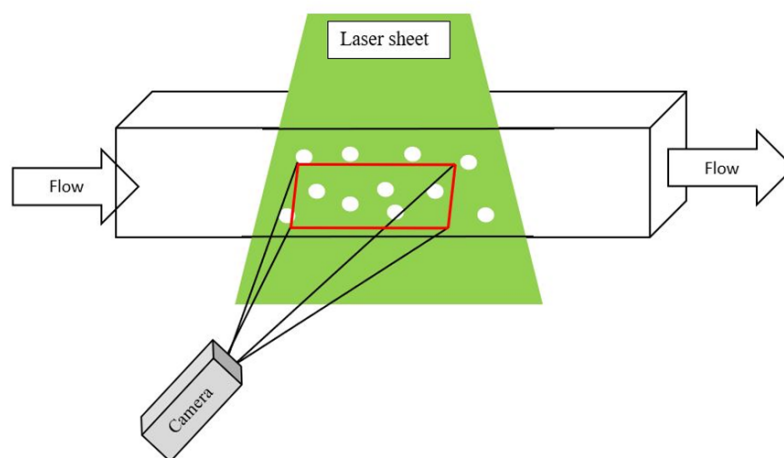
Figure 3.1: General PIV setup

Tritico et al. (2007) designed a miniature submersible PIV system with a main goal of portability. This design consisted of separate boxes to house the laser and the camera, connected by a cable and additionally connected to a computer for data storage. This system used a 90 mW battery-powered laser and a 1 megapixel, 30 fps camera. 50 image pairs were collected, with 15 being used for analysis. When examining flow conditions common within river systems and boundary layers, this system measured velocity within 10% of acoustic doppler velocimeter (ADV) measured values and vorticity within 3.5% of values measured by a laboratory PIV system. The system cost $7500 and was operable by two people. While capable of capturing the turbulence metrics of interest, this design suffered from a lack of ruggedness due to the need for a computer in the field and the large amount of waterproofing. As this system is meant for field use, the care this system requires is a limitation.

Katija and Dabiri (2008) constructed a portable handheld PIV device for divers to examine interactions of aquatic animals and their surroundings in-situ. This system used a 300 mW battery-powered laser and a high speed camera, their waterproofed casings connected through a locking extendable arm ensuring perpendicularity. They conducted analysis over 1 s of flow, with measurements taken at night for image quality. The authors note that 60 fps setting on the camera is sufficient, despite their camera being capable of higher temporal resolutions. While portable and accurate, the accessibility of this system to wider use is limited due to its expensive cost, around $90,000. This system's handheld nature inherently introduces error through its reduced stability and by interrupting the flow pattern near the system. Additionally, the authors note that its inability to examine three-dimensional flow structures meaningfully is another limitation.

To study flow patterns through vegetated marshes, Morgan (2013) designed and used a

PIV system to measure flow around softstem bulrush on the shore of the Huron River in Ann Arbor, Michigan. This system consisted of a 6 megapixel 60 fps digital camera and a 750 mW laser each stored in its own separate waterproofed box, connected through a rigid arm to allow for the perpendicular setup needed. The camera was connected through a cable to a computer to control the camera and enable real-time viewing of the images. Video was continuously recorded and frames pulled from the video to provide for the paired images needed. While this system was able to accurately measure vorticity, it also struggled from flow interruption and a need for increased field ruggedness. Its relatively large nature also served as a portability challenge. This system used the open source PIV analysis software PIVlab (Thielicke & Stamhuis 2014) to process the images, using 20 frames for analysis. The temporal average of these frames was used to determine average flow characteristics.

Jin (2019) developed an underwater PIV system with the intention of measuring deep, benthic boundary layer turbulence. This system consisted of three separately waterproofed parts – a laser unit, containing a 15 W laser facing downward through a cylindrical lens for a vertical laser sheet, a 30 fps combined camera-and-computer unit positioned orthogonally to the laser unit to be able to image the laser, and a separate battery unit. These units were connected to a rigid frame consisting of cast iron pipes and fittings, to allow for easy assembly and to ensure the necessary perpendicularity of the camera and laser. The camera-and-computer unit was connected to the battery and laser units through underwater eight-pin cables. Due to the deep nature of the measurements taken with this system, daytime measurement was possible, although a small 'shading board' helped improve the quality of the contrast of images further, as some sunlight still reached the depth being measured of 55 m. The author noted that a challenge to this system was the low natural particle density in the deep measurement location.

Overall, the development of such systems has yielded working techniques. However, they overwhelmingly suffer from a challenge to portability, high costs, and partial flow obstruction. The system described here is designed to address these challenges.

3.3 Design

The goal of the novel PIV system introduced here is to create a less-invasive, low-cost, reliable, highly portable instrument. This design has five parts—laser, cylindrical lens, waterproofed laser box, metal framing system, and camera. Figure 3.2 gives a top and side view of the design (a), and an image of the system (b).

The system's base is a rectangular aluminum extrusion frame with three cross bars. A battery powered laser and the cylindrical lens used to split the laser beam into a sheet are housed within a waterproof box at one end of the frame. This box is placed on stilts, and is attached to a fixed crossbar and the end of the frame. On another crossbar, a GoPro camera is attached, with the lens facing upwards to be able to image the horizontal laser sheet. PIV image recording is done through videoing the laser sheet for an extended period of time, and later pulling frames of the video to act as image pairs. Further details on each element of the design are given in the subsections below.
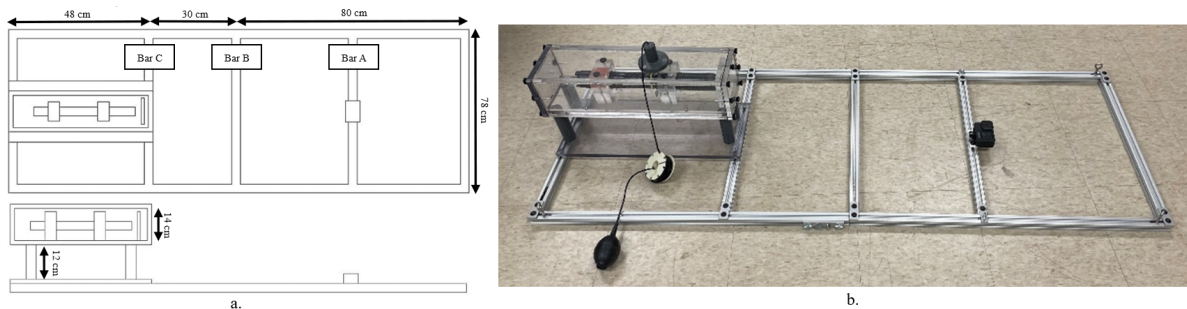
Figure 3.2: Novel PIV system diagram (a) and image (b)

3.3.1 Laser, Lens, and Housing Box

The battery-powered laser used here emits a continuous, 1 W, 532 nm, 2 mm diameter beam. It is triggered using a 6 m air shutter release (a device originally designed for photographers, used to manually depress buttons from afar), allowing control of lasing from a distance. The lens used to split the laser into a sheet is a plano-concave cylindrical lens with a focal length of 1.27 cm, secured into the center of an acrylic square and held in place 2 cm in front of the laser. This acrylic square is able to be rotated 90°, offering flexibility in the orientation of the laser sheet (vertical or horizontal) and therefore in the orientation of flow patterns the system is able to capture.

The box used to house the laser and lens is constructed of 1.5 cm thick acrylic, with four 12 cm long cylindrical legs attached to the bottom, one on each corner. Additional legs with different lengths can be constructed to alter distance between camera and laser sheet, offering the ability to change the size of the field of view (FOV) or the depth of the recorded flow. Below these legs is a 1.5 cm thick acrylic sheet that enhances support for the box and legs while attached to the metal frame. Four holes are drilled in this base, one at each corner, to facilitate attachment of the laser-lens-housing box system to the frame. Both ends of the box are removable to allow for the necessary adjustments inside of the box, but must be secured in place before the system is used underwater. The aforementioned air shutter release is placed through the top of the box, with the trigger aligned with the laser 'on' button. As this requires a hole in the acrylic, a watertight seal surrounding it keeps the system waterproof.

3.3.2 Metal Framing and Camera

The frame system, designed to ensure perpendicularity between laser sheet and camera, is constructed from aluminum extrusion frame which gives freedom to adjust the setup as needed.

Additionally, it allows the system to easily be broken down and reassembled by hand in the field. The various bars are connected by plates and screws, allowing maximum flexibility in the design. Figure 3.2a shows a diagram of the frame and gives the dimensions.

From Figure 3.2a, bar A supports the camera, and its placement is adjustable to allow for varying distance between the camera and laser box as needed. Here we use a GoPro HERO9 Black, and with the current length of the cylindrical legs, this results in a maximum FOV of 20 cm x 27 cm. Bar B increases bracing and structural integrity of the design, and bar C together with the end of the frame supports the waterproof laser box. If a vertical laser sheet is desired, an attachment can be constructed and attached to the frame to hold the camera in such a position to accommodate this. Figure 3.3 shows an example of such an attachment, although this is not the only design possible for such an alteration; the adjustability of the frame allows for a wide variety of designs to fulfill such a need.

The camera frame rate, FOV, and laser power are limiting factors to the setup described here. We focus on low velocity habitats, thus the setup is adequate; the system's use can be expanded by altering the camera and laser used.

Figure 3.3: Sample attachment for capturing data in a vertical laser sheet

3.3.3 Design Benefits

This system costs approximately $1100 USD to construct, making it affordable to most organizations that may be interested in acquiring this type of system, such as conservation groups. Using a GoPro camera increases field ruggedness, and its small stature reduces flow obstruction. The small battery-powered laser reduces cost and system size while further increasing system ruggedness through eliminating the need for cables and cords. The frame's ability to completely break down enables easy portability and adjustability in the field; its flatness and distance from the laser sheet reduces its footprint in the recorded flow.

This system described here is designed to take measurements in a relatively small FOV where detailed hydrodynamics are desired, not large river-scale characteristics. A major benefit of the system's design is its adaptability. By using a higher power laser, altering dimensions such as the distance from the laser to the camera, using a high-speed camera, or capturing longer datasets, its use can be expanded to larger areas or higher speed flows.

3.4 Methods

3.4.1 General Recommendations

To ensure good quality data, the project team makes the following recommendations.

1. Measurements should be taken at night. The reduced light enhances contrast with the laser, giving better image quality. Nautical twilight was sufficient for the laser tested here, although this is dependent on the power of the laser being used.

2. In similar environments to those examined here, a frame rate of 60 fps captures sufficient detail, can be edited and processed using most editing softwares, and does not unnecessarily consume large amounts of data storage.

3. The GoPro HERO9 Black needs to be set to 'Linear'. This setting internally corrects for the fisheye lens on the camera, reducing the need to do this correction in post-processing of the data.

4. Taking data facing upstream minimizes disturbance to the captured flow by the system.

5. This system works best in environments 1 m deep and shallower, as stability becomes difficult to ensure with higher depths. The minimum usable depth is directly related to the length of the legs attached to the laser box. Thus, different sets of legs can be constructed to expand the range of the instrument.

6. A pixel-to-actual distance calibration photo is needed and can be easily taken outside of the measurement site prior to or after field data collection. The calibration photo used here was an image of a ruler in the laser sheet, to show distance in the correct plane.

7. High turbidity is a limitation to the system, as it is to all PIV analysis. In areas with very murky flows, image quality may be too degraded to effectively perform analysis using this system.

8. In areas with low natural seeding, eco-friendly particles such as milk powder or flour can be added to the flow to perform analysis.

9. If horizontality is needed, a level can be added to the frame to ensure this metric is met.

3.4.2 Data Collection

The following procedures are followed for data collection with this system.

1. Adjust bar A's placement to be as far from the laser as needed to get an adequate FOV. This distance depends on laser power and the flow of interest.

2. Turn the laser's safety off, and waterproof the system. Begin recording a video prior to placement in the water.

3. Place the system in the area of interest, facing such that data is recorded upstream of the laser box. Ensure it is still and stable.

4. Trigger the laser using the air shutter release. Record as long as necessary to capture all flow structures of interest; ideal data collection length will depend on flow behavior. Length of recordings is limited by camera storage capacity and laser-related limitations, including battery life or potential safety shutoffs.

5. Turn the laser off prior to removal from the water for safety purposes using the air shutter release. Remove the system from the water. Stop recording.

3.4.3 Data Processing

Data processing and analysis is done through the following method.

1. Edit the data to have enhanced contrast and to be greyscale. Here Adobe Premiere Pro was used, although many programs are capable of doing this.

2. Load the edited video into PIVlab, choosing the frames of interest for analysis. The number of frames needed to accurately capture average flow characteristics can be ascertained through testing convergence of metrics of interest, i.e. by averaging across several different time periods (e.g. 0.5 s, 1 s, 1.5 s, etc) to determine when average values converge within an error range acceptable to the application. This error range will be highly situationally-dependent and therefore is to be determined by the user.

3. Calibrate the pixel-to-distance ratio using the calibration photo, and mask any areas not of interest or of poor image quality.

4. Adjust PIVlab's PIV settings to what is needed for accurately analyzing the dataset. This varies based on flow conditions (Adrian, 2005; Raffel et al., 2018).

5. Analyze all frames. After initial analysis is done, PIVlab can provide many important

    turbulence and flow metrics. The ones examined here are velocity magnitude, velocity

    components to calculate TKE, and vorticity.

3.5 Laboratory Validation

Validation testing was performed in a water tunnel on both uniform flow and flow around

a cylinder to ensure the system's ability to accurately measure velocity and TKE. Vorticity was

qualitatively explored in the lab but quantitatively validated in the field; this is described below

in *3.6 Field Testing*.

3.5.1 Laboratory Velocity Validation

Velocity was measured at several different settings in the water tunnel using the novel

PIV system, a Hach FH950 electromagnetic flowmeter, and an ADV sampling a volume of 7 mm

vertically at a high frequency of 200 Hz. The water tunnel had a water depth of 53.5 cm, and all

velocity measurements were taken 32 cm from the water surface to capture the approximate

average velocity in the tunnel. The ADV and Hach FH950 were centered transversely in the

tunnel, and their measurements were time averaged over 1 s. PIV results were spatially averaged

(see the FOV shown in Figure 3.6a), and temporally averaged over 1 s to allow for meaningful

comparison with the other point methods. Error was determined for the PIV and ADV by

comparing repeat datasets, and error for the Hach FH950 was determined through the

instrument's specifications. The outcome of this comparison is shown in Figure 3.4.

The error bars of the PIV measurements fall within the same range as the other two

methods for all but the highest velocity (between 48.6 – 53.6 cm/s) examined. At this velocity,

the high end of the PIV's error range aligns with the low end of the Hach FH950's error range,
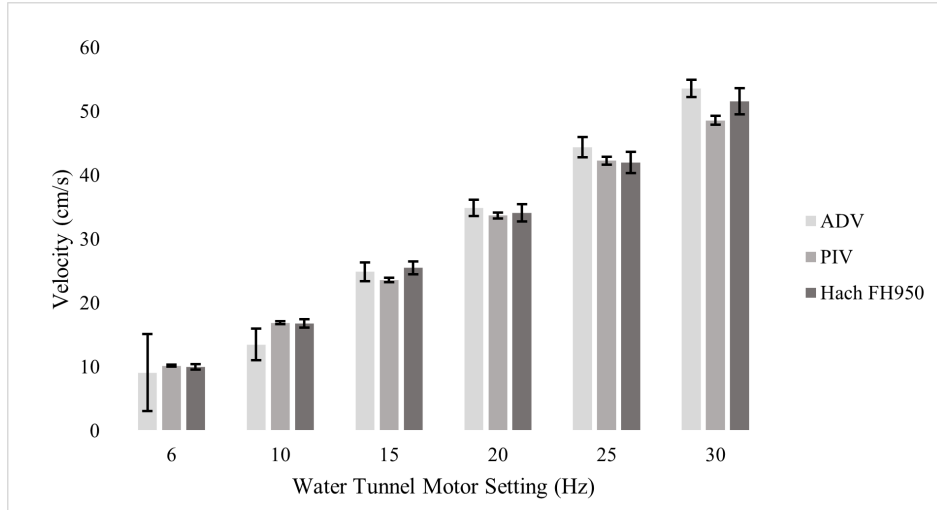
Figure 3.4: Laboratory velocity measurements using ADV, novel PIV, and Hach FH950
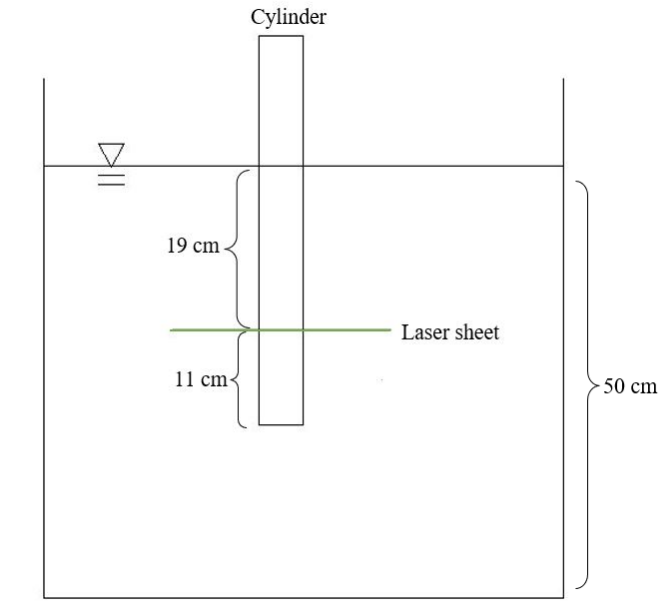
Figure 3.5: Laboratory setup for turbulence validation measurements

with the average PIV velocity being within 10% of all measurements at this setting. This indicates possible slight but insignificant underestimation of the velocity at this setting by the PIV. Thus, at the range of velocities examined here, the novel PIV agrees with the ADV and the Hach FH950, and the system is able to measure average flow velocity reliably.

3.5.2 Laboratory Turbulence Validation

The strength of the novel PIV system lies in its ability to capture two-dimensional turbulence information in the field. To validate its ability to do so, flow behind a 5.1 cm diameter cylinder was recorded by both the novel PIV and an ADV at two water tunnel motor settings (6 and 10 Hz). The overall test setup is shown in Figure 3.5.

The ADV is unable to directly measure vorticity due to its nature of recording point measurements; PIV, however, can capture this metric. Figure 3.6a provides an example of vorticity captured by the novel PIV in the water tunnel at 6 and 10 Hz. As would be expected due to the higher water velocity in the tunnel at this setting, the 10 Hz run recorded consistently higher levels of vorticity spread throughout more of the flow. Qualitatively this agrees with intuition; quantitative vorticity validation is discussed in the section below, *3.6 Field Testing*, at Field Site 1.

TKE was analyzed using both the novel PIV and an ADV. Figure 3.6b shows average TKE at 6 Hz and 10 Hz measured using the PIV. The black 'X' in this figure indicates placement of the ADV, with the values from both systems at this point compared in Figure 3.6c. As the PIV system is only able to measure velocities in the x- and y-direction here, z-direction velocities measured by the ADV are excluded from its TKE calculation to maintain uniform analysis across both methods. From Figure 3.6c, despite the PIV's larger error range, there is overwhelming agreement between the two methods. It is therefore clear that the novel PIV agrees with the

a. Vorticity (1/s)

b. TKE (m^2/s^2)

Note: cylinder placed above center of vorticity and TKE maps
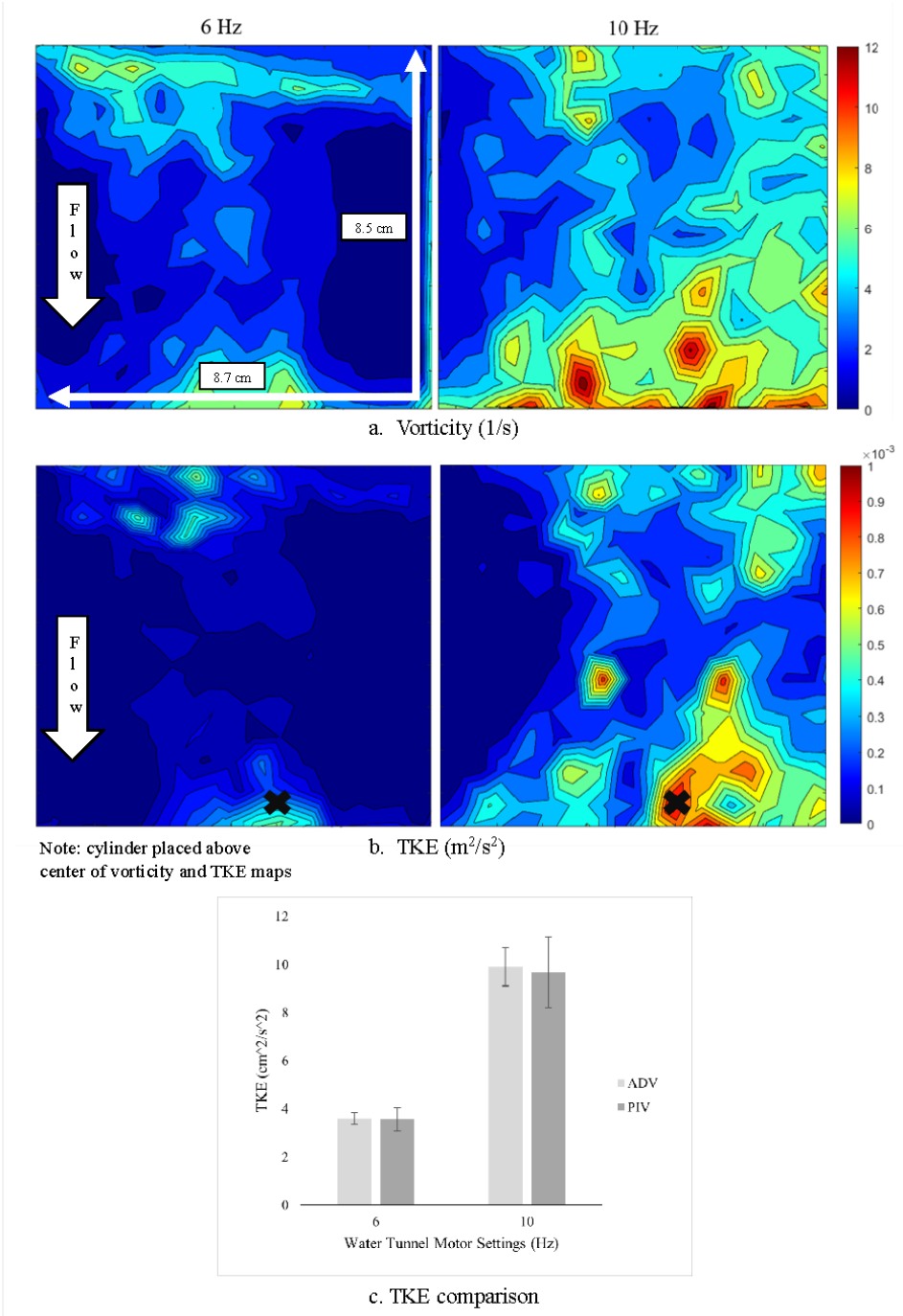
c. TKE comparison

Figure 3.6: Laboratory turbulence validation results – a) vorticity data from novel PIV, b) TKE data from novel PIV, where the black 'X' indicates ADV placement, and c) comparison of novel PIV and ADV results

ADV, and can accurately capture TKE information.

3.5.3 Laboratory Validation Conclusions

Laboratory validation of the novel system reveals a high level of dependability for both TKE and average velocity measurements. While no measurement technique is perfect and without its flaws, this PIV system gives close results to two accepted forms of field measurements—an electromagnetic flowmeter and an ADV—indicating its results are acceptable and reliable.

3.6 Field Testing

Field testing was performed at three sites exhibiting a variety of flow conditions in the Huron River in Ann Arbor, Michigan from July through October 2021. Each of these measurements were taken during nautical twilight to give good contrast between the laser and its background. Figure 3.7 shows the locations of each site, and Figure 3.8 shows the FOV for data at each.

3.6.1 Field Site 1 – Barton Dam Bulrush Patch

Field site 1 was a bulrush patch directly downstream from Barton Dam (see Figure 3.7a), located at 42°18'27.5"N 83°45'21.7"W on the Huron River in Ann Arbor, Michigan. The water depth in this patch was approximately 44 cm, and measurements were taken approximately 3.5 m directly offshore. Figure 3.8a exemplifies the data captured and analyzed at this location following conversion to greyscale. The solid red area is considered 'masked', and is excluded from PIV analysis due to poor image quality. The area within the blue box was used for analysis at this field site. Relative to this image, bulrush was surrounding the top, left, and right sides, with flow moving as indicated on the figure. The water was somewhat murky at this site, hence

a. Barton Dam Bulrush Patch – 'X' indicates patch location

b. Bandemer Park locations

c. Island Park Boulder – 'X' indicates boulder location
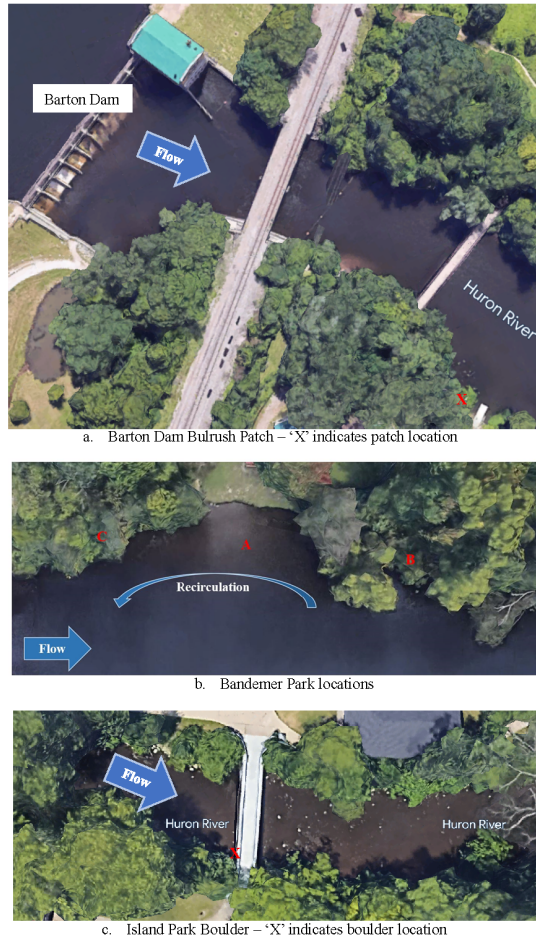
Figure 3.7: Locations of field sites 1 (a), 2 (b), and 3 (c)

a. Barton Dam Bulrush Patch

b. Bandemer Park

c. Island Park Boulder
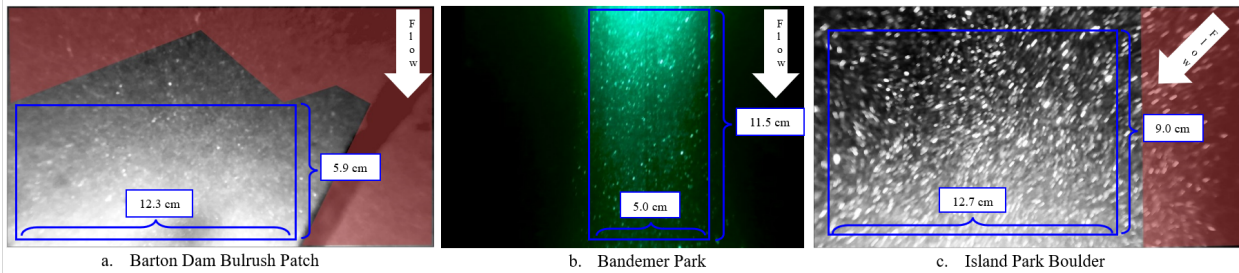
Figure 3.8: FOV of field data sets at field site 1 (a), 2 (b), and 3 (c)

the reduced contrast between the particles and the background. However, robust PIV analysis was still able to be performed on part of the data collected, the results of which are presented here.

Figure 3.9 gives velocity magnitude, vorticity magnitude, and TKE temporally averaged over 1 s (60 frames) at this location. In this environment, eddies are created as the flow passes by each individual reed, with some eventually merging. This results in relatively complicated vorticity and turbulence patterns. This is qualitatively reflected in Figure 3.9, with vorticity and TKE being highly variable across the entire FOV.

Previous PIV measurements have been taken at this location (Morgan 2013). These measurements were taken nearly a decade prior, under different river and plant growth conditions. However, due to the site's location a short distance downstream from a dam (see Figure 3.7a) and its therefore controlled flow nature, typical flow conditions will not have varied greatly over time. Table 3.1 compares both sets of turbulence measurements at this site; the novel system's results align well with these previous measurements, showing reliability.

3.6.1.1 Field Site 1 Conclusions

Barton Dam Bulrush Patch is a particularly useful field site to test the novel system's accuracy in vorticity and eddy characteristic measurements due to the location having previous measurements that provide a baseline for comparison; this offers the opportunity for quantitative validation for these turbulence characteristics. Based on Table 3.1, both peak and average vorticity fall within the previously measured range, indicating valid measurements. When examining eddy diameter and circulation at this site, the novel PIV system found similar values but a wider range than the previous measurements. This new range is well within an order of magnitude of the validating measurements, and is therefore most likely due to changes in plant
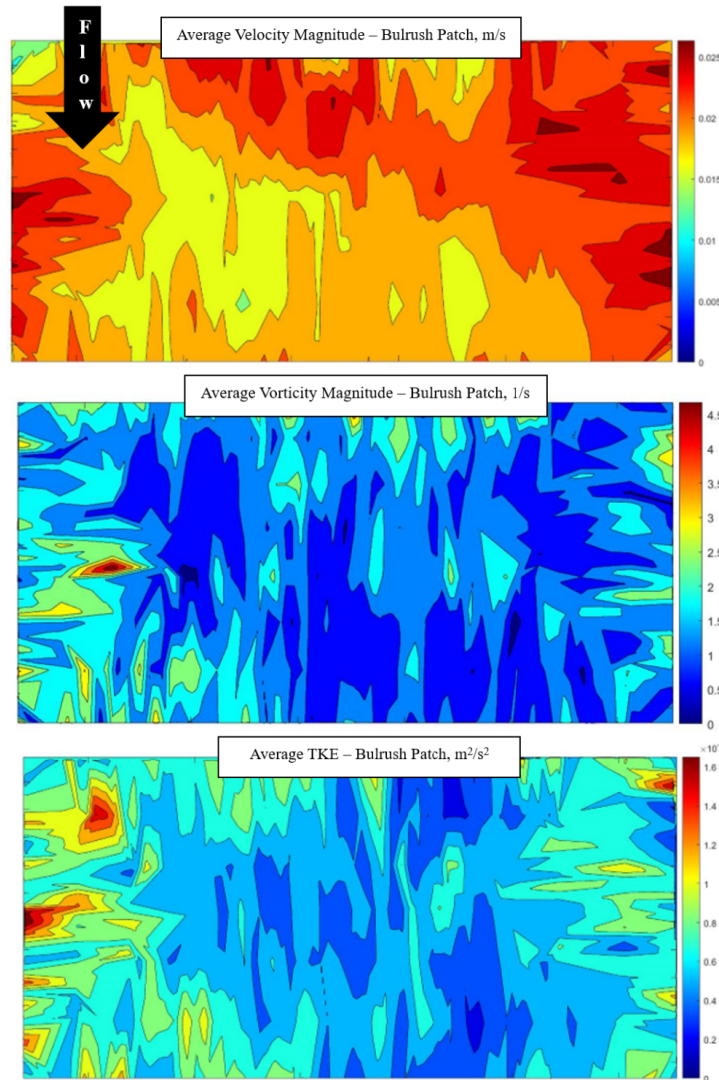
Figure 3.9: Field site 1 PIV data results – average velocity magnitude (top), average vorticity magnitude (middle), and average TKE (bottom)

Table 3.1: Peak vorticity (1/s), average vorticity (1/s), average eddy diameter (cm), and average circulation (cm^2/s) at field site 1 from previous measurements and field PIV

	Previous Measurements Range	Novel System
Peak vorticity (1/s)	2.5-10	5.2 ± 0.44
Average vorticity (1/s)	0.7-4.5	1.6 ± 0.07
Average eddy diameter (cm)	0.56-0.7	0.63 ± 0.13
Average circulation (cm^2/s)	0.3-1.1	1.46 ± 1.11

growth conditions over the approximate decade since the last measurements were taken.

At Field Site 1, the novel system quantitatively compared well to the baseline measurements, indicating adequacy of the system for analyzing vorticity, TKE, eddy diameters, and eddy circulation in vegetated marsh environments. Considering the complexity of the flow pattern and turbulence structure in such locations, this speaks to the system's ability to analyze complicated eddy-dominated flows. Additionally, these environments play important roles in a wide variety of river restoration objectives. From reducing velocities and therefore minimizing bank erosion and encouraging sediment deposition, to removing pollutants from the water, to acting as specialized fish habitat (Palmer 1988; Parkos et al. 2011), these types of environments and the conditions within them are of interest. This novel system is able to capture the flow conditions of vegetated marshes accurately, providing essential physical parameters for conservation applications there.

3.6.2 Field Site 2 – Bandemer Park

The second field site is at Bandemer Park, located at 42°18'12"N 83°44'45"W in Ann Arbor, Michigan. This is located in a bend of the Huron River, in an area of recirculation downstream from field site 1. Velocities are reduced here due to widening of the river. Three different locations at this site were used to test the novel PIV.

Each of these locations are close in proximity to each other, but exhibit variance in flow patterns. As such, this site tests the PIV's ability to capture similarities and differences in related flows. Figure 3.7b briefly illustrates the placement of each site, with further details given for each below. Figure 3.8b gives an example of the raw data collected at this location. Each location's velocity was also recorded by a Hach FH950 for comparison purposes.

These three Bandemer Park locations can be separated into two categories – relatively

uniform flow, and complex turbulent flow. Location A had relatively uniform flow. It was 5.8 m directly offshore in an open area approximately 0.51 m deep, with no nearby vegetation or large rocks to perturb the flow. Measurements were taken in a horizontal plane approximately 15.2 cm from the riverbed. Figure 3.10 demonstrates that Location A has more uniform velocity (a) and vorticity (b), and lower TKE (c), than Locations B and C; this agrees with expectation. Additionally, Location A's relatively rectilinear flow nature means its overall velocity magnitude should agree with that recorded by the Hach FH950, as the Hach FH950 can only measure velocity in one direction and the velocity here is dominated by unidirectional flow. The Hach FH950 measured the velocity in this location to be approximately 9 cm/s, which was also measured by the novel PIV in Figure 3.10a. Note the data presented in Figure 3.10 is temporally averaged over 1 s of flow, or 60 frames of data.

Locations B and C were more turbulent due to their placement among vegetation and woody debris. Location B was downstream from Location A in the recirculating flow, 2.1 m offshore in a patch of vegetation near a large boulder. The water depth was approximately 0.48 m. This location had gravelly, sandy substrate, and due to the vegetative patch and boulder the flow was much more turbulent than Location A. Location C was upstream of Location A in the recirculation, in the center of another vegetative group. Measurements here were taken 3.8 m offshore, with a water depth of approximately 0.30 m deep. Again, heightened turbulence and vorticity are expected at both of these locations due to the presence of vegetation and boulders, and this expectation is reflected in Figures 3.10b and c. From Figure 3.10, Location B and C have similar vorticity levels (b) while Location B has lower velocity magnitudes (a) – this leads to the discrepancy in TKE between Locations B and C (c), as generally higher velocities in turbulent flows will lead to more drastic velocity fluctuations and therefore higher TKE.

a. Average velocity magnitude, m/s

b. Average vorticity magnitude, 1/s
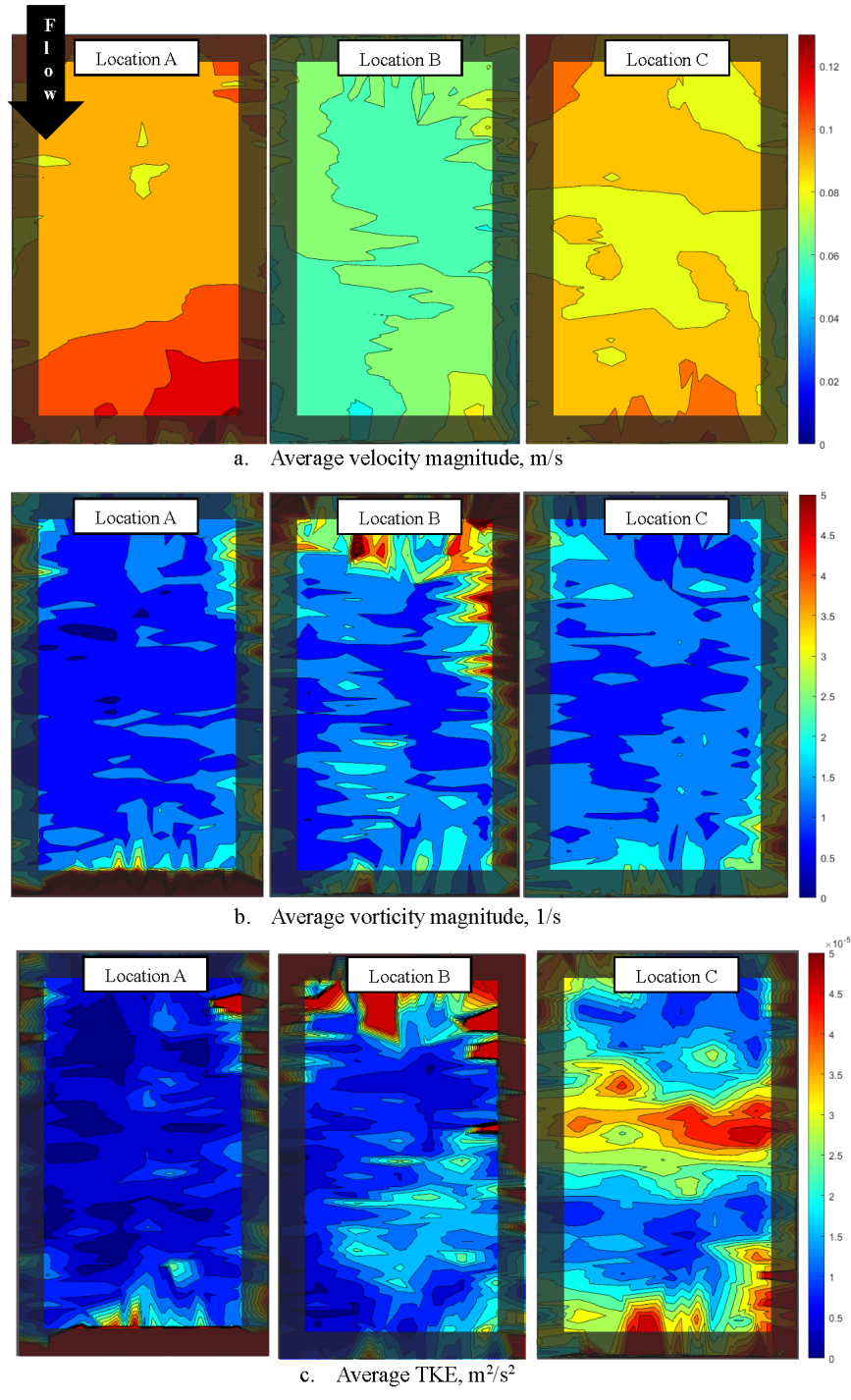
c. Average TKE, m²/s²

Figure 3.10: Field site 2 PIV data results at locations A (left), B (middle), and C (right) – a) average velocity magnitude, b) average vorticity magnitude, c) average TKE

3.6.2.1 Field Site 2 Conclusions

Bandemer Park measurements are intended to provide proof-of-concept for the novel system, exploring qualitative agreement between the data and intuitive expectations at this site. Despite proximity of the three locations, the system was able to obtain expected, detailed results in each that clearly differentiated each flow condition. These captured variances demonstrate the system's sensitivity to subtle changes in a flow, a necessary characteristic when considering differences or changes in turbulent regimes. Further, two of these three locations are vegetated environments. Such areas are of particular interest as they are a common habitat for a variety of species. Fish have been shown to respond to TKE, vorticity, and eddy size distributions within their habitat, and so being able to measure such values both increases knowledge on habitat preferences and can inform restoration efforts in degraded areas.

3.6.3 Field Site 3 – Island Park Boulder

Field Site 3 examined flow around a boulder in Island Park on the Huron River, located at 42°17'24.5"N 83°43'48"W (Figure 3.7c). Figure 3.8c shows an example of the data collected at this site following conversion to greyscale. The blue box indicates the region of analysis. Eddies were periodically shed behind the boulder, such that in some frames flow with an eddy passing through was captured and in other frames flow with no specific eddy structure is captured. Both of these flows are analyzed here – the background flow with no eddies present, and the flow with eddies present (FEP). Between these flows, velocity magnitude, vorticity, and TKE can be examined to determine the system's ability to capture their differences (Figure 3.11). This site also tests the system's ability to measure background flows when flow structures such as eddies are imposed upon them. These results are once again temporally averaged over 1 s, or 60 frames, of data.

Background flow   FEP

a. Average velocity magnitude (m/s)

b. Average vorticity magnitude (1/s)

c. Average TKE (m²/s²)

Note: boulder positioned above upper right corner with respect to images
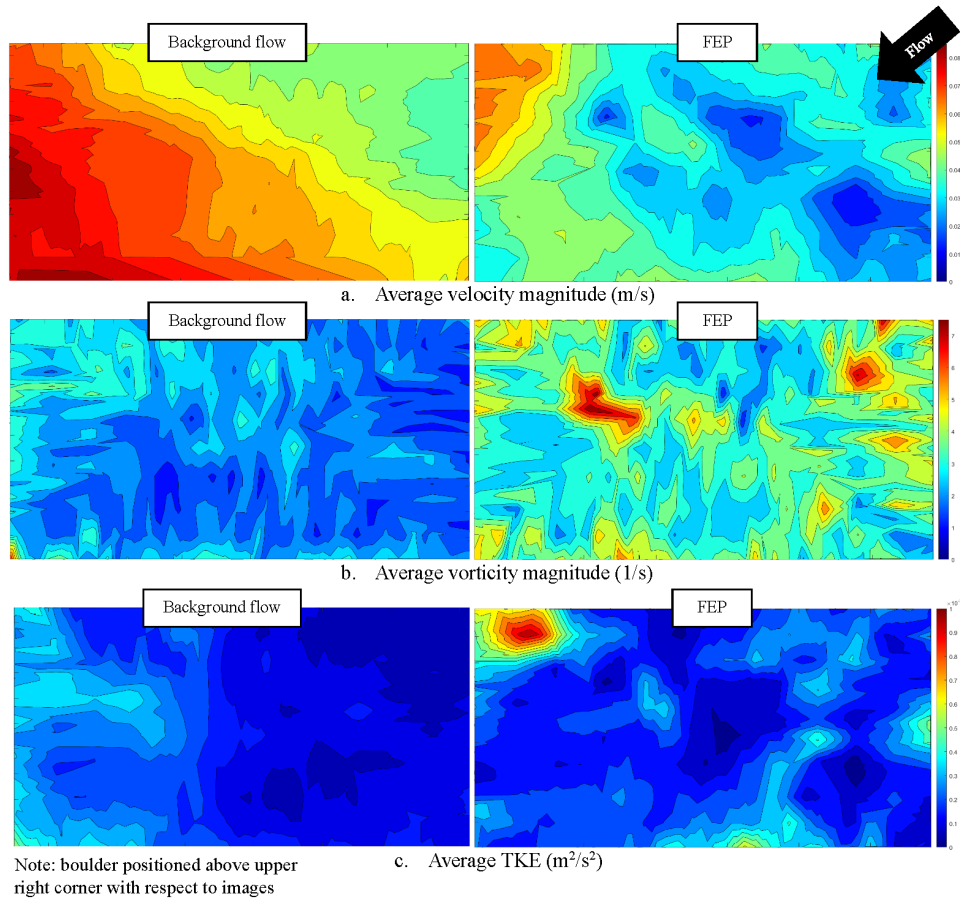
Figure 3.11: Field site 3 PIV data results for background flow (left) and FEP (right) – a) average velocity magnitude, b) average vorticity magnitude, c) average TKE

Table 3.2: Field site 3 velocity magnitude (cm/s), vorticity (1/s), and TKE (cm²/s²) ranges in FEP and background flow

	Background flow	FEP
Velocity magnitude (cm/s)	3.9 – 8.6	1.2 – 7.0
Vorticity (s⁻¹)	1.0 – 4.1	1.2 – 7.9
TKE (cm²/s²)	0.59 – 5.4	0.40 – 10.0

This site serves as additional proof-of-concept in a different environment of interest, and for this flow the following qualitative expectations are examined: 1) the background flow should have greater velocity magnitudes yet a smaller range of values, due to a lack of the high velocity differentials imparted into the flow by eddies, 2) velocity magnitudes in the background flow should be lowest directly behind the boulder, in the wake, and steadily increase away from the boulder, as the flow reattaches, 3) relatively uniform vorticity is expected in the background flow since there are no eddies creating high vorticity areas, and it should therefore reflect the general vorticity found in the river flow, 4) the minimum vorticity and TKE of FEP should be similar to overall background flow values, 5) FEP should have higher maximum vorticity values concentrated in small areas due to eddies, and therefore a larger range of vorticity values by the reasoning in expectation 4, and 6) FEP should have higher maximum TKE than background flow due to the eddies increasing turbulent velocity fluctuations in the flow, and thus a larger TKE range. Table 3.2 gives the ranges for each of these metrics for each flow type, and matches the intuitive expectations described here.

The background flow's range of velocity magnitudes is approximately 81% that of FEP, and is composed of larger values (FEP's median velocity magnitude is 4.1 cm/s, background flow's is 6.25 cm/s – see Table 3.2), aligning with expectation 1. Demonstrating expectation 2, Figure 3.11a shows the distribution of velocity magnitudes in the background flow, with the magnitude increasing away from the boulder. Further, Figure 3.11a shows how eddies perturb this flow pattern when being shed from the boulder.

Exploring turbulence characteristics at this site, and qualitatively confirming expectation 3, Figure 3.11b visually shows that vorticity in the background flow is more uniform than in FEP. Table 3.2 reflects expectation 4, as the minimum values of TKE (0.40 and 0.59 cm^2/s^2

respectively) and vorticity (1.2 s^{-1} and 1.0 s^{-1} respectively) in FEP and background flow are similar. This can additionally be visualized through Figures 3.11b and c.

Table 3.2 and Figure 3.11b agree with expectation 5, with FEP's maximum vorticity being 7.9 s^{-1} as opposed to background flow's 4.1 s^{-1}; Figure 3.11b shows FEP's maximum vorticity levels to be concentrated in areas, reflecting eddies. Further, FEP's vorticity range is approximately 216% that of the background flow, reflecting the larger variation in vorticity expected. Addressing expectation 6, FEP has a significantly larger range of TKE than the background flow (approximately 199.6%), and a significantly higher maximum TKE (10.0 versus 5.4 cm^2/s^2).

3.6.3.1 Field Site 3 Conclusions

Island Park Boulder provides an opportunity to examine how the novel system distinguishes changes of flow regime in eddy-dominated turbulent flows that periodically change in time. Since both the background flow itself and the flow with eddies imposed upon it are separately recorded, this location also demonstrates how the novel system works with complex combined flow structures. Similar to site 2, the results' overwhelming agreement with qualitative expectations explores how the system can effectively measure turbulence in this setting for these types of flows.

3.7 Conclusions

Lack of in-situ data has been a limiting factor to restoration and conservation efforts in aquatic ecosystems for decades; the PIV system detailed here is a technique that can help remedy this data gap. Building off previous designs and addressing several of their shortcomings, this system is able to effectively measure velocity and a variety of turbulence metrics in shallow environments, including a vegetated marsh, an open area of river flow, patches of coarse woody

debris, and flow surrounding a boulder. The modular design of the system means that its current limitations, such as depth or image quality, can be addressed through minor modifications of the system's design. For example, longer legs may be built for the laser box, or a higher frame rate camera or alternate analysis methods may be used in the case of streaked images from high velocities. This novel PIV therefore has the potential to be used in a wide variety of situations through small modification when necessary.

The system can reliably measure turbulence metrics including eddy dynamics such as size and circulation, vorticity, and turbulent kinetic energy. These were measured due to their significance to conservation efforts; this system can be used outside of conservation applications as well, e.g. in-situ boundary layer behaviors. 1 s of data was used to calculate mean flow characteristics to allow comparison across instruments and field sites; future users may need to either increase or decrease the averaging period depending on their specific field site and parameters of interest. By expanding upon the system's design and analysis focus, this PIV system can remain simple and accessible while continuing to be a widely versatile tool.

3.8 Acknowledgments

3.9 References

Adrian, R. J. (2005). Twenty years of particle image velocimetry. Experimental Fluids, 39(2), 159–169. https://doi.org/10.1007/s00348-005-0991-7

Baiandina, I. S., & Khanaychenko, A. N. (2018). Water turbulence effect on egg survival and characteristics of hatched larvae of the Black Sea turbot Scophthalmus maeoticus (Pallas, 1814). Marine Biological Journal, 3(4), Article 4. https://doi.org/10.21072/mbj.2018.03.4.11

Cada, G. F., & Odeh, M. (2001). Turbulence at Hydroelectric Power Plants and its Potential Effects on Fish. (DOE/BP-26531-1). Bonneville Power Administration, Portland, OR (US).

Cotel, A.J., Webb, P.W. (2015). Living in a Turbulent World—A New Conceptual Framework for the Interactions of Fish and Eddies. Integrative and Comparative Biology, 55, 662–672. https://doi.org/10.1093/icb/icv085

Cotel, A. J., Webb, P. W., & Tritico, H. (2006). Do Brown Trout Choose Locations with Reduced Turbulence? Transactions of the American Fisheries Society, 135(3), 610-619. https://doi.org/10.1577/T04-196.1

Dimotakis, P. E. (2005). Turbulent Mixing. Annual Review of Fluid Mechanics, 37, 329–356. https://doi.org/10.1146/annurev.fluid.36.050802.122015

Dower, J. F., Miller, T. J., & Leggett, W. C. (1997). The Role of Microscale Turbulence in the Feeding Ecology of Larval Fish. In J. H. S. Blaxter & A. J. Southward (Eds.), Advances in Marine Biology, 31, 169-220. https://doi.org/10.1016/S0065-2881(08)60223-0

Drucker, E. G., & Lauder, G. V. (1999). Locomotor forces on a swimming fish: Three-dimensional vortex wake dynamics quantified using digital particle image velocimetry. Journal of Experimental Biology, 202(18), 2393–2412. https://doi.org/10.1242/jeb.202.18.2393

Higham, T. E., Stewart, W. J., & Wainwright, P. C. (2015). Turbulence, Temperature, and Turbidity: The Ecomechanics of Predator–Prey Interactions in Fishes. Integrative and Comparative Biology, 55(1), 6–20. https://doi.org/ 10.1093/icb/icv052

Hilder, P. E., Cobcroft, J. M., & Battaglene, S. C. (2017). Factors affecting the feeding response of larval southern bluefin tuna, Thunnus maccoyii (Castelnau, 1872). Aquaculture Research, 48(6), 2752–2766. https://doi.org/10.1111/are.13108

Hockley, F. A., Wilson, C. A. M. E., Brew, A., & Cable, J. (2014). Fish responses to flow velocity and turbulence in relation to size, sex and parasite load. Journal of the Royal Society Interface, 11(91). https://doi.org/10.1098/rsif.2013.0814

Jin, T. (2019). Underwater Particle Image Velocimetry (PIV) Measurement of Turbulence Over Mussel Bed in a Deepsite of Lake Michigan [Thesis]. https://dc.uwm.edu/etd/2313/

Katija, K., & Dabiri, J. O. (2008). In situ field measurements of aquatic animal-fluid interactions using a Self-Contained Underwater Velocimetry Apparatus (SCUVA). Limnology and Oceanography Methods, 6(4), 162–171. https://doi.org/10.4319/lom.2008.6.162

Li, M., Shi, X., Jin, Z., Ke, S., Lin, C., An, R., Li, J., & Katopodis, C. (2021). Behaviour and ability of a cyprinid (Schizopygopsis younghusbandi) to cope with accelerating flows when migrating downstream. River Research and Applications, 37(8), 1168–1179. https://doi.org/10.1002/rra.3686

Liao, J. C. (2007). A review of fish swimming mechanics and behaviour in altered flows. Philosophical Transactions of the Royal Society B, 362(1487), 1973–1993. https://doi.org/10.1098/rstb.2007.2082

Liao, J. C., Beal, D. N., Lauder, G. V., & Triantafyllou, M. S. (2003). Fish Exploiting Vortices Decrease Muscle Activity. Science, 302(5650), 1566–1569. https://doi.org/10.1126/science.1088295

Lupandin, A. I. (2005). Effect of Flow Turbulence on Swimming Speed of Fish. Biological Bulletin, 32(5), 461–466. https://doi.org/10.1007/s10525-005-0125-z

Marrase, C., Costello, J. H., Granata, T., & Strickler, J. R. (1990). Grazing in a Turbulent Environment: Energy Dissipation, Encounter Rates, and Efficacy of Feeding Currents in Centropages Hamatus. Proceedings of the National Academy of Sciences of the United States of America, 87(5), 1653–1657. https://doi.org/10.1073/pnas.87.5.1653

Megrey, B. A., & Hinckley, S. (2001). Effect of turbulence on feeding of larval fishes: A sensitivity analysis using an individual-based model. ICES Journal of Marine Science, 58(5), 1015–1029. https://doi.org/10.1006/jmsc.2001.1104

Morgan, J. K. (2013). Flow Characterization in a Vegetated Marsh Environment [Thesis]. https://deepblue.lib.umich.edu/handle/2027.42/99882

Navarro, A., Boys, C. A., Robinson, W., Baumgartner, L. J., Miller, B., Deng, Z. D., & Finlayson, C. M. (2019). Tolerable ranges of fluid shear for early life-stage fishes: Implications for safe fish passage at hydropower and irrigation infrastructure. Marine and Freshwater Research, 70(11), 1503–1512. https://doi.org/10.1071/MF18131

Neitzel, D. A., Dauble, D. D., Cada, G. F., Richmond, M. C., Guensch, G. R., Mueller, R. P., Abernethy, C. S., & Amidan, B. (2004). Survival Estimates for Juvenile Fish Subjected to a Laboratory-Generated Shear Environment. Transactions of the American Fisheries Society, 133(2), 447–454. https://doi.org/10.1577/02-021

Nikora, V. I., Aberle, J., Biggs, B. J. F., Jowett, I. G., & Sykes, J. R. E. (2003). Effects of fish size, time-to-fatigue and turbulence on swimming performance: A case study of Galaxias maculatus. Journal of Fish Biology, 63(6), 1365–1382. https://doi.org/10.1111/j.1095-8649.2003.00241.x

Odeh, M., Noreika, J. F., & Haro, A. (2002). Evaluation of the Effects of Turbulence on the Behavior of Migratory Fish, Final Report 2002. (DOE/BP-00000022-1). Bonneville Power Administration (BPA), Portland, OR (United States).

Palmer, M. A. (1988). Epibenthic Predators and Marine Meiofauna: Separating Predation, Disturbance, and Hydrodynamic Effects. Ecology, 69(4), 1251–1259. https://doi.org/10.2307/1941280

Parkos, J. J., Ruetz, C. R., & Trexler, J. C. (2011). Disturbance regime and limits on benefits of refuge use for fishes in a fluctuating hydroscape. Oikos, 120(10), 1519–1530. https://doi.org/10.1111/j.1600-0706.2011.19178.x

Pekcan-Hekim, Z., Hellén, N., Härkönen, L., Nilsson, P. A., Nurminen, L., & Horppila, J. (2016). Bridge under troubled water: Turbulence and niche partitioning in fish foraging. Ecology and Evolution, 6(24), 8919–8930. https://doi.org/10.1002/ece3.2593

Prada, A. F., George, A. E., Stahlschmidt, B. H., Chapman, D. C., & Tinoco, R. O. (2018). Survival and drifting patterns of grass carp eggs and larvae in response to interactions with flow and sediment in a grass carp eggs and larvae in response to interactions with flow and sediment in a laboratory. PLoS ONE, 13(12). https://doi.org/10.1371/journal.pone.0208326

Prada, A. F., George, A. E., Stahlschmidt, B. H., Jackson, P. R., Chapman, D. C., & Tinoco, R. O. (2019). Influence of turbulence and in-stream structures on the transport and survival of grass carp eggs and larvae at various developmental stages. Aquatic Sciences, 82(1), 16. https://doi.org/10.1007/s00027-019-0689-1

Raffel, M., Willert, C. E., Scarano, F., Kähler, C. J., Wereley, S. T., & Kompenhans, J. (2018). Particle Image Velocimetry: A Practical Guide. Springer. https://doi.org/10.1007/978-3-319-68852-7

Rehmann, C. R., Stoeckel, J. A., & Schneider, D. W. (2003). Effect of turbulence on the mortality of zebra mussel veligers. Canadian Journal of Zoology, 81(6), 1063–1069. https://doi.org/10.1139/z03-090

Rothschild, B. J., & Osborn, T. R. (1988). Small-scale turbulence and plankton contact rates. Journal of Plankton Research, 10(3), 465–474. https://doi.org/10.1093/plankt/10.3.465

Silva, A. T., Katopodis, C., Santos, J. M., Ferreira, M. T., & Pinheiro, A. N. (2012). Cyprinid swimming behaviour in response to turbulent flow. Ecological Engineering, 44, 314–328. https://doi.org/10.1016/j.ecoleng.2012.04.015

Thielicke, W., & Stamhuis, E. J. (2014). PIVlab – Towards User-friendly, Affordable and Accurate Digital Particle Image Velocimetry in MATLAB. Journal of Open Research Software, 2. https://doi.org/10.5334/jors.bl

Trinci, G., Harvey, G. L., Henshaw, A. J., Bertoldi, W., & Hölker, F. (2020). Turbulence, instream wood and fish: Ecohydraulic interactions under field conditions. Ecohydrology, 13(5). https://doi.org/10.1002/eco.2211

Tritico, H. M. (2009). The Effects of Turbulence on Habitat Selection and Swimming Kinematics of Fishes [Thesis]. http://deepblue.lib.umich.edu/handle/2027.42/62393

Tritico, H. M., & Cotel, A. J. (2010). The effects of turbulent eddies on the stability and critical swimming speed of creek chub (Semotilus atromaculatus). Journal of Experimental Biology, 213(13), 2284–2293. https://doi.org/10.1242/jeb.041806

Tritico, H. M., Cotel, A. J., & Clarke, J. N. (2007). Development, testing and demonstration of a portable submersible miniature particle imaging velocimetry device. Measurement Science and Technology, 18. https://doi.org/10.1088/0957-0233/18/8/031

Wang, H., & Chanson, H. (2018). On upstream fish passage in standard box culverts: Interactions between fish and turbulence. Journal of Ecohydraulics, 3(1), 18–29. https://doi.org/10.1080/24705357.2018.1440183

Webb, P. W., & Cotel, A. J. (2010). Turbulence: Does Vorticity Affect the Structure and Shape of Body and Fin Propulsors? Integrative and Comparative Biology, 50(6), 1155–1166. https://doi.org/10.1093/icb/icq020

Wu, J. Z., Ma, H. Y., & Zhou, M. D. (2015). Fundamentals of Fluid Dynamics. In J. Z. Wu, H. Y. Ma, & M. D. Zhou (Eds.), Vortical Flows. 1–38. Springer.

Zha, W., Huang, M., & Zeng, Y. (2019). Swimming behavior of crucian carp in an open channel with sudden expansion. River Research and Applications, 35(9), 1499–1510. https://doi.org/ 10.1002/rra.3500

Chapter 4 The Hydrodynamics of Low-Slope Denil Fishways

4.1 Introduction

A commonly used fishway design is the Denil fishway, a sloped concrete channel with evenly spaced baffles along the sides and bottom, a diagram of which is shown in Figure 4.1 (Kamula & Bärthel, 2000). Despite being widely implemented, this is one of the least efficient fishway types (Noonan et al., 2012). Typically built at 10-25% grades, recent design suggestions recommend a slope of 10% or less to improve passage success (Mallen-Cooper & Stuart, 2007). As passage rates depend on the detailed hydraulics fishes encounter within the fishway (Fouché & Heath, 2013; Jones & Cotel, 2023; Tritico et al., 2009; Tritico & Cotel, 2010), the goal with these updated recommendations is to alter the hydrodynamics to be more amenable to passage.
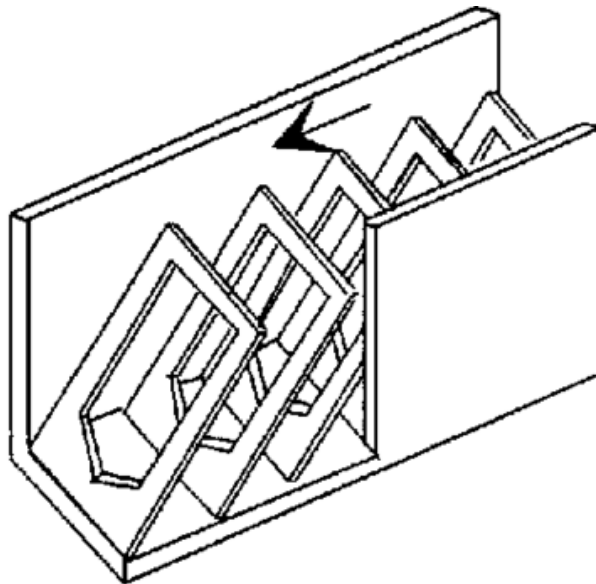
Figure 4.1: Diagram of Denil fishway (Kamula & Bärthel, 2000)

The fluid dynamics of Denil fishways have been coarsely examined experimentally (Rajaratnam et al., 1997; Rajaratnam & Katopodis, 1984) and modelled computationally (Mahmoudian et al., 2019). Previous experimental efforts do not offer insight into detailed hydrodynamics, only large-scale flow directions in different regions of the baffle sections. Additionally, previous computational models have fallen short of accurately reflecting flow conditions, as their results do not align with observation (Duguay et al., 2017). Specifically, numerical models show two flow regions within Denil fishways—a top region of high-speed through flow, and a rolling, low-speed flow structure below that. So far, this lower rolling flow pattern has not been observed in laboratory settings or in full-scale Denil fishways. Therefore, it is essential to experimentally measure the detailed hydrodynamics using reliable laboratory methods to gain an understanding of the flow conditions present under the updated slope recommendations. To achieve this, this experimental study quantified the hydraulics of Denil fishways using Particle Image Velocimetry (PIV) at 0%, 5%, and 10% grades.

4.2 Methods

4.2.1 Laboratory Methods

A scaled-down physical model of a Denil fishway, designed based on federal guidelines (U.S. Department of Agriculture, 2007), was constructed, consisting of three baffles placed 45° to the model bottom which created two flow windows. The model was able to be adjusted to 0%, 5%, and 10% grades. Figure 4.2 offers a diagram of a side view of the model, and the details and dimensions of the baffles. This model was placed in a water tunnel to measure flow patterns at several flowrates. Flow patterns were recorded in Windows 1 and 2 (illustrated in Figure 4.3) at flowrates of approximately 0.032 ± 0.001 m³/s, 0.037 ± 0.001 m³/s, and 0.043 ± 0.001 m³/s.
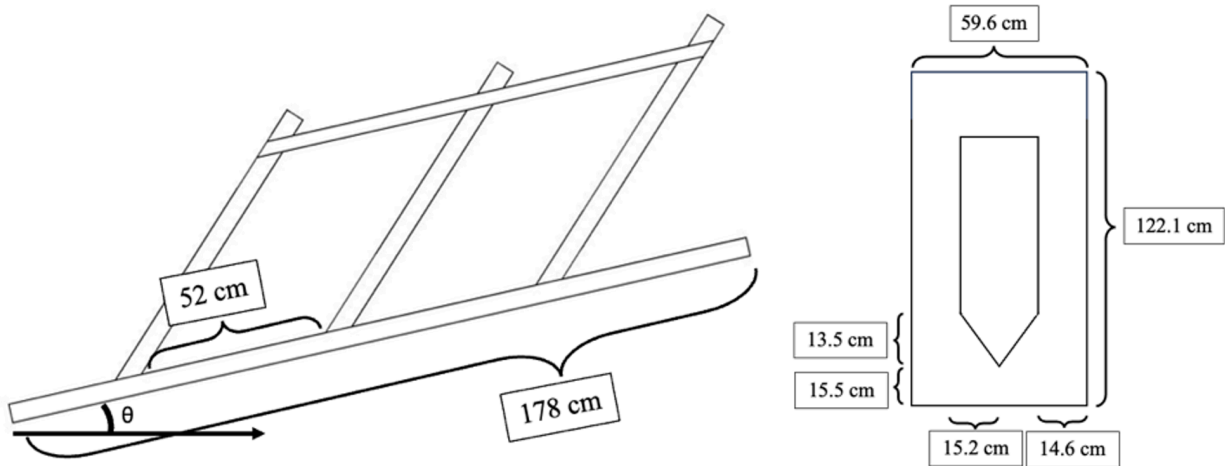
Figure 4.2: Side view of Denil fishway model (left) and front view of baffles (right)
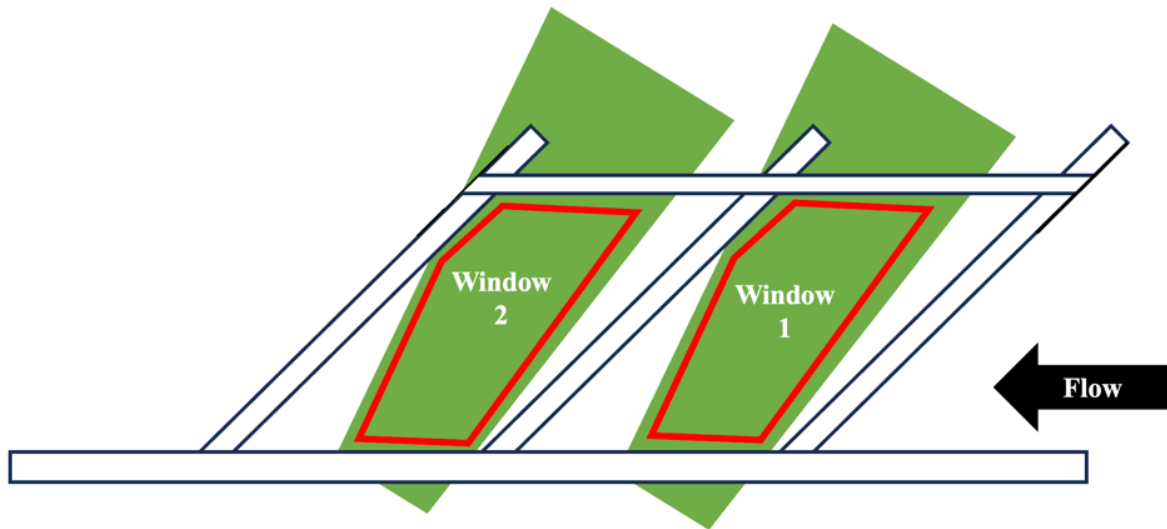
Figure 4.3: Data viewing windows

These flowrates are similar to those examined in previous experimental efforts (Rajaratnam &

Katopodis, 1984).

Based on conservation of mass, the different settings correspond to approximate cross-

sectionally averaged velocities through the baffles of 25.2 ± 1.0 cm/s, 29.4 ± 1.0 cm/s, and 33.8

± 1.0 cm/s, and Reynolds numbers (Re) based on baffle width of approximately 76,000, 89,000,

and 103,000. For real-world Denil fishways, goal Re depends on the target species; for adult

chinook salmon (*Oncorhynchus tshawytscha*) for example, a typical Denil design would aim for

Re of less than approximately 1,000,000, but for young striped bass (*Morone saxatilis*) in the

same design, a target Re would be less than approximately 43,000 (U.S. Department of

Agriculture, 2007). The large variability in real-world Denil fishway Re values makes exact

Reynolds similarity between the model and full-scale structures difficult; however, through

maintaining Re in the turbulent range, this study captures the expected turbulence structure.

Additionally, since this study's focus is on hydrodynamic impacts of varying slopes, the limited

range of flowrates is used to ensure that the turbulent patterns discovered are not strictly unique

to one flow condition.

Measurements were taken using PIV, an optical flow measurement technique that utilizes

a laser sheet, seeding particles, and a camera to illuminate and track flow within a two-

dimensional plane (Raffel et al., 2018). A sample PIV diagram is shown in Figure 3.1; for more

details on the method, see *Chapter 3*. The flow was seeded using 10 μm-diameter hollow glass

spheres, and was illuminated using a continuous, 1 W, 532 nm wavelength laser shown through a

1.27 cm focal length cylindrical lens to split the laser beam into a sheet. PIV data was imaged

using a Nikon D5200 DSLR camera recording video data at 60 fps.

4.2.2 Analysis Methods

Data analysis was performed using PIVlab (Thielicke & Stamhuis, 2014), an open source MATLAB-based PIV software. Video frames were used as image pairs in the cross-correlation analysis to determine particle displacement.

Temporally averaged flow data was sought to gain a general understanding of flow conditions within these fishways. Average velocity convergence testing was performed on 13 randomly selected data points at different flowrates, slope settings, and viewing windows in order to determine the averaging period that offers representative mean flow patterns. Figure 4.4 shows the results of this convergence test. For all test data points, at averaging periods greater than two seconds, the mean velocity stayed within 20% of the two-second mean, and it was therefore determined that a two-second average value reflects overall typical conditions.

4.3 Results

Figure 4.5 illustrates the flows observed within the Denil fishway model, which generally
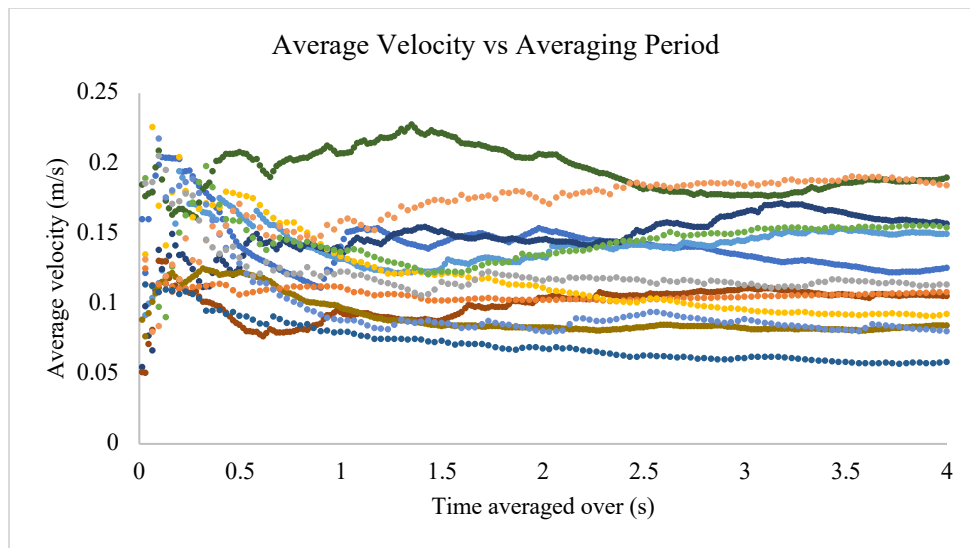
Figure 4.4: Velocity convergence test results. Each color represents a different data point examined.

consisted of three regions—an upper area of downstream-directed through flow, below which an elongated region of low velocity exists perpendicular to the baffle, where eddies are periodically shed. At the bottom of the baffle section, a third domain of upward- and/or upstream-directed flow was consistently observed. The exact details of each changed with slope of the model but the trend remained the same. More details are given below.

4.3.1 0% Grade

Figure 4.6 shows average velocity magnitudes (m/s) measured at a 0% slope. This grade was examined to determine the baseline hydrodynamics imparted by only the fishway geometry, when gravitational effects do not increase as flow proceeds, and to determine flow conditions at very low slopes. Across speeds and upstream/downstream placement, there is faster flow through the top of the baffle section and reduced speeds lower in the sections. Specifically, under the high-speed flow, velocities taper to a small low-speed region perpendicular to the baffle that extends transversely across the field of view. Below this low-speed region, an area of intermediate velocity is observed at the bottom of the section.

To predict fish behavioral responses to these flow conditions, more than velocity must be considered. Fish respond to vorticity dynamics within flow (Cotel & Webb, 2015; Jones & Cotel, 2023; Liao, 2007; Liao et al., 2003; Tritico et al., 2009), and thus it is useful to also study this quantity under the updated guidelines. Note that vorticity has an orientation (positive or negative) that indicates eddy rotational direction (clockwise or counterclockwise). A strong positive and a strong negative value therefore speak to high vorticity magnitudes induced by eddies with rotational directions opposite to one another. As the temporal averages presented in this chapter have been taken across all vorticity values recorded during the averaging period, which may be both positive and negative, the mean values do not solely speak to the magnitudes

0% grade   5% grade   10% grade
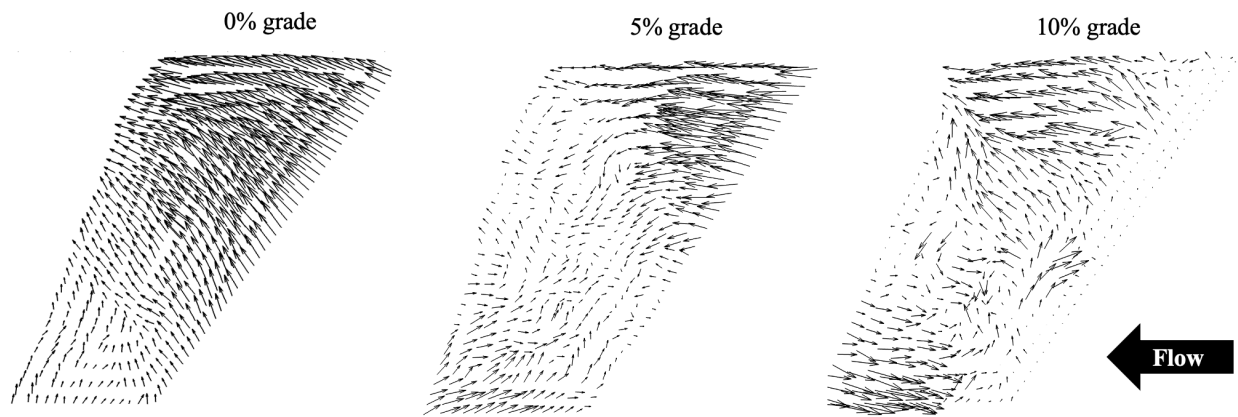
Flow

Figure 4.5: Average flow direction for all cases in Window 2 at 0.037 m³/s

Window 2   Window 1

0.032 m³/s

0.037 m³/s

0.043 m³/s

Side view

Scale

20 cm

Flow
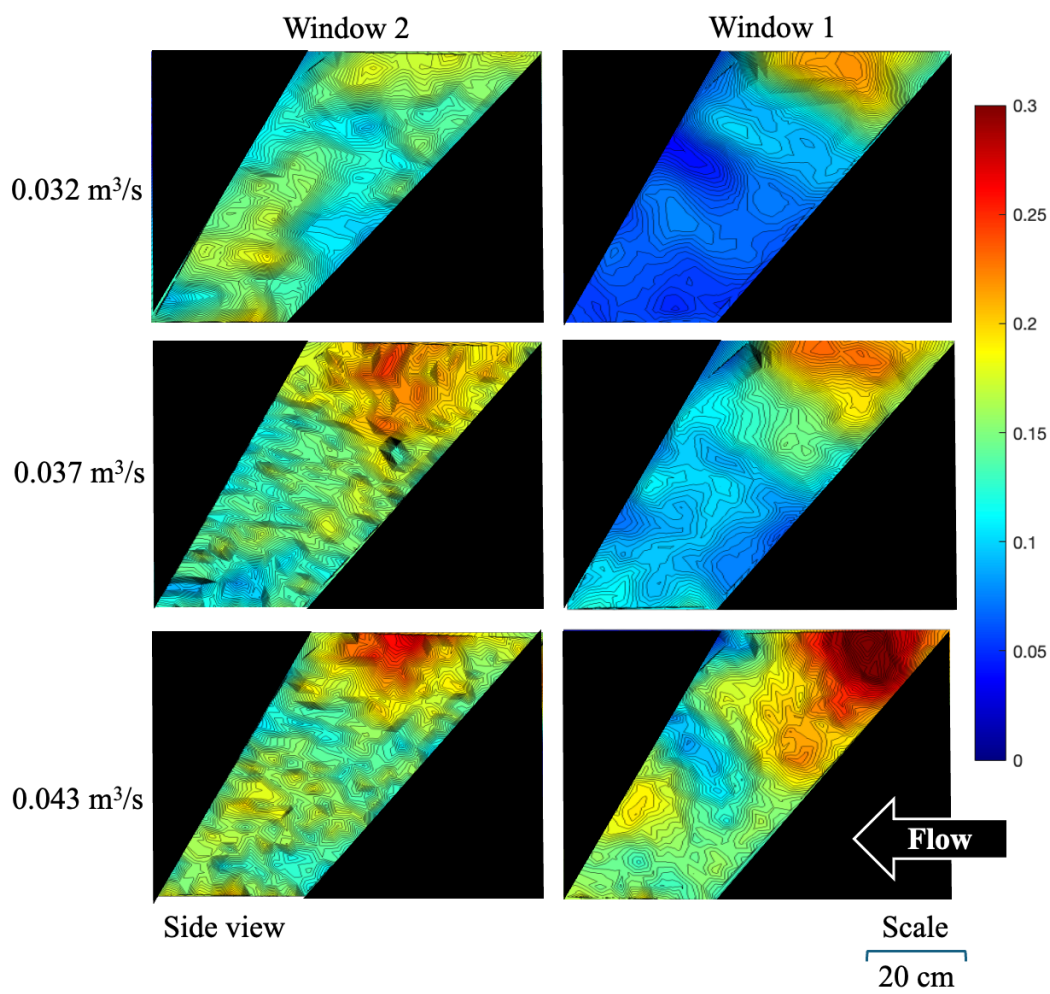
Figure 4.6: Average velocity magnitudes (m/s) at 0% grade. Side views.

experienced. For example, if at two points in time a region has two separate eddies of strong positive vorticity, the average value from those two eddies will be a strong positive value. However, if a region has an eddy of strong positive vorticity at one point in time, and an eddy with strong negative vorticity at another, the average value from those eddies will be close to zero. Therefore, the averages here can be used to also interpret vortical consistency. Note that in regions with consistent vorticity, the average values reflect the typical magnitudes present as well.

Figure 4.7 shows average vorticity (s^{-1}) within the flow and reveals more about the eddy structure within the fishway. Contrary to previous computational models, there are no large eddies observed in the lower portion of the flow in either window. Further, there are significant differences in upstream versus downstream vorticity. Generally, the upstream Window 1 has regions of high vorticity magnitude perpendicular to the baffle, corresponding to the low velocity magnitude planes observed in Figure 4.6. These regions indicate consistently oriented, strong eddies being shed from the baffles, directly above the triangular gap as shown in Figure 4.8. In downstream Window 2, as turbulence has further developed, these regions of strong positive and negative vorticity are no longer present; rather, isotropic turbulence is observed with eddy diameters ranging from approximately 2-17 cm depending on flowrate.

4.3.2 5% Grade

Figure 4.9 shows average velocity magnitudes (m/s) measured at a 5% slope. The same regions of reduced velocity perpendicular to the baffle seen in the 0% grade case are also observed at this slope, although the flows above and below exhibit more complexity due to the increased gravitational effects introduced by a sloped channel. A significant difference between these flow patterns and that of the baseline flows observed at 0% grade is the location of regions
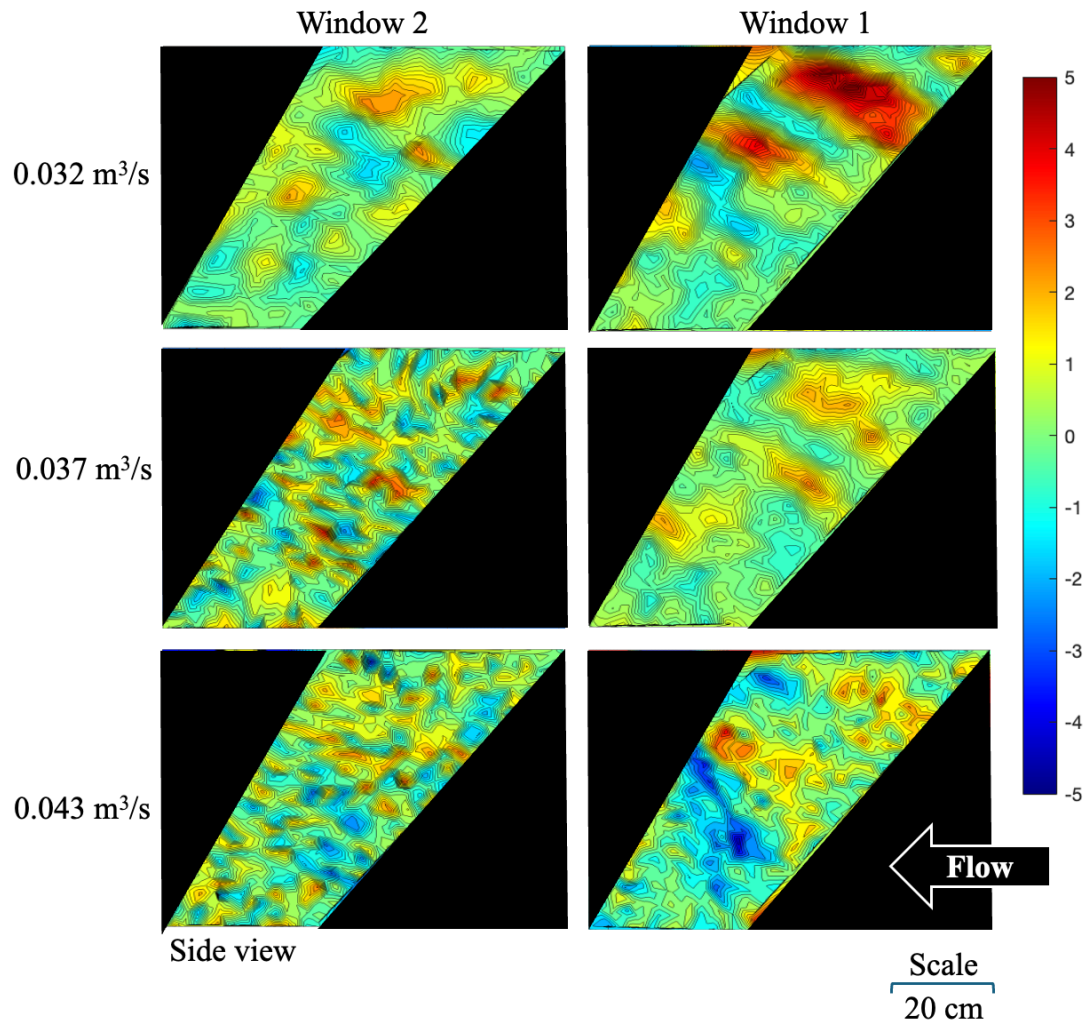
Figure 4.7: Average vorticity (s^{-1}) at 0% grade. Side views.
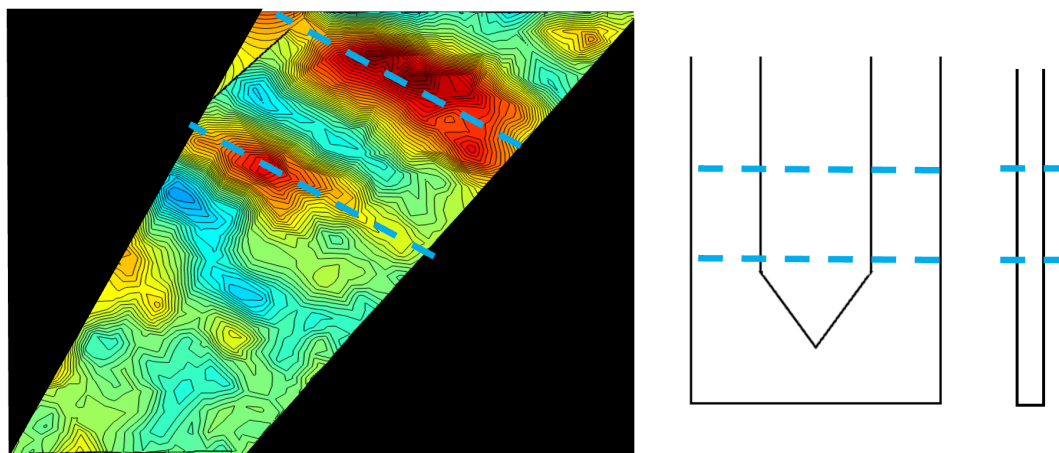
Figure 4.8: Placement along baffle of high vorticity regions at 0% grade. Placement in vorticity map (left), placement along front of baffle (middle), placement along side of baffle (right). These regions are induced by eddies shedding past the baffle openings.

of high velocity—when considering only the geometry of the fishway as the 0% grade case does, regions of highest velocity are strictly at the top of the fishway. This changes once the fishway is sloped—at a 5% grade, some cases' highest velocity region is at the top of the window (e.g. Window 2 at 0.037 m^3/s), others have high velocity regions at both the top and bottom of the window (e.g. Window 2 at 0.032 m^3/s), and yet others' highest velocity region is at the bottom of the window (e.g. Window 1 at 0.037 m^3/s). Thus, once fishways are sloped, the regions of high and low speeds change location, with the change being variable across baffle section and flowrate.

Figure 4.10 shows average vorticity (s^{-1}) measured at a 5% slope. The average vorticity magnitudes are lower in this case, due to less consistency in eddy orientation at this design grade. However, some patterns are still present. The region of heightened vorticity perpendicular to the baffle angle remains. As flowrate increases, this region disperses and expands farther along the baffle. Additionally, in the downstream Window 2, there is another region of consistent vorticity near the baffle opening where the flow exits the window.

4.3.3 10% Grade

Figure 4.11 shows the average velocity magnitudes (m/s) for a 10% slope. In Window 1, there are two distinct regions of reduced velocity—one perpendicular to the baffle angle as seen in the previous cases, and one horizontal just below the baffle opening (see Figure 4.12), near the bottom of the viewing window. Additionally, a pocket of high-speed flow exists near where the flow exits the baffle section, which expands in size with increasing flowrate. Downstream in Window 2 as the flow develops, the reduced velocity plane perpendicular to the baffles is still observed; however, the velocity magnitude of the flow around it is more uniform, retaining a high speed. Further, the horizontal low-speed pocket in Window 1 is not present in Window 2.
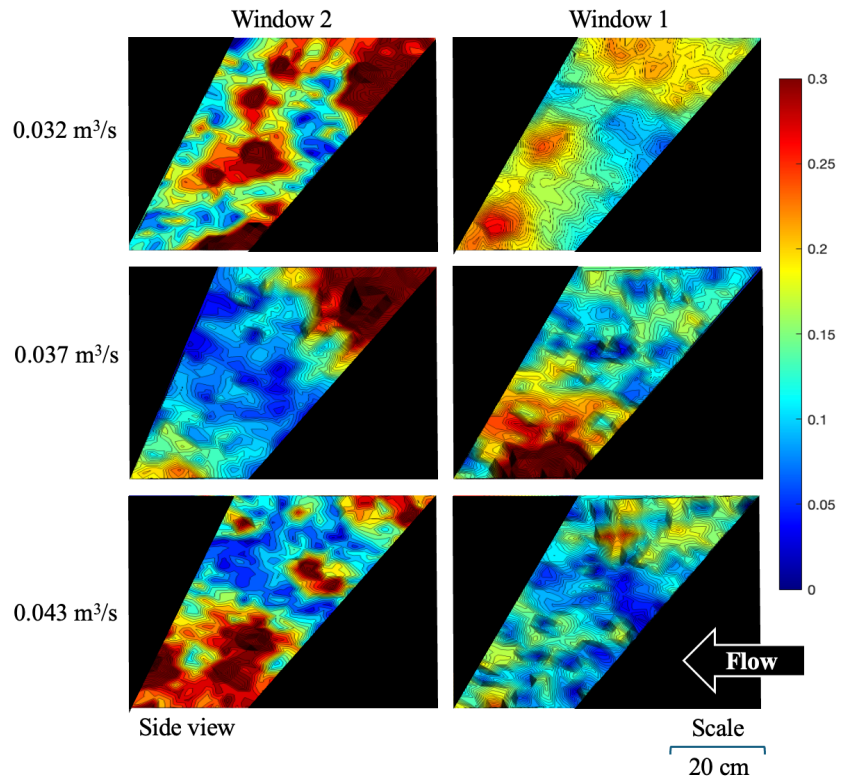
Figure 4.9: Average velocity magnitudes (m/s) at 5% grade. Side views.
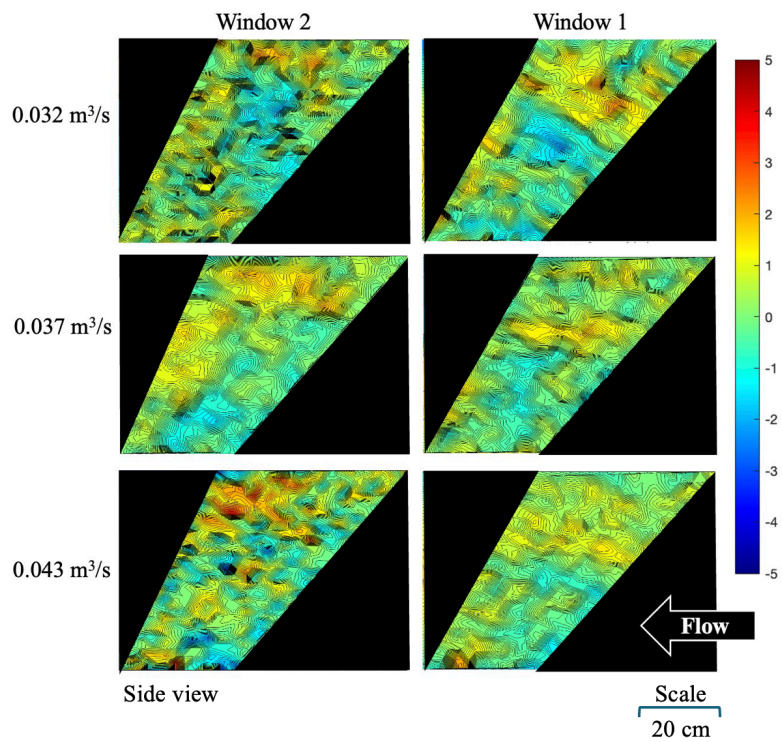
Figure 4.10: Average vorticity (s^{-1}) at 5% grade. Side views.
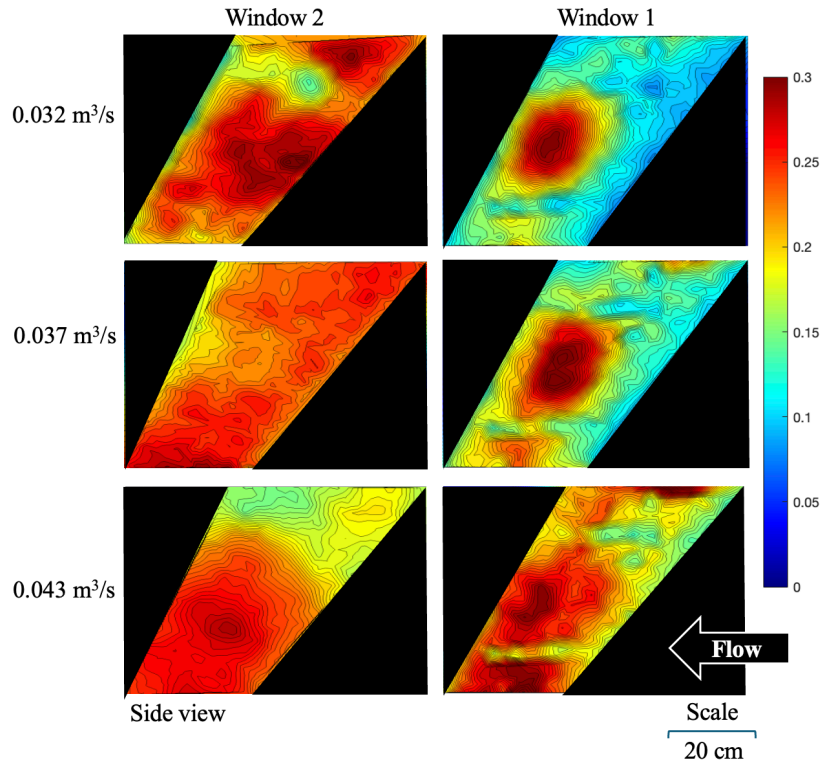
Figure 4.11: Average velocity magnitudes (m/s) at 10% grade. Side views.
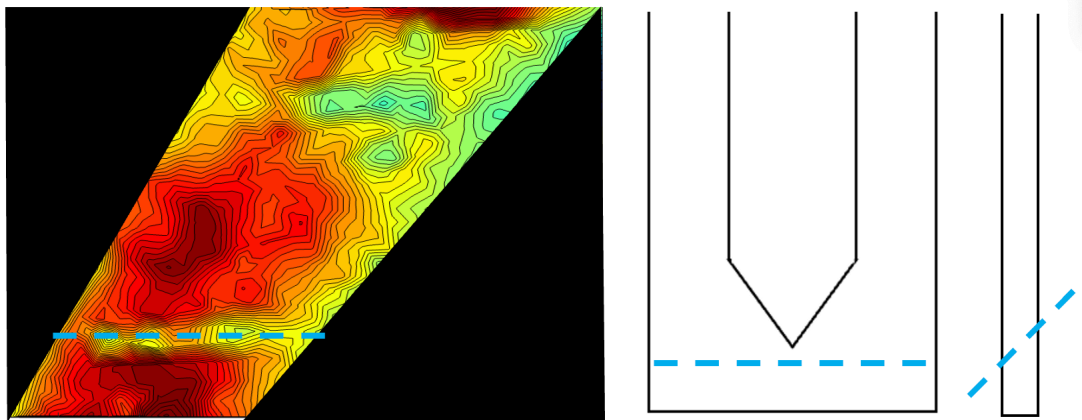
Figure 4.12: Placement along baffle of horizontal low-speed region at 10% grade. Placement in velocity magnitude map (left), placement along baffle front (middle), and placement along baffle side (right). This region appears to be created by flow separation at the bottom of the baffle opening; more work is needed to determine the definitive cause.
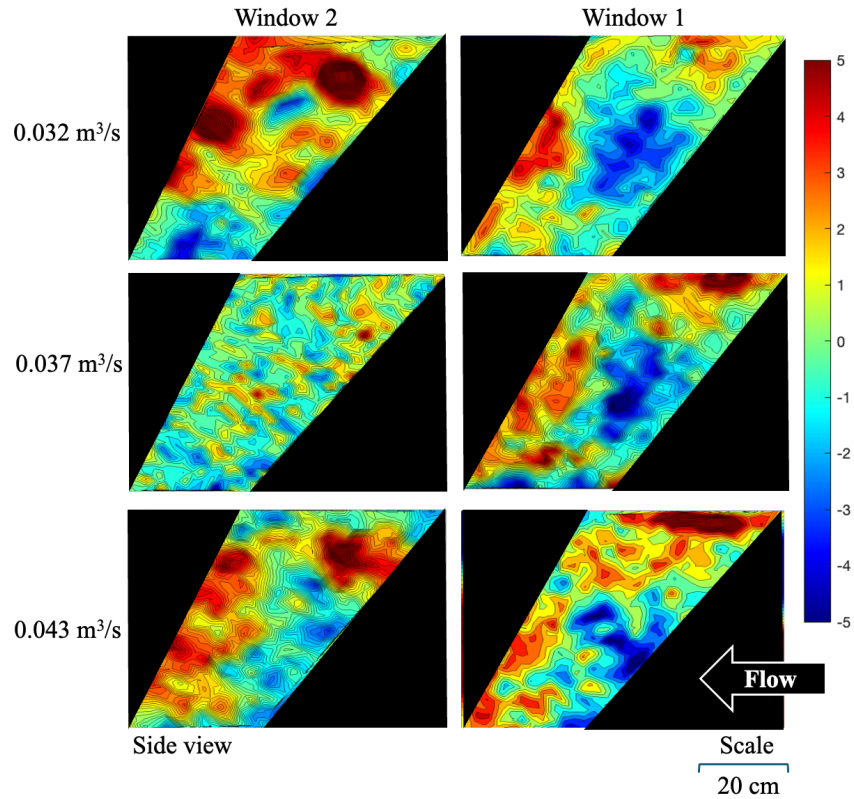
Figure 4.13: Average vorticity (s^{-1}) at 10% grade. Side views.

Thus, as the flow develops in the fishway at this slope, areas of low speed disappear and regions of high speed disperse, resulting in velocity magnitudes increasing overall and becoming more uniform throughout.

Figure 4.13 shows the average vorticity (s^{-1}) for a 10% slope. In Window 1, regions of high average vorticity magnitude exist near both baffle openings (a region of strong negative vorticity where the flow enters the baffle section, and a region of strong positive vorticity where the flow exits the baffle section). In downstream Window 2, the region of strong positive vorticity where the flow exits the baffle section is also present, in addition to the region of consistent, strong vorticity perpendicular to the baffle observed in all previous cases. These patterns align with the consistent eddy regions seen at a 5% slope, but with higher magnitude.

The presence of these patterns at 5% and 10% slopes, but not in the flat 0% case, indicates that these regions are caused by gravitational effects on the flow imparted by a sloped channel.

4.4 Conclusions

The distinct turbulent patterns measured across flowrates, slopes, and upstream/downstream placement within the Denil fishway model offer insight into what flow elements contribute to the low passage success of these structures. The 0% grade case is used to understand the baseline turbulence in the fishways, induced only by their geometry. Figure 4.7 shows an elongated region of heightened vorticity perpendicular to the baffle that extends across the flow window, directly in the path fishes must take to continue upstream. Since strong vorticity is an obstacle to fish swimming capability (Cotel & Webb, 2015; Liao, 2007; Tritico et al., 2009; Tritico & Cotel, 2010), the location of this region hinders passage. Further, at a 0% slope, this structure is most notable in upstream Window 1—once turbulence has developed further as in Window 2, the flow more resembles an isotropic pattern. The fact that this change occurs after the flow has only proceeded approximately 1 m, in the second baffle section, shows that turbulence develops very rapidly within these structures. Considering the real-world designs of tens or more baffle sections that fishes must swim through, most of the journey is highly turbulent and therefore difficult and stressful. Once the additional flow patterns discussed above in *4.3.2 5% Grade* and *4.3.3 10% Grade* that stem from sloping the channel are imposed on top of this isotropic pattern, the flow becomes even less navigable.

Velocity magnitude maps across the cases reveal significant hydrodynamic changes once gravitational effects have greater influence. While a region of low flow perpendicular to the baffle is always observed, the surrounding flow patterns are different—in the 0% case, the fastest flow is at the top of the flow window, with a low-speed region below that, and an area of

intermediate velocity near the bottom. In the 5% case, across the different flowrates and baffle sections, high speed flow is observed both above and below the low-speed region. At the steepest 10% case, the highest speed is consistently below the low-speed region. Thus, as slope of the design increases, the bottom region of low-speed flow that is seen in the flat case and in previous computational models decreases or diminishes altogether. These regions are essential to successful fish passage, as they act as refuges for fishes navigating the fishway. Without such areas, fishes experience greater stress, and in the sloped cases examined here, these regions do not reliably exist. This lack of low-speed refuges is one hydraulic obstacle to fishes within these designs.

The average vorticity maps for the 5% and 10% cases exhibit more complexity than the flat 0% case. For all cases, a region of heightened average vorticity perpendicular to the baffle exists; at 5% and 10% slopes, regions of consistent vorticity aligned with the baffle openings are additionally present. Therefore, as slope increases and gravitational effects on the flow become more significant, more regions of heightened vorticity develop in the fish pathway, escalating passage difficulty. These patches of consistent, high-magnitude vorticity are another hydrodynamic hurdle fishes must overcome during passage across Denil fishways.

There are also notable differences between the flat and sloped cases when examining vorticity development in upstream versus downstream sections of the fishway. For the flat 0% case, the downstream Window 2 loses the structure observed in the upstream Window 1, i.e. becoming isotropic. For the sloped cases, more of the structure from Window 1 is preserved in Window 2. Thus, when slopes are increased, regions of vorticity that make passing difficult spread throughout more baffle sections; fishes must encounter and swim through them multiple times, increasing stress and difficulty of the journey. Further, many of these regions are on the
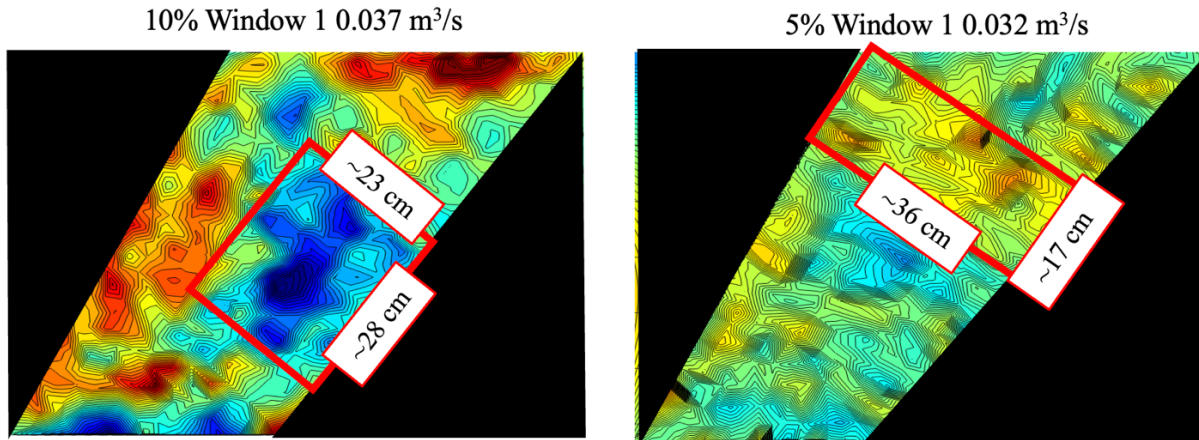
Figure 4.14: Approximate size of two example regions of consistent vorticity

same order of magnitude of size as a passing fish (e.g. Figure 4.14). As eddies similar in size to fishes particularly impair swimming ability and increase energy expenditure (Cotel & Webb, 2015; Jones et al., 2022), high vorticity regions in this size range exceptionally impede passing fishes. This exacerbates the negative effects patches of heightened vorticity already have.

Generally, as slope increases, flow characteristics that inhibit swimming compound in the flow. This study found two specific phenomena that may significantly hinder passage: low-velocity refuges are lost, and regions of increased vorticity that have high potential to destabilize and fatigue fishes develop directly in the swimming path. The updated recommendations should therefore improve passage rates, as requiring milder design grades would dampen the effects that intensify with increasing slope. Based on the results found in this study, there are two more management and design recommendations that would improve passage efficiency. First, managing flowrate if possible is important, as the loss of low-speed regions means fishes have no respite from high flows within this fishway design. As fishes must continually navigate in high-speed conditions, lessening flowrate and thus velocity would reduce necessary energy expenditure and decrease chance of fatigue. Additionally, adjusting baffle design (e.g. altering

geometry in a way that induces smaller or weaker eddies to shed into the baffle section, such as including small vortex generators along the edges) to dissipate areas of high vorticity directly along the baffle openings would reduce the number of high-vorticity regions fishes must traverse. Adjusting these regions to contain smaller or weaker eddies would improve performance, as such eddies would carry less momentum and not disrupt swimming mechanics as significantly.

4.5 Future Work

This study is limited in the placement and number of fields of view of the flow. Certainly three-dimensional hydraulic structures exist within these fishways that are not reflected when examining only the transverse center of the baffle sections as done here. Measuring more planes of flow both parallel and perpendicular to the main flow direction would expand understanding of the fluid dynamics influencing Denil fishway success. Additionally, only two baffle sections were examined in this study due to size limitation of the facility—data farther downstream may be needed to fully understand how turbulence develops as flow proceeds through this infrastructure. Measuring the hydrodynamics of additional downstream baffle sections would further advance knowledge of how slope impacts the hydraulic conditions in real-world Denil fishways. Finally, developing a holistic design framework with more explicit connections between the flow patterns characterized here and fish response to these flows (see Cotel & Webb, 2015) would be useful in informing Denil fishway design to improve passage success moving forward.

4.6 Acknowledgments

4.7 References

Cotel, A. J., & Webb, P. W. (2015). Living in a Turbulent World—A New Conceptual Framework for the Interactions of Fish and Eddies. Integrative and Comparative Biology, 55(4), 662–672. https://doi.org/10.1093/icb/icv085

Duguay, J. M., Lacey, R. W. J., & Gaucher, J. (2017). A case study of a pool and weir fishway modeled with OpenFOAM and FLOW-3D. Ecological Engineering, 103. https://doi.org/10.1016/j.ecoleng.2017.01.042

Fouché, P., & Heath, R. (2013). Functionality evaluation of the Xikundu fishway, Luvuvhu River, South Africa. African Journal of Aquatic Science, 38(sup1), 69–84. https://doi.org/10.2989/16085914.2013.773418

Jones, K., & Cotel, A. J. (2023). A hydrodynamics-based framework to evaluate the impact of fishways on drifting lake sturgeon larvae. Journal of Great Lakes Research, 49(1), 332–338. https://doi.org/10.1016/j.jglr.2022.11.006

Jones, K., Cotel, A. J., & Webb, P. W. (2022). Stability and turbulence. In Reference Module in Life Sciences. Elsevier. https://doi.org/10.1016/B978-0-323-90801-6.00018-5

Kamula, R., & Bärthel, J. (2000). Effects of modifications on the hydraulics of Denil fishways. Boreal Environment Research, 5.

Liao, J. C. (2007). A review of fish swimming mechanics and behaviour in altered flows. Philosophical Transactions of the Royal Society B: Biological Sciences, 362(1487), 1973–1993. https://doi.org/10.1098/rstb.2007.2082

Liao, J. C., Beal, D. N., Lauder, G. V., & Triantafyllou, M. S. (2003). Fish Exploiting Vortices Decrease Muscle Activity. Science, 302(5650), 1566–1569. https://doi.org/10.1126/science.1088295

Mahmoudian, Z., Baharvand, S., & Lashkarara, B. (2019). Investigating the Flow Pattern in Baffle Fishway Denil Type. Irrigation Sciences and Engineering, 42(3), 179–196. https://doi.org/10.22055/jise.2019.23693.1689

Mallen-Cooper, M., & Stuart, I. G. (2007). Optimising Denil fishways for passage of small and large fishes. Fisheries Management and Ecology, 14(1), 61–71. https://doi.org/10.1111/j.1365-2400.2006.00524.x

Noonan, M. J., Grant, J. W. A., & Jackson, C. D. (2012). A quantitative assessment of fish passage efficiency. Fish and Fisheries, 13(4), 450–464. https://doi.org/10.1111/j.1467-2979.2011.00445.x

Raffel, M., Willert, C. E., Scarano, F., Kähler, C. J., Wereley, S. T., & Kompenhans, J. (2018). Particle Image Velocimetry: A Practical Guide. Springer. https://doi.org/10.1007/978-3-319-68852-7

Rajaratnam, N., & Katopodis, C. (1984). Hydraulics of Denil Fishways. Journal of Hydraulic Engineering, 110(9), 1219–1233. https://doi.org/10.1061/(ASCE)0733-9429(1984)110:9(1219)

Rajaratnam, N., Katopodis, C., Wu, S., & Sabur, M. A. (1997). Hydraulics of Resting Pools for Denil Fishways. Journal of Hydraulic Engineering, 123(7), 632–638. https://doi.org/10.1061/(ASCE)0733-9429(1997)123:7(632)

Technical Supplement 14N -- Fish Passage and Screening Design. (2007). U.S. Department of Agriculture. https://directives.sc.egov.usda.gov/17824.wba

Thielicke, W., & Stamhuis, E. J. (2014). PIVlab – Towards User-friendly, Affordable and Accurate Digital Particle Image Velocimetry in MATLAB. Journal of Open Research Software, 2. https://doi.org/10.5334/jors.bl

Tritico, H. M., & Cotel, A. J. (2010). The effects of turbulent eddies on the stability and critical swimming speed of creek chub (Semotilus atromaculatus). Journal of Experimental Biology, 213(13), 2284–2293. https://doi.org/10.1242/jeb.041806

Tritico, H. M. (2009). The Effects of Turbulence on Habitat Selection and Swimming Kinematics of Fishes [Thesis]. http://deepblue.lib.umich.edu/handle/2027.42/62393

Chapter 5 An Ecohydraulic Investigation into Sea Lamprey Trap Entrance Rates

5.1 Introduction

Sea lampreys (*Petromyzon marinus*) are parasitic fish invasive to the Laurentian Great Lakes. For the last century, after reaching the lakes through the current Welland Canal (Beaulaurier, 2014; Crowe, 1975; Jensen & Jones, 2018; Robinson et al., 2021; Smith & Tibbles, 1980), they have proliferated throughout much of this freshwater system, harming many fish populations of the lakes and having a steep negative impact on the local commercial fisheries. To attempt to combat their growth, sea lamprey control efforts have been undertaken since the 1950s, primarily through use of lampricides, with additional efforts including barriers, traps, pheromones, and alarm cues (Lavis, 2003; Lawrence et al., 2021; Miehls et al., 2020). While these efforts have been effective in reducing sea lamprey numbers, they result in negative side effects; namely, lampricides target native lampreys in addition to invasive ones (Neave et al., 2021), and emerging research shows these chemicals harm other fishes as well (Newton et al., 2023; Pratt et al., 2021; Sakamoto et al., 2016). Thus, there is increased interest in moving away from lampricide as the main control measure; since traps are already used for monitoring, improving trapping for use in sea lamprey population control is the logical next step and a current goal (Holbrook et al., 2016).

Sea lamprey traps are inefficient, capturing approximately 20% of the lampreys who approach them (McLean et al., 2015). This is believed to be due in part to the traps' "attraction flows", the downstream flow patterns induced by the trap that lampreys feel and respond to during approach. Despite these flows' significance in guiding lampreys into traps (McLaughlin et

al., 2007), they are yet to be characterized. This chapter experimentally quantifies attraction flows for two common sea lamprey trap designs and explores how they affect the entrance behaviors of approaching sea lampreys in a laboratory setting.

5.2 Background

5.2.1 Sea Lampreys in the Laurentian Great Lakes

Due to significantly increased cargo demand through the Welland Canal, in the 1920s, it was enlarged and deepened to accommodate heavier traffic. By 1930, the canal was opened to shipping (Styran & Taylor, 2016). While this expansion project allowed for greater transportation of goods, it unfortunately also enabled sea lampreys to widely disperse throughout the North American Great Lakes. This would begin a century-long fight for the health of the lakes' biological communities.

Sea lampreys' parasitization of ecologically significant native species had far-reaching ripple effects. Through their near elimination of burbot (*Lota lota*) and lake trout (*Salvelinus namaycush*)—two top predators in the Great Lakes—and a variety of other species such as walleye (*Sander vitreus*), the fish assemblage distribution changed drastically (Miehls et al., 2020). The populations of other species such as alewife (*Alosa pseudoharengus*) increased dramatically, surpassing sustainable levels, leading to eventual hazardous mass die offs (Miehls et al., 2020; Oosten, 1947).

The rapidly-developing consequences from the presence of sea lampreys were not restricted to ecological health of the lakes, and the economy of the region suffered as well. One anecdotal estimate in 1951 by a longtime commercial fisherman asserted that their profits had fallen 50% due to the presence and predation of sea lampreys (Gaden et al., 2021). The sea lamprey invasion of the lakes was the final motivation to develop the Great Lakes Fishery

Commission (GLFC), an international body between the United States and Canada with the mission of controlling Great Lakes sea lamprey populations (Gaden et al., 2021; *Great Lakes Fishery Commission - About*, 2023).

5.2.2 Sea Lamprey Control

Sea lamprey control has been attempted through various means since the 1950s. Lampricide application is the main method, supplemented with barrier use, trapping, and sterile male releases. Due to the downsides of lampricides, there is interest in improving trapping. One avenue to improve traps is exploiting attraction flows to increase entrance and capture rates.

There are many different designs of sea lamprey traps (Beaulaurier, 2014; McLaughlin et al., 2007), and just as many attraction flow signatures—however, there are some common features across traps. They have multiple chambers with mesh funnels between each for the lampreys to swim into and continue into upstream chambers of the trap. Additionally, the downstream-most face of the trap where lampreys first enter generally has one of two designs— either a mesh face, or a solid face. Mesh face traps have an entirely mesh front. Solid face traps have a solid front, typically either concrete or metal, with a hole where the mesh funnel is placed. Figure 5.1 shows examples of mesh and solid faces on traps. This study characterizes the attraction flows induced by these two trap face types, and studies sea lamprey response to these flows.

5.3 Methods

To quantify flow patterns induced by sea lamprey traps, two physical models were built—one of a mesh face trap, and one of a solid face trap, each with centrally located funnels on the downstream-most panel. A diagram of each is shown in Figure 5.2. Experiments were

Figure 5.1: Mesh face trap (left) and solid face trap (right) examples. View from inside trap facing downstream.
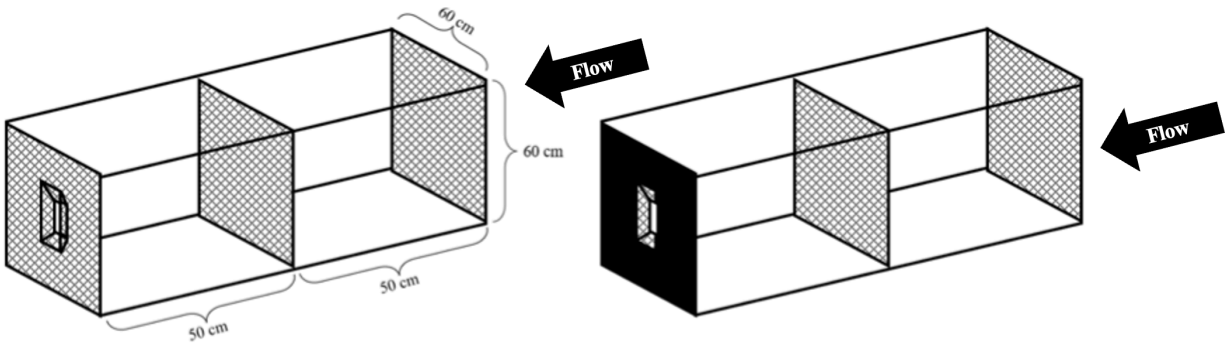
Figure 5.2: Diagram of mesh face (left) and solid face (right) trap models. Dimensions remain the same across both models

Table 5.1: Reynolds number comparison between flow conditions at real-world trap, mesh face model, and solid face model. Average Re is the average taken across bulk Re values at all flow conditions.

Note: approximate values	Based on funnel width		Based on funnel depth	
	Range of Re	Average Re	Range of Re	Average Re
Real-world trap	7600 - 61600	28800	14700 - 119200	55600
Mesh face model	9300 - 25100	17200	14800 - 40200	27500
Solid face model	8900 - 17800	12700	14300 - 28500	20300

performed in flumes in two different laboratories, and therefore these models were sized to fit the smaller flume. The funnel was scaled down to maintain approximate Reynolds flow similarity with a sample real-world trap. Table 5.1 gives details on Re for flow conditions at the sample trap, and during the hydraulic experiments presented in this study.

Each flume was chosen for different purposes. The first smaller flume (60 cm x 60 cm cross-section) had low background turbulence, and therefore was used to explore the baseline flows induced by only trap geometry. This laboratory utilized city water, and exclusively hydraulic experiments were run. The second flume (122 cm x 60 cm cross-section) had higher background turbulence and was fed using water from Lake Huron—it was used both to examine how the hydrodynamics change with increased background turbulence as would be encountered in real-world traps, and further to observe sea lamprey response to the recorded flows. In this second laboratory, both hydraulic and sea lamprey behavioral experiments were performed. The methods used in each part of the study are detailed below.

5.3.1 University of Michigan Hydraulics Lab Methods

The models were placed in a water tunnel at the University of Michigan Hydraulics Lab (UMHL) from September 2022 – April 2023. Flow patterns induced by the trap models at flowrates of approximately $0.00231 – 0.0931$ m^3/s were measured using Particle Image Velocimetry (PIV) (see *Chapter 3* for details on this method), although not all datasets were analyzed due to image quality limitations. Flow was seeded using 10 μm-diameter hollow glass spheres, and illuminated using a continuous, 1 W, 532 nm wavelength laser split into a sheet through a 1.27 cm focal length cylindrical lens. Video data at 60 fps was recorded using a Nikon D5200 DSLR camera.

The hydrodynamics lampreys interact with while approaching a trap are the flows of

Table 5.2: Water tunnel flowrates and velocity conditions measured in the University of Michigan Hydraulics Lab. Flowrates across solid face and mesh face with same number of asterisks indicate comparable downstream velocity conditions.

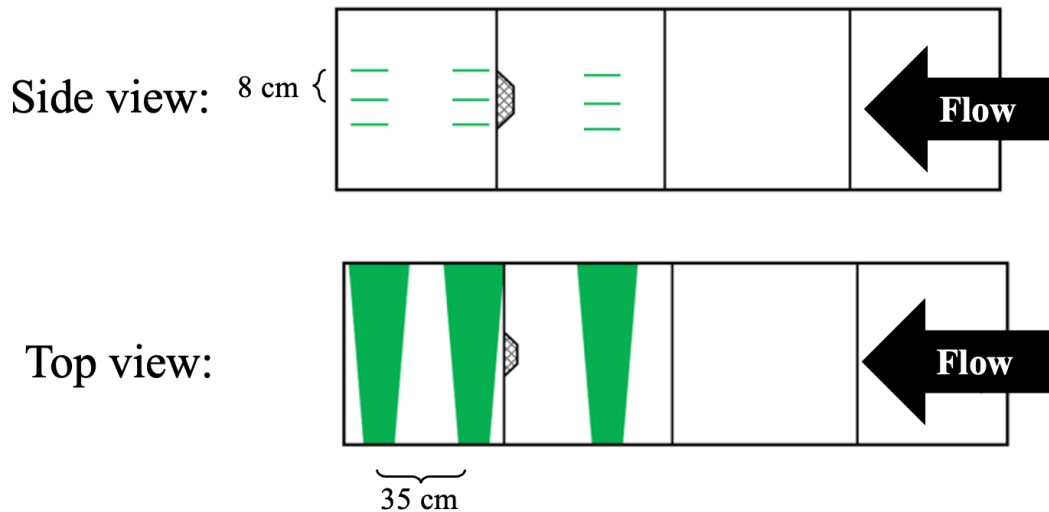| Trap type	Water tunnel flowrate (m^3/s)	Incoming velocity (cm/s)	Approximate velocity downstream of funnel (cm/s)
Solid	0.00231*	0.7 ± 0.3	10
	0.00396**	1.2 ± 0.4	12
	0.0066***	2.0 ± 0.2	15
	0.00891****	2.7 ± 0.5	20
Mesh	0.0343*	10.4 ± 0.2	10
	0.0409**	12.4 ± 0.2	12
	0.0472***	14.3 ± 0.3	14
	0.0528***	16.0 ± 0.2	16
	0.0594	18.0 ± 0.3	18
	0.0677****	20.5 ± 0.3	21
	0.0733	22.2 ± 0.2	22
	0.0802	24.3 ± 0.3	24
	0.0868	26.3 ± 0.2	26
	0.0931	28.2 ± 0.4	28

Figure 5.3: Locations of PIV measurements for trap in UMHL

interest to this study, thus for meaningful comparison of trap face designs, similar downstream velocity conditions between the trap models were sought. Since the solid face trap significantly accelerates flow through the funnel, it was therefore necessary to analyze different incoming flowrates between trap models. Table 5.2 gives upstream and downstream velocity conditions for each flowrate analyzed in both models. Horizontal flow patterns were measured at nine locations at each trap for the flowrate conditions listed in Table 5.2. Figure 5.3 shows these PIV measurement locations.

5.3.2 Hammond Bay Biological Station Methods

Hammond Bay Biological Station (HBBS) is a United States Geological Survey field station on the shore of Lake Huron in Millersburg, Michigan that studies sea lampreys. Two flumes in this facility were used to run hydrodynamic experiments with heightened background turbulence, and to observe sea lamprey behavior in response to the measured flows.

5.3.2.1 HBBS Hydraulic Experimental Methods

At HBBS, there are several large concrete raceways fed by the lake—hydraulic experiments were performed by placing the trap models into two of the raceways. Flow patterns induced by the traps in this more turbulent setting were measured using the PIV system detailed in *Chapter 3*. Attraction flows for each trap type were characterized at two flow settings—high and low—at 18 locations. Table 5.3 gives details on the flow settings, and Figure 5.4 shows PIV measurement locations. Both near the trap face and farther downstream, three horizontal PIV measurements—to the left, middle, and right of the funnel—were needed due to the field equipment used at HBBS; to get a larger field of view (FOV) of the flow at the front of the trap, these three different datasets were separately taken and analyzed, their results later combined.

Experiments were performed at HBBS from June 2, 2023 – June 27, 2023, the schedule

Table 5.3: Flow settings measured at HBBS

Flow setting	Approximate flow velocity downstream of solid face trap funnel (cm/s)	Approximate flow velocity downstream of mesh face trap funnel (cm/s)
High	55	35
Low	35	10-15
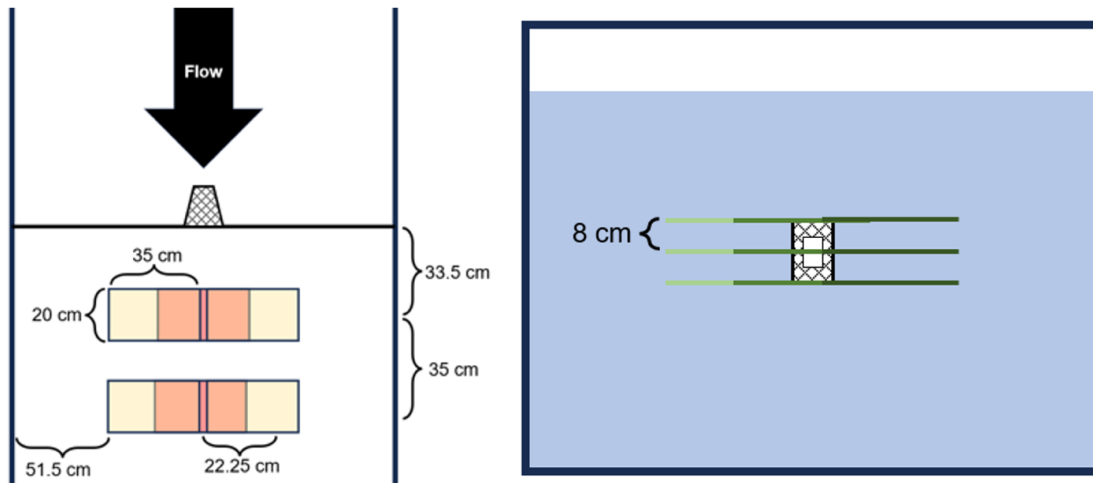
Figure 5.4: HBBS measurement locations. Top view (left) showing six total FOV, illustrated by yellow and pink boxes. Three FOV are at the left, middle, and right both near the funnel and farther downstream. Front view (right) showing nine total FOV, illustrated by varying colors of green lines; three are at the left, center, and right at each of the top, middle, and bottom of funnel. Note all FOV have overlap with other FOV

Table 5.4: Experimental schedule at HBBS

	PIV + behavioral data taken			Behavioral data taken	
Week 1, high flow	June 2	June 3	June 4	June 5	June 6
Week 2, low flow	June 9	June 10	June 11	June 12	June 13
Week 3, high flow	June 16	June 17	June 18	June 19	June 20
Week 4, low flow	June 23	June 24	June 25	June 26	June 27

split into four 5-day long segments. The data collection schedule is given in Table 5.4. Data collection extending over the course of a month allowed the study to control for potential differences in sea lamprey behavior that may arise due to timing of the measurements and change in water temperature.

5.3.2.2 HBBS Behavioral Experimental Methods

This work was primarily performed by a collaborator at University of Guelph, Deven Nicholson. Sea lampreys are photoresponsive (e.g. Haro et al., 2020), and thus red light was placed around the raceways to enhance working condition safety while minimally altering swimming behavior. Cameras were placed in the raceways to record details of lamprey movement—Figure 5.5 shows the setup in each raceway. Due to sea lampreys' preference for nocturnal migration (Stamplecoskie et al., 2012), behavioral experiments were run at night according to the schedule in Table 5.4, beginning around 10 PM and running until between 3-5 AM. Sea lampreys were run one at a time in each raceway, thus two at a time overall, twelve times each experimental night for a total of 24 sea lampreys observed each night. A total of 480 sea lampreys were therefore used in the trials, 96 per trap type per flow treatment (384 total for experiments) and 96 as controls.

Each sea lamprey was given 15 minutes to acclimate in the release cage, and two minutes to leave the cage after it was opened. If the lamprey did not leave within two minutes, it was physically prodded. Each lamprey then had 20 minutes to swim up the raceway and enter the trap; if it entered before the 20-minute trial finished, it was removed from the trap and raceway. If it did not enter during those 20 minutes, it was removed from the raceway after the trial period had finished. Trap type, flow setting, water temperature, timing of run (week 1, week 2, etc), left versus right raceway, sex, length, and weight were recorded for each lamprey.
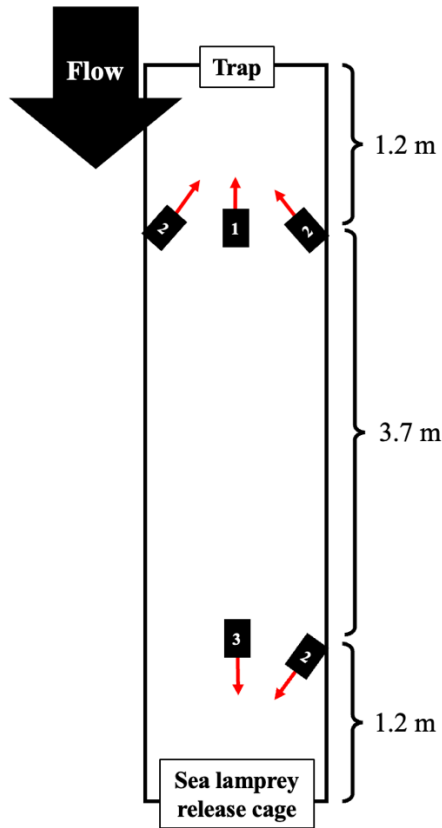
Figure 5.5: Camera setup in each raceway at HBBS. "1" indicates placement of both an overhead and underwater camera, "2" indicates placement of only an underwater camera, and "3" indicates placement of only an overhead camera
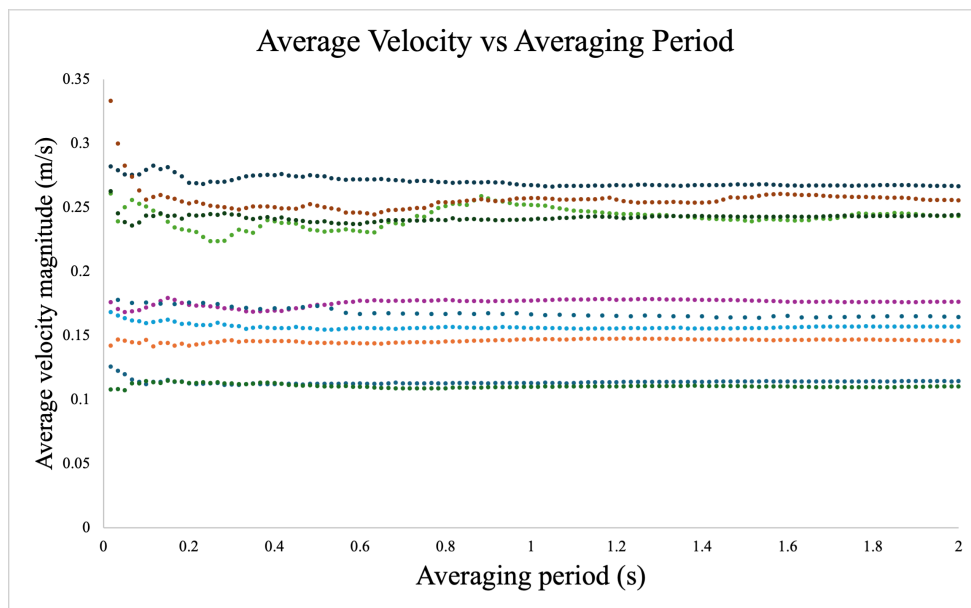

Figure 5.6: Velocity convergence testing result for data taken at UMHL

5.3.3 Analysis Methods

5.3.3.1 Hydraulics Analysis

Analysis on both UMHL data and HBBS hydraulic data was performed using PIVlab (Thielicke & Stamhuis, 2014) to obtain two-second temporal averages of the flow conditions. Two-second averages were determined to be representative flow patterns through average velocity convergence testing. Ten random data points from different trap types and flowrates were selected from UMHL data, and were tested for average velocity convergence. The results are shown in Figure 5.6. By the one-second averaging period, mean velocities had converged— all mean velocities averaged over time periods greater than one second remained within 5% of the one-second average. A two-second average is therefore representative of the flow while containing more data than using only the convergence period of one second. Two-second temporal averages were also used for HBBS hydraulic data to allow for direct comparison across flumes.

Hydraulic analysis differed slightly between UMHL and HBBS due to the limitation on FOV of the HBBS data. In UMHL, PIV analysis was performed on one dataset per measurement location; at HBBS, it was necessary to perform PIV analysis on three datasets, each overlapping the right/left of one another, and later combine the results. Because of the highly turbulent nature of the flow, the results do not align perfectly and are discontinuous (e.g. Figure 5.9); however, they give a qualitative view of the overall flow patterns, and provide quantitative information on expected vorticity and velocity values surrounding sea lamprey traps.

5.3.3.2 Behavioral Analysis

Sea lamprey behavioral analysis was performed by collaborators at University of Guelph, Dr. Robert McLaughlin and Deven Nicholson. Using the videos taken and recorded variables

listed in *5.3.2.2 HBBS Behavioral Experimental Methods*, the following eight behaviors were recorded: 1) time to first approach, defined as a lamprey making contact with the raceway near the front wall of the trap and exhibiting searching behavior, 2) number of approaches, 3) time from approach to searching trap face, defined as a lamprey exhibiting searching behavior at the front face of the trap, 4) time spent searching, 5) time to discovery of funnel opening, defined as a lamprey exhibiting searching behavior at the funnel, 6) time to first entrance attempt, 7) number of entrance attempts, and 8) successful versus unsuccessful entrance. Searching behavior was defined by a lamprey pacing side-to-side within 5 cm of the wall or trap face, and entrance attempts were defined by a lamprey placing their body at the funnel opening, orienting perpendicularly to the trap face, and increasing tailbeat frequency and amplitude.

A base generalized linear regression model was developed to examine entry as it related to trap type, flow, and trap type:flow interaction. Additional general linear models were created to examine the relationship between the base model and experimental setup variables (water temperature, timing of run, left versus right raceway), the relationship between the base model and biological variables (lamprey sex, length, weight), and the relationship between the base model and all variables; many of these results are outside the scope of this chapter, and only entry behavior as it varies between trap types in relation to their hydrodynamic footprints is discussed below.

5.4 Results

In UMHL, both mesh and solid face traps had distinct turbulent footprints. At HBBS, these footprints changed due to the increased background turbulence. Details of the experimental results are given below.

5.4.1 Mesh Face Traps

It was hypothesized that mesh traps had no notable turbulent footprint and instead would impart isotropic turbulence into the flow; this was incorrect. The edges of the funnel were found to create wakes in the flow. Figure 5.7 gives average velocity magnitude (m/s) and vorticity (s^{-1}) maps for the mesh face trap model at several flowrates in UMHL. In these FOVs, the two regions with reduced velocity and heightened vorticity, directly downstream of the funnel, are the wake locations. The vorticity structure of the wakes consists of two parts—one of strong positive vorticity, and one of strong negative vorticity. This is due to the nature of wakes, where eddies of different orientation are shed directly side-by-side with one another (e.g. Carmer, 2005). This pattern was seen across all flowrate settings in UMHL; Appendix Figure A5.1 shows results at each center measurement location for the mesh face trap at all flowrates in UMHL.

It is further illuminating to examine transverse velocity gradients at the trap funnels, as this flow characteristic acts as an obstacle to and generally alters fish swimming (Coutant & Whitney, 2000; Enders et al., 2012; Li et al., 2021; Vowles et al., 2014). Figure 5.8 shows both the velocity (m/s) and velocity gradient (s^{-1}) profiles taken at the centerline of the PIV FOV for the mesh face trap model at each flowrate. Across all flow conditions, the centerline velocity profile remains similar—the wakes from the edges of the funnel are reflected in the simultaneous reduction in velocity and significant velocity gradient fluctuation. Notably, despite approximately a threefold increase in flowrate, velocity gradient magnitudes remain similar.

Mesh face trap attraction flows changed slightly with the more turbulent background flow conditions at HBBS. Figure 5.9 shows average velocity magnitude (m/s) and vorticity (s^{-1}) measured in HBBS, downstream from the center of the funnel. As the incoming flow becomes more turbulent, the wakes are not as clear; however, this trap type still has a notable downstream
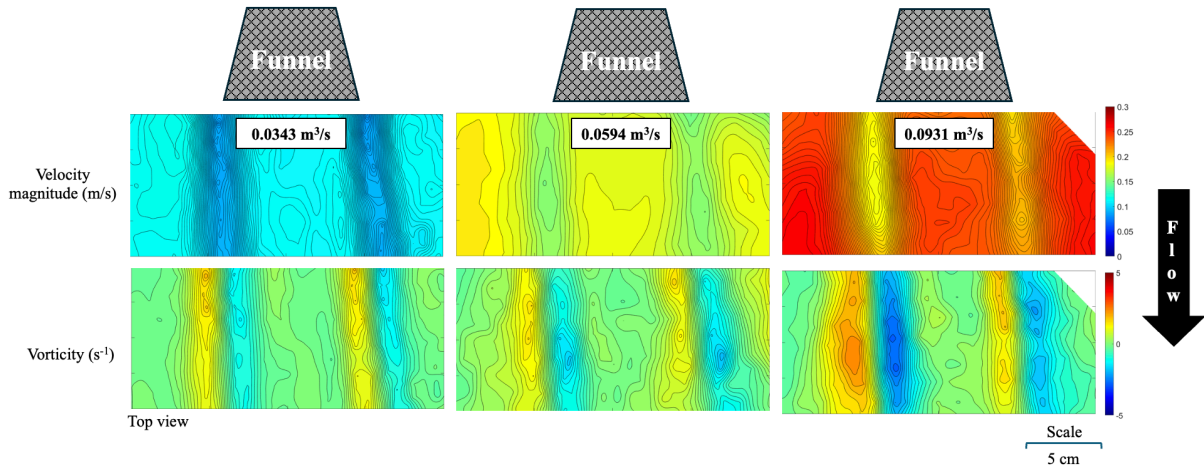
Figure 5.7: Average velocity magnitude (top) and average vorticity (bottom) maps downstream of funnel center for selected velocity conditions for the mesh trap model in UMHL. Top views.

Figure 5.8: Centerline velocity profile (left) and velocity gradient profile (right) for all flowrates for the mesh trap model in UMHL
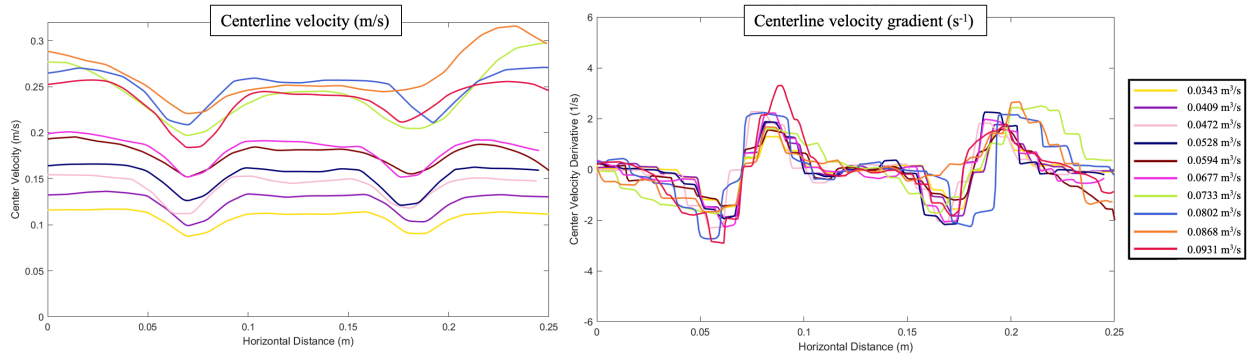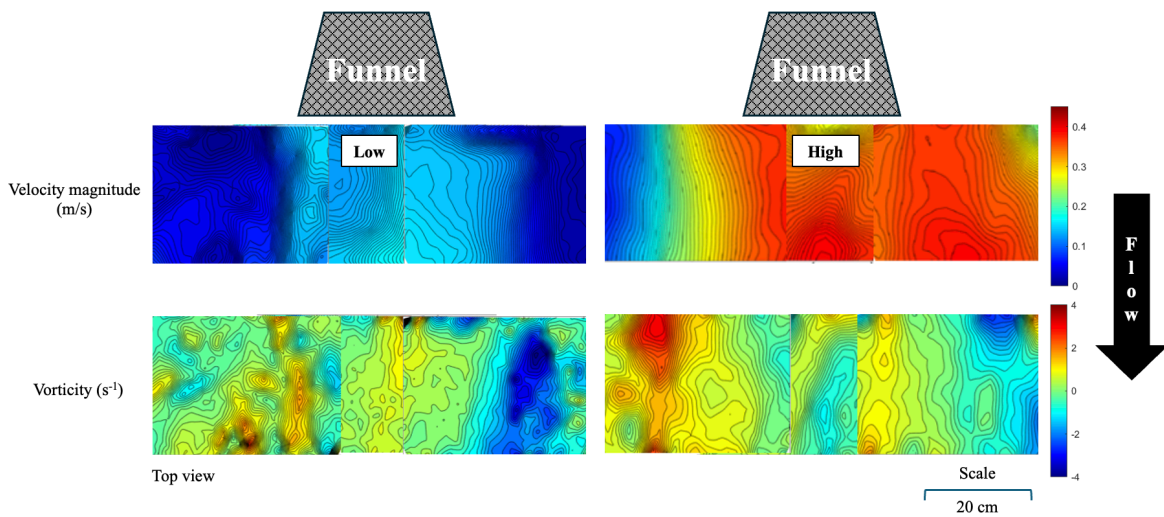

Figure 5.9: Average velocity magnitude (top) and average vorticity (bottom) maps directly downstream of funnel for the mesh trap model in HBBS. Top views.

flow footprint. The HBBS velocity magnitude maps resemble a widened jet, as the turbulence rapidly disperses the wake structure. The wakes consisting of side-by-side oppositely oriented eddies are therefore no longer present; however, regions with strong velocity gradients still exist, in addition to stand-alone areas of strong positive or negative vorticity. Further, the peak average vorticity magnitudes at HBBS (approximately 4.0 s^{-1}) are higher than those in UMHL (approximately 2.8 s^{-1}) because of the increased background turbulence imposed on the induced flow patterns; thus, despite the lack of a "clean" wake structure, eddy placement and orientation remain consistent, and vorticity maintains a notable pattern.

5.4.2 Solid Face Traps

It was hypothesized that solid face traps create a strong turbulent jet; in UMHL, this was the observed pattern. Figure 5.10 shows average velocity magnitude (m/s) and vorticity (s^{-1}) directly downstream of the solid face trap funnel for the flowrates listed in Table 5.2; Appendix Figure A5.2 shows results at each center measurement location for the solid face trap in UMHL. As flowrate increases, vorticity values remain similar (see Figure 5.11), and while hydrodynamic pattern does not change significantly, the jet disperses more widely into the flow.

Figure 5.12 shows solid face trap centerline velocity (m/s) and velocity gradient (s^{-1}) profiles for UMHL. Across flowrates, velocity gradient profile pattern and magnitude remain similar. Centerline velocity pattern, however, changes as flowrate increases—at lower flows, maximum velocity is achieved approximately 2.5 cm from jet center and maintained for approximately 5 cm across the jet width, resulting in the flattened velocity profile shown in Figure 5.12 for 0.00231 and 0.00396 m^3/s. At higher flows, this does not occur, and velocity peaks at the midpoint of the jet, resulting in the rounded velocity profile shown for 0.0066 and 0.00891 m^3/s. Both of these profiles are typical of turbulent jets (e.g. Abramovich, 2003).

Figure 5.10: Average velocity magnitude (top) and average vorticity (bottom) maps directly downstream of funnel for the solid trap model in UMHL. Top views.

Maximum and Minimum Average Vorticity Magnitude (s⁻¹) vs Flowrate (m³/s)

Figure 5.11: Maximum and minimum average vorticity magnitude (s⁻¹) at each flowrate for solid face trap model in UMHL. Red dashed line indicates average maximum vorticity magnitude value across the datasets.
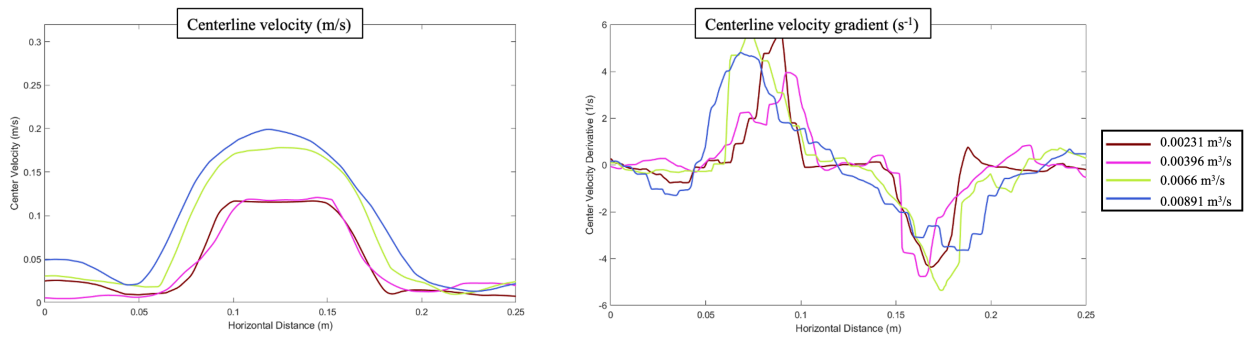
Figure 5.12: Centerline velocity profile (left) and velocity gradient profile (right) for all velocity conditions for the solid trap model in UMHL

In UMHL, the solid face trap produced a clean turbulent jet in the flow. With additional background turbulence at HBBS, the flow becomes more complex. Figure 5.13 shows average velocity magnitude (m/s) and vorticity (s^{-1}) for the solid face trap measured at HBBS. The velocity magnitude maps still vaguely resemble a jet, with highest velocities in the center and low velocities near the edges of the flow FOV. The vorticity maps, however, no longer resemble a jet; rather, they reflect random vortical distributions, ranging from areas of isotropic turbulence to areas of sustained high vorticity. This change is caused by two flow phenomena in HBBS—jet meander, and severe turbulent fluctuations in the flow.

Figure 5.14 shows frames from the videos taken in HBBS, with the jet position highlighted in red. This illustrates the jet meander seen at HBBS, induced by the difference in flume geometry. The HBBS raceways are significantly wider than the UMHL water tunnel, and the flow being directed through the trap funnel therefore has more significant transverse velocity components, increasing sideways movement of the jet. This velocity structure, combined with increased turbulence of the raceways, imparts randomness into the eddy structure of the flow, eliminating the predictable maps seen in UMHL. Additionally, average vorticity values are lower in HBBS (peak average vorticity magnitude approximately 3.5 s^{-1}) than UMHL (peak average vorticity magnitude approximately 5.0 s^{-1})—this is because these attraction flows lack a consistent vorticity pattern. As high magnitudes of average vorticity also reflect consistency in eddy orientation (i.e. the vorticity induced by two strong eddies of the same rotational orientation will average to a value similar to that of the eddies, whereas the vorticity caused by two strong eddies of different rotational orientation will average to approximately zero), the lack of spatial consistency results in lower averages.

Two additional sets of analysis were performed on solid face trap HBBS data to check
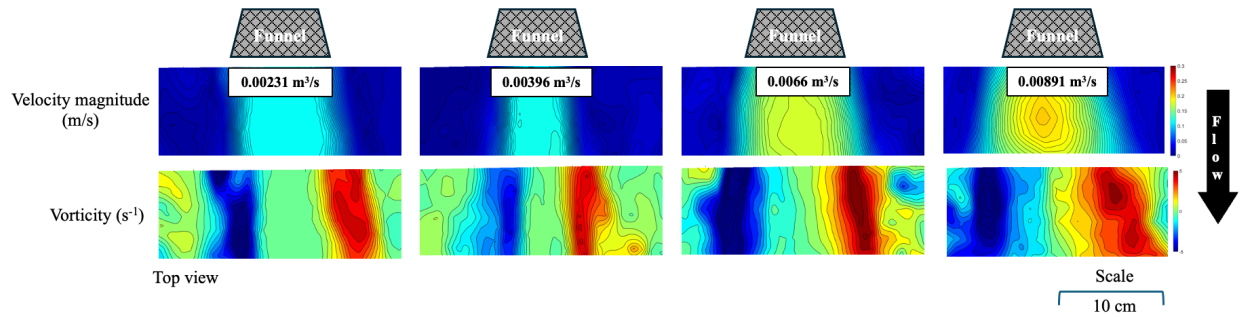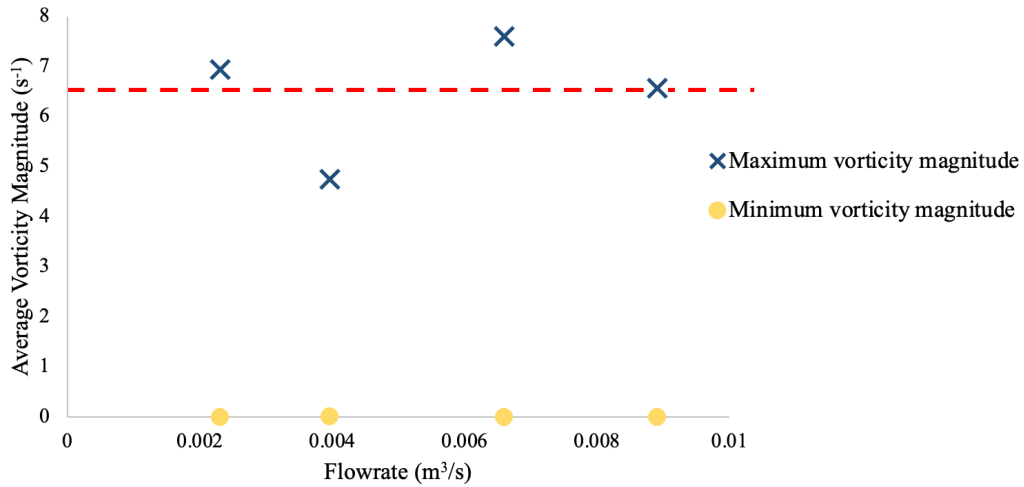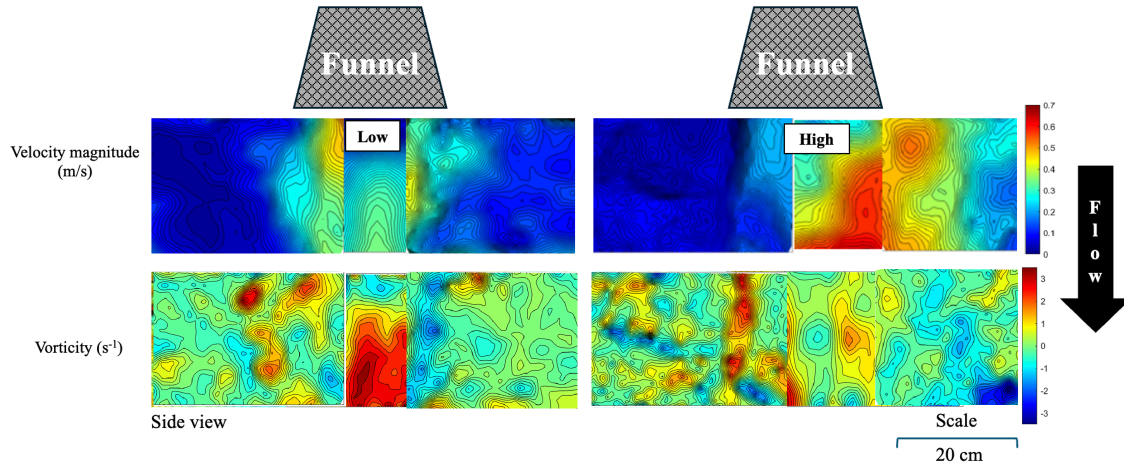
Figure 5.13: Average velocity magnitude (top) and average vorticity (bottom) maps directly downstream of funnel for the solid trap model in HBBS. Top views.
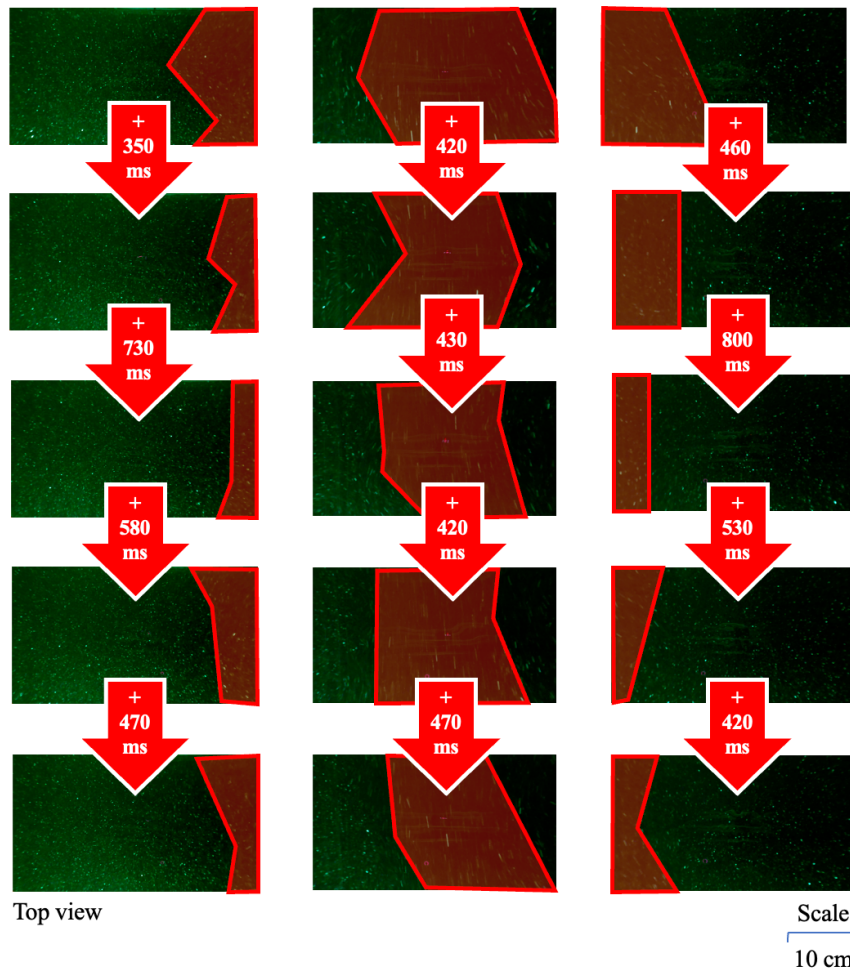
Figure 5.14: Example of jet meander for the solid trap at high flow in HBBS. Frames from video taken to the left of jet (left), video taken with jet centered (center), and video taken to the right of jet (right). Time on arrows indicates time step length between images. Red illustrates jet placement in the frame. Top views.

that the results do indeed reflect stochasticity in the flow and not error. First, analysis was repeated over a different two-second high flow dataset, the results of which are shown in Figure 5.15. This second dataset exhibits both similarities and differences to the original analysis. The velocity magnitude map still resembles a jet, although the second dataset has less velocity magnitude continuity across the different FOVs. Overall however, the highest velocities are still seen at the center with lower velocities on the outer edges of the FOV.

Comparing vorticity map results, both sets of analysis exhibit a random structure, but the details of the random structure differs across them. In Figure 5.13, the majority of the center jet region exhibits sustained high positive vorticity. In Figure 5.15, this same area is split into domains of strong positive and negative vorticity, with a small region of minimal vorticity between them. The structure of the outer areas also differs between analysis sets; these outside regions in Figure 5.15 have lower average vorticity values and are more consistent than those in Figure 5.13. These two datasets therefore both show random variation in vortical pattern. The large difference in the specific random structure across both datasets further confirms the stochastic nature of vorticity in this flow.

The second method used to validate randomness in the vorticity patterns was to examine flows over a longer 20-second average. Results are shown in Figure 5.16. Compared to Figure 5.13, both average velocity magnitude and vorticity maps are significantly smoother. The velocity magnitude map clearly shows a classic turbulent jet structure. Thus, the longer the averaging period, the more fluctuations are averaged out of the flow. This indicates that the fluctuations are indeed random and confirms that the discontinuity seen in Figure 5.13 is due to jet meander. Further, the vorticity in Figure 5.16 is significantly lower than Figure 5.13. This reflects lack of consistency in eddy structure of the flow—average vorticity approaching zero as

100
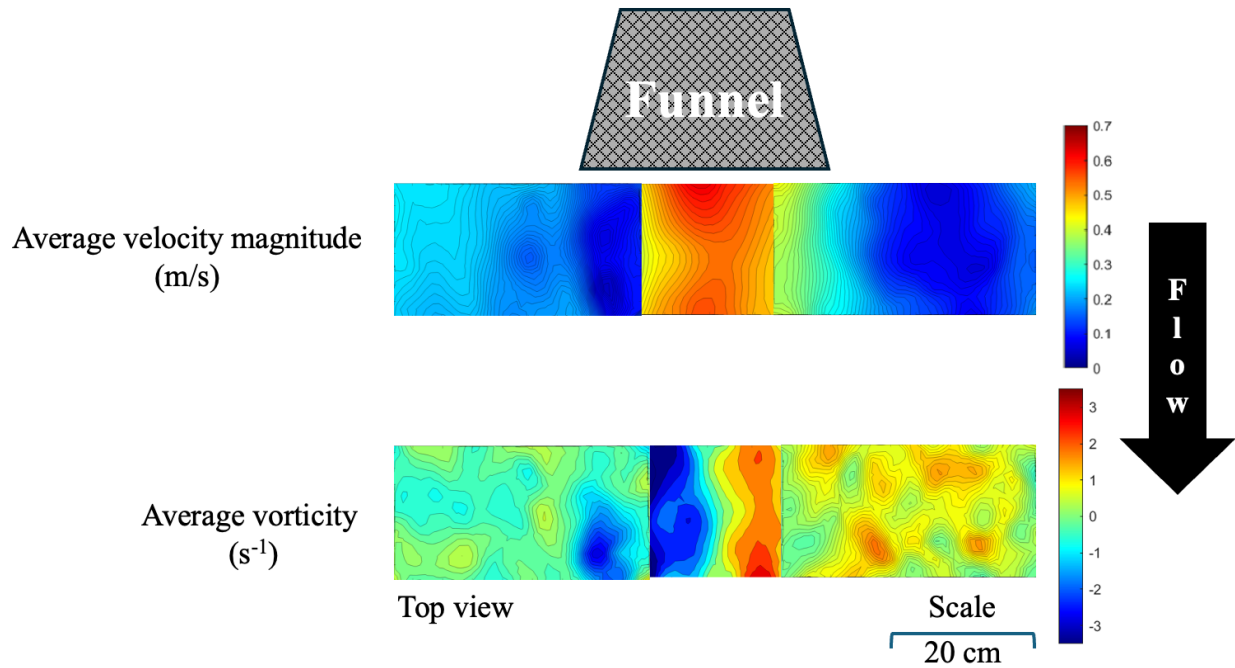
Figure 5.15: Additional 2 second snapshot analysis for HBBS solid trap at high flow. Top views.
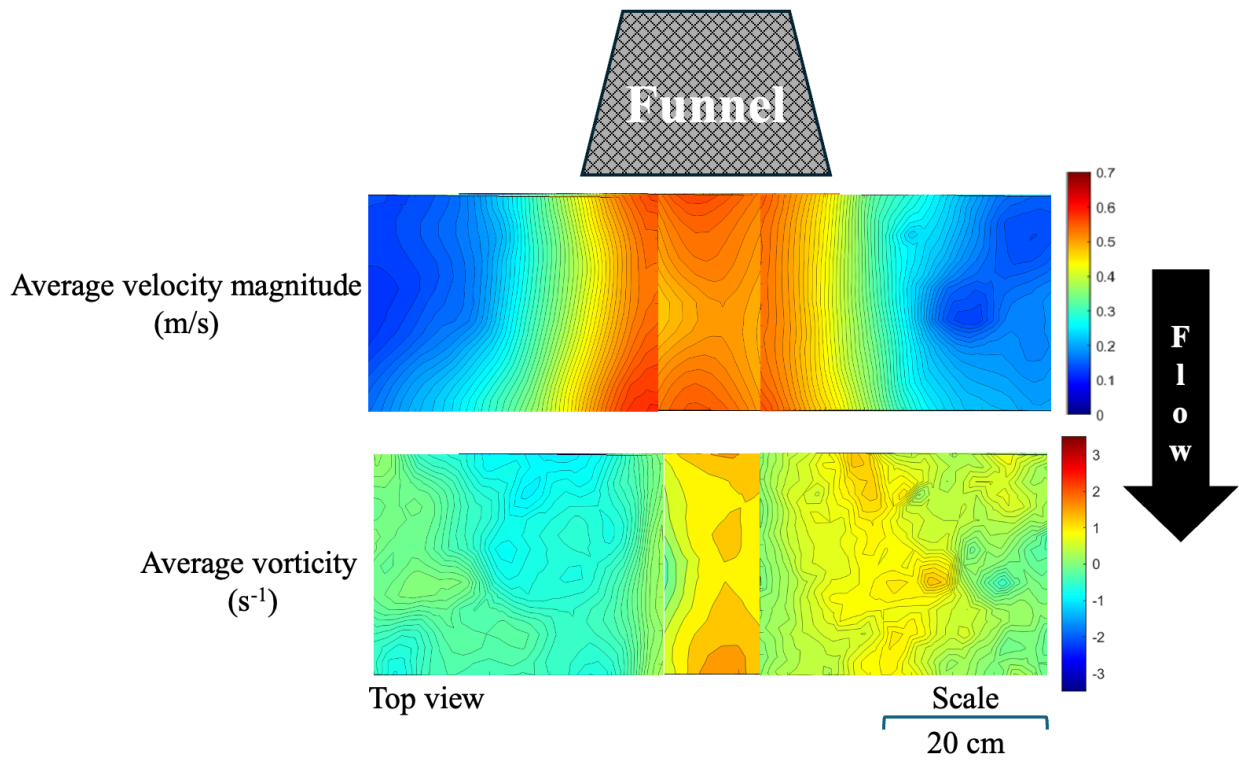
Figure 5.16: Average velocity magnitude (m/s) and vorticity (s^{-1}) averaged over 20 s for solid trap at high flow in HBBS. Top views.

the averaging period becomes longer indicates more eddies of different orientation being included in the average. Therefore, from Figures 5.13, 5.14, 5.15, and 5.16, once solid face traps are placed in turbulent background flow, their downstream vorticity structure becomes unpredictable.

5.4.3 Sea Lamprey Response

Entrance rates across the trap types and flow conditions at HBBS are shown in Figure 5.17. For the mesh face trap model, all sea lampreys who attempted to enter did so successfully. Mesh trap performance varied between the two flow settings, as high flow had approximately 2.5x more entrances than low flow. For the solid face trap model, not all sea lampreys that attempted to enter were able to; for low flow, only 68.1% of sea lampreys who attempted entry were successful. The solid trap under high flow conditions performed even worse, with 35.3% of lampreys who attempted entry finding success.
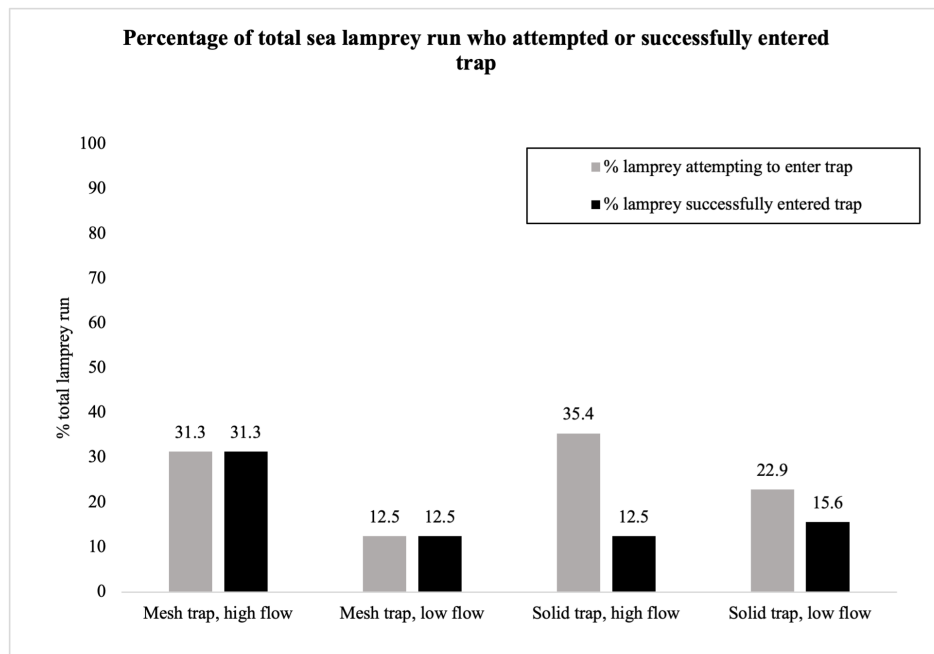
Figure 5.17: Sea lamprey trap entrance attempts and success

While it had low entry rates, the solid face trap under high flow conditions was the only trap/flow combination to consistently have lampreys try entrance multiple times. For the lampreys that attempted to enter, the average number of attempts for this trap/flow combination was 1.2; for the same trap at low flow, only one lamprey attempted multiple entrances. This discrepancy indicates the hydrodynamics induced by solid face traps under specifically high flow conditions are motivating to approaching lampreys. For the mesh face traps under both flow conditions, every lamprey who attempted entry only attempted once, since they were able to enter on their first try.

Despite the solid face trap model under high flow conditions motivating lamprey movement into the trap, this trap/flow combination had one of the lowest successful entry rates. Thus, this flow pattern may be attractive to a lamprey near the funnel, but serves as an obstacle to entrance, ultimately negating the positive impact its attractive effect may have on trapping rates. Overall, the mesh face model under high flow conditions was the most successful trapping condition by a significant amount—this trap/flow combination was 2.5x more successful than both the same trap under low flow conditions and the solid trap under high flow conditions, and was twice as successful as the solid trap under low flow conditions. This indicates that the hydrodynamics induced by this trap design under high flow conditions are both attractive to lampreys and easily navigable, two desirable characteristics of attraction flows.

Attraction effects downstream versus near the trap were also explored. Figure 5.18 shows the time to initial trap approach for the different trap types and flow settings at HBBS. This metric illustrates trap performance downstream—e.g. a significantly faster initial approach time for one trap/flow combination would indicate that sea lampreys are being attracted by that trap's hydrodynamics far downstream. From Figure 5.18, there is no significant difference across all

trap/flow combinations; thus, downstream from the traps, lampreys do not perceive a difference in attractiveness between the different trap hydraulics.

Figure 5.19 demonstrates attractiveness of flows near the traps. It illustrates time from lampreys approaching the trap to finding the funnel, and here there is a pronounced difference in attraction flow effect. Figure 5.19 shows that when in close range of the trap, lampreys are able to find the solid face funnel more quickly—this remains true across both flow conditions. Therefore, near the trap, solid face trap flows may be more attractive, but downstream there is no significant difference.

5.5 Conclusions

To understand sea lamprey trap efficiency, hydraulic and biological data must be considered in tandem. In HBBS, the mesh face trap model at high flow setting had by far the highest entry rates; it is notable that these rates were double that of the solid face trap model at low flow setting, as these two trap/flow combinations have the same downstream velocity conditions (see Table 5.3). This means entrance is influenced by more than bulk velocity. Considering Figures 5.9 and 5.13, under the turbulent conditions at HBBS, mesh traps maintained a predictable and consistent vorticity map, whereas solid traps did not. This may explain the lower success of the solid face traps—the unpredictable turbulence structure makes the flow both more difficult to "read" and to navigate, deterring sea lampreys from moving into the trap.

Under high flow conditions, entrance attempts were similar across trap model types, but entry success was not. Considering the multiple entrance attempts made by lampreys in the solid face model under these flow conditions and Figure 5.19, the much lower entry rates of the solid face traps are not due to their downstream hydrodynamics being unattractive. Rather, the inferior
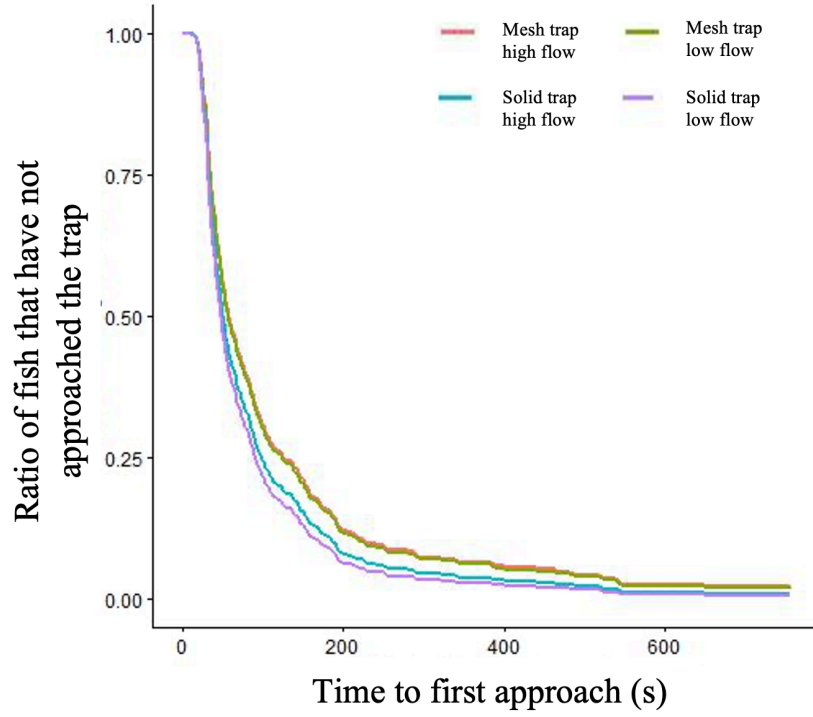
104

Figure 5.18: Time to first approach of lamprey for different trap types and flow conditions
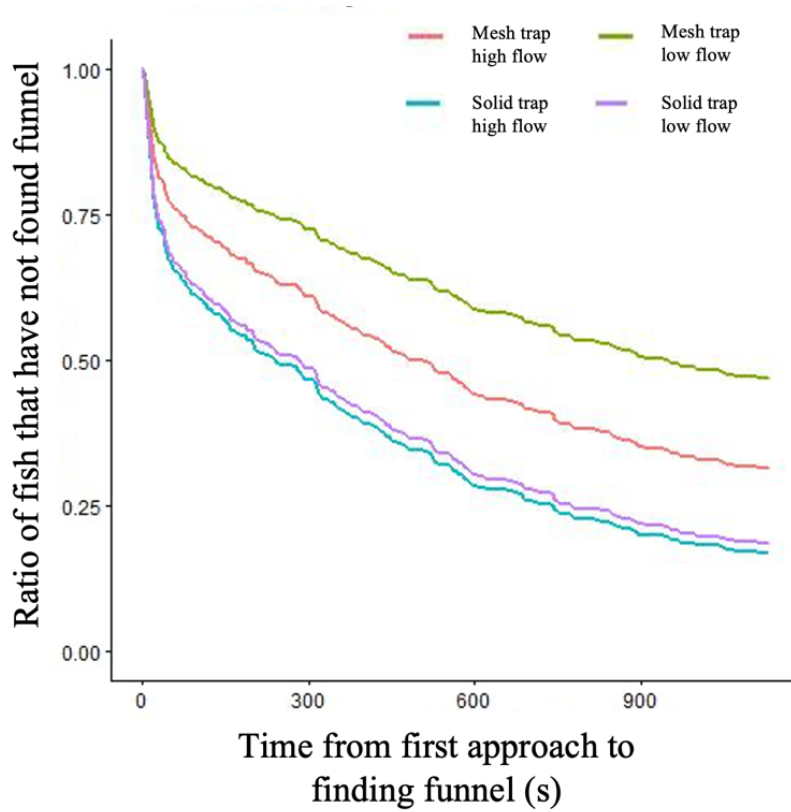

Figure 5.19: Time from lamprey first approach to finding funnel for different trap types and flow conditions

105

entry rates may be explained both by the random vortical structure of the flow as discussed above, and its velocity gradients. From Figures 5.8 and 5.12, even in a low turbulence laboratory setting, solid face traps had velocity gradients approximately twice as strong as those in mesh face traps. As velocity gradient is a known obstacle to fish swimming (e.g. Enders et al., 2012), this is expected to impede trap entry. The randomly fluctuating nature of the HBBS solid face attraction flows would place these gradients erratically throughout the flow field, exacerbating the difficulty they pose. Compared to the flows measured downstream of the mesh face model, which were more consistent and carried lower baseline velocity gradients, this flow feature would particularly challenge lampreys approaching a solid face trap.

Previously, it was theorized that solid face traps may be superior to mesh face traps due to their strong footprint in the flow (Bravener & McLaughlin, 2013; McLaughlin et al., 2007); this study found that this is not the case. Mesh face traps do impart a notable turbulence signature into the flow (see Figures 5.7 and 5.9), and the more stable flow conditions ease entrance for lampreys. This study would therefore recommend that new traps moving forward should focus on designs that induce hydrodynamics with the following features: enhanced stability and predictability such that flow remains readable and navigable, and minimized velocity gradients and fluctuations that sea lampreys struggle to overcome.

5.6 Future Work

The work presented in this chapter is currently being expanded in two ways. First, computational models are being developed and verified to examine attraction flows under a greater range of flow conditions. Field work is also planned to analyze how lamprey behavior and flow conditions change in-situ. Moving forward, this work could have a greater impact on

sea lamprey control efforts if the hydrodynamics induced by specific other trap geometries are studied, to advance knowledge of flow conditions at traps at a wide variety of trap designs.

5.7 Acknowledgments

Thank you to Justin Roelofs and Steve Donajkowski for their help in sea lamprey trap model construction. Thank you to Mariana Fernández Correa and Julien Malherbe for their help in UMHL data collection and analysis. Thank you to Deven Nicholson for his work with the sea lampreys, the biological analysis, and his assistance with data collection at Hammond Bay Biological Station.

5.8 References

Abramovich, G. N. (2003). The Theory of Turbulent Jets. The MIT Press. https://doi.org/10.7551/mitpress/6781.001.0001

Beaulaurier, J. J. (2014). Factors Affecting the Behavior of Great Lakes Sea Lamprey (petromyzon marinus) at Traps [Thesis]. http://deepblue.lib.umich.edu/handle/2027.42/117733

Bravener, G. A., & McLaughlin, R. L. (2013). A behavioural framework for trapping success and its application to invasive sea lamprey. Canadian Journal of Fisheries and Aquatic Sciences, 70(10), 1438–1447. https://doi.org/10.1139/cjfas-2012-0473

Carmer, C.F.V. (2005). Shallow Turbulent Wake Flows: Momentum and Mass Transfer due to Large-Scale Coherent Vortical Structures [Thesis]. https://doi.org/10.5445/KSP/1000003453

Coutant, C. C., & Whitney, R. R. (2000). Fish Behavior in Relation to Passage through Hydropower Turbines: A Review. Transactions of the American Fisheries Society, 129(2), 351–380. https://doi.org/10.1577/1548-8659(2000)129<0351:FBIRTP>2.0.CO;2

Crowe, W. R. (1975). Great Lakes Fishery Commission History, Program, and Progress. Great Lakes Fishery Commission.

Enders, E. C., Gessel, M. H., Anderson, J. J., & Williams, J. G. (2012). Effects of Decelerating and Accelerating Flows on Juvenile Salmonid Behavior. Transactions of the American Fisheries Society, 141(2), 357–364. https://doi.org/10.1080/00028487.2012.664604

Gaden, M., O. Brant, C., & Lambe, R. (2021). Why a Great Lakes Fishery Commission? The seven-decade pursuit of a Canada-U.S. fishery treaty. Journal of Great Lakes Research, 47, 11–23. https://doi.org/10.1016/j.jglr.2021.01.003

Great Lakes Fishery Commission—About. (2023). http://www.glfc.org/about.php

Haro, A., Miehls, S., Johnson, N. S., & Wagner, C. M. (2020). Evaluation of Visible Light as a Cue for Guiding Downstream Migrant Juvenile Sea Lamprey. Transactions of the American Fisheries Society, 149(5), 635–647. https://doi.org/10.1002/tafs.10261

Holbrook, C. M., Bergstedt, R. A., Barber, J., Bravener, G. A., Jones, M. L., & Krueger, C. C. (2016). Evaluating harvest-based control of invasive fish with telemetry: Performance of sea lamprey traps in the Great Lakes. Ecological Applications, 26(6), 1595–1609. https://doi.org/10.1890/15-2251.1

Jensen, A. J., & Jones, M. L. (2018). Forecasting the response of Great Lakes sea lamprey (Petromyzon marinus) to barrier removals. Canadian Journal of Fisheries and Aquatic Sciences, 75(9), 1415–1427. https://doi.org/10.1139/cjfas-2017-0243

Lavis, D. S. ; H. (2003). History of and Advances in Barriers as an Alternative Method to Suppress Sea Lampreys in the Great Lakes (Vol. 29, pp. 362–372). International Association of Great Lakes Research. https://doi.org/10.1016/S0380-1330(03)70500-0

Lawrence, M. J., Mitrovic, D., Foubister, D., Bragg, L. M., Sutherby, J., Docker, M. F., Servos, M. R., Wilkie, M. P., & Jeffries, K. M. (2021). Contrasting physiological responses between invasive sea lamprey and non-target bluegill in response to acute lampricide exposure. Aquatic Toxicology, 237, 105848. https://doi.org/10.1016/j.aquatox.2021.105848

Li, M., Shi, X., Jin, Z., Ke, S., Lin, C., An, R., Li, J., & Katopodis, C. (2021). Behaviour and ability of a cyprinid (Schizopygopsis younghusbandi) to cope with accelerating flows when migrating downstream. River Research and Applications, 37(8), 1168–1179. https://doi.org/10.1002/rra.3686

McLaughlin, R. L., Hallett, A., Pratt, T. C., O'Connor, L. M., & Gordon McDonald, D. (2007). Research to Guide Use of Barriers, Traps, and Fishways to Control Sea Lamprey. Journal of Great Lakes Research, 33, 7–19. https://doi.org/10.3394/0380-1330(2007)33[7:RTGUOB]2.0.CO;2

McLean, A. R., Barber, J., Bravener, G., Rous, A. M., & McLaughlin, R. L. (2015). Understanding low success trapping invasive sea lampreys: An entry-level analysis. Canadian Journal of Fisheries and Aquatic Sciences, 72(12), 1876–1885. https://doi.org/10.1139/cjfas-2015-0140

Miehls, S., Sullivan, P., Twohey, M., Barber, J., & McDonald, R. (2020). The future of barriers and trapping methods in the sea lamprey (Petromyzon marinus) control program in the Laurentian Great Lakes. Reviews in Fish Biology and Fisheries, 30(1), 1–24. https://doi.org/10.1007/s11160-019-09587-7

Neave, F. B., Booth, R. M. W., Philipps, R. R., Keffer, D. A., Bravener, G. A., & Coombs, N. (2021). Changes in native lamprey populations in the Great Lakes since the onset of sea lamprey (Petromyzon marinus) control. Journal of Great Lakes Research, 47, S378–S387. https://doi.org/10.1016/j.jglr.2020.10.005

Newton, T. J., Boogaard, M. A., Schloesser, N. A., Kirkeeng, C. A., Schueller, J. R., & Toribio, S. G. (2023). Behavioral and reproductive effects of the lampricides TFM and TFM:1% Niclosamide on native freshwater mussels. Journal of Great Lakes Research, 49(1), 303–317. https://doi.org/10.1016/j.jglr.2022.11.007

Oosten, J. V. (1947). Mortality of smelt, Osmerus mordax (Mitchill), in Lakes Huron and Michigan during the fall and winter of 1942-1943. Transactions of the American Fisheries Society, 74(1), 310–337. https://doi.org/10.1577/1548-8659(1944)74[310:MOSOMM]2.0.CO;2

Pratt, T. C., Morrison, B. J., Quinlan, H. R., Elliott, R. F., Grunder, S. A., Chiotti, J. A., & Young, B. A. (2021). Implications of the sea lamprey control program for lake sturgeon conservation and rehabilitation efforts. Journal of Great Lakes Research, 47, 421–429. https://doi.org/10.1016/j.jglr.2020.06.014

Robinson, K. F., Miehls, S. M., & Siefkes, M. J. (2021). Understanding sea lamprey abundances in the Great Lakes prior to broad implementation of sea lamprey control. Journal of Great Lakes Research, 47, S328–S334. https://doi.org/10.1016/j.jglr.2021.04.002

Sakamoto, K., Dew, W. A., Hecnar, S. J., & Pyle, G. G. (2016). Effects of Lampricide on Olfaction and Behavior in Young-of-the-Year Lake Sturgeon (Acipenser fulvescens). Environmental Science & Technology, 50(7), 3462–3468. https://doi.org/10.1021/acs.est.6b01051

Smith, B. R., & Tibbles, J. J. (1980). Sea lamprey (Petromyzon marinus) in Lakes Huron, Michigan, and Superior: History of Invasion and Control, 1936-78. Canadian Journal of Fisheries and Aquatic Sciences, 37, 1780–1801. https://doi.org/10.1139/f80-222

Stamplecoskie, K. M., Binder, T. R., Lower, N., Cottenie, K., McLaughlin, R. L., & McDonald, D. G. (2012). Response of Migratory Sea Lampreys to Artificial Lighting in Portable Traps. North American Journal of Fisheries Management, 32(3), 563–572. https://doi.org/10.1080/02755947.2012.675963

Styran, R. M., & Taylor, R. R. (2016). This Colossal Project: Building the Welland Ship Canal, 1913-1932. McGill-Queen's University Press. https://www.jstor.org/stable/j.ctt1hj9wv3

Thielicke, W., & Stamhuis, E. J. (2014). PIVlab – Towards User-friendly, Affordable and
Accurate Digital Particle Image Velocimetry in MATLAB. Journal of Open Research
Software, 2. https://doi.org/10.5334/jors.bl

Vowles, A. S., Anderson, J. J., Gessel, M. H., Williams, J. G., & Kemp, P. S. (2014). Effects of
avoidance behaviour on downstream fish passage through areas of accelerating flow
when light and dark. Animal Behaviour, 92, 101–109.
https://doi.org/10.1016/j.anbehav.2014.03.00

Appendix: All Flow Patterns at Center of Funnel in UMHL

Appendix Figure A5.1 shows all flow patterns at the center of the funnel in UMHL for the mesh face trap model, and Appendix Figure A5.2 shows all flow patterns at the center of the funnel in UMHL for the solid face trap model.
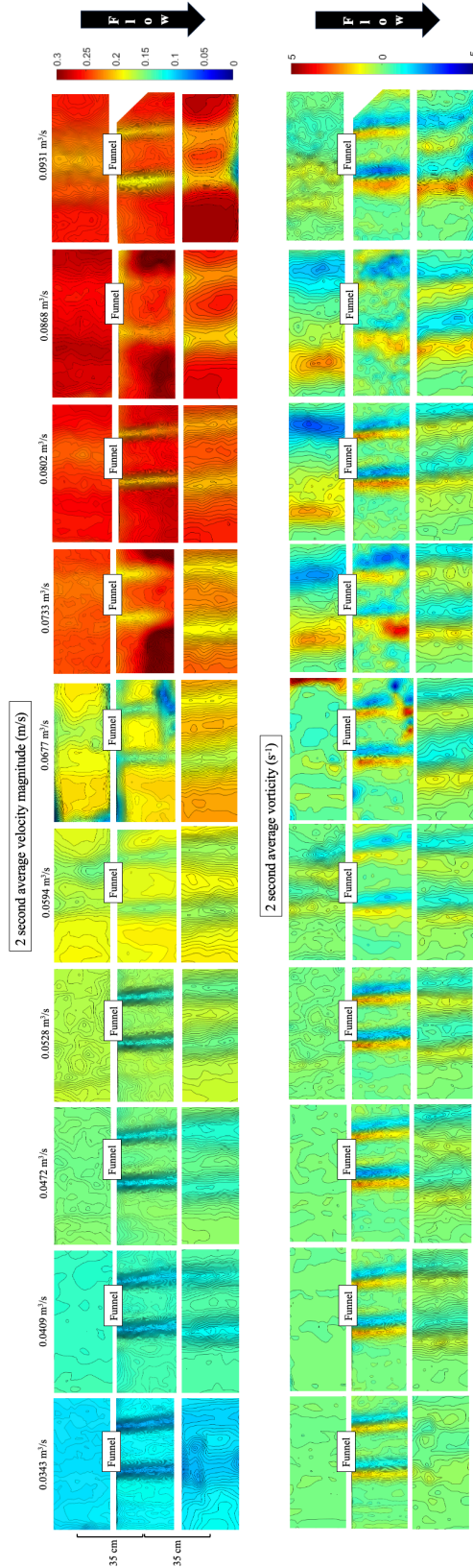
Appendix Figure A5.1: All flow patterns at center of funnel for mesh face trap at UMHL. Top views.
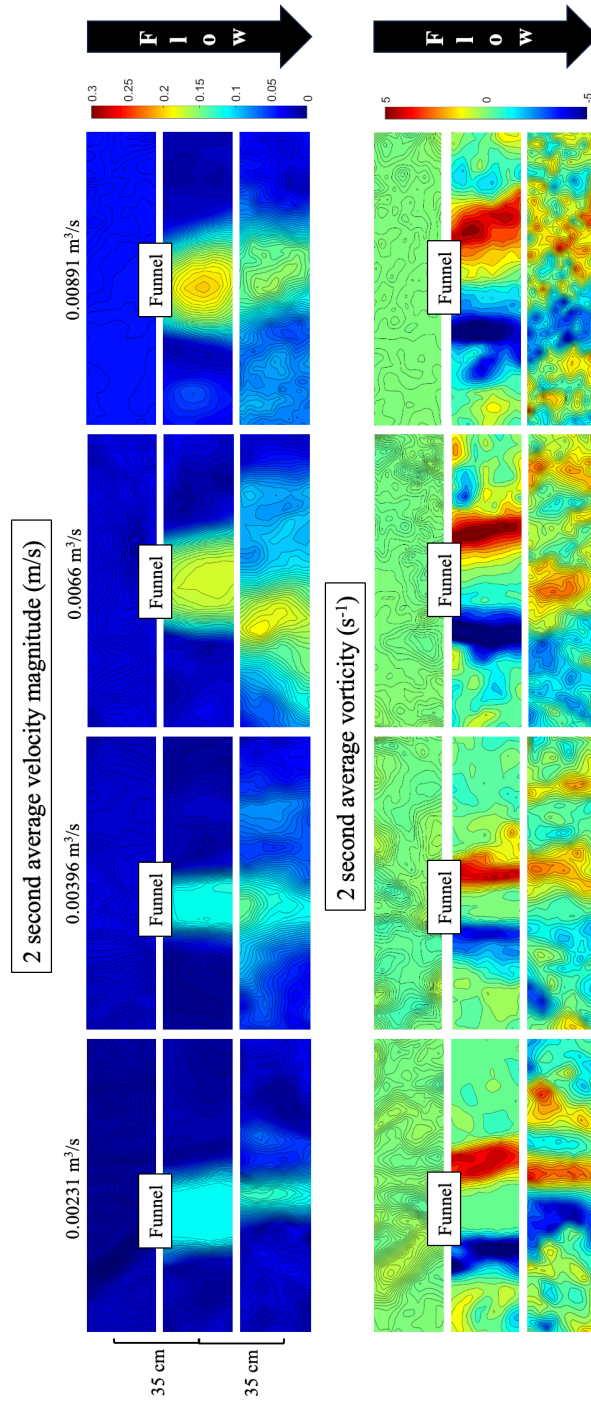
Appendix Figure A5.2: All flow patterns at center of funnel for solid face trap at UMHL. Top views.

Chapter 6 Conclusions

Human interference in fluvial environments has allowed societies to take advantage of the many benefits these freshwater systems can offer; unfortunately, these benefits often carry an ecological cost. This dissertation is one of many current research efforts investigating the balance between the needs of people with restoration and maintenance of a healthy environment. The studies presented here develop a body of work on turbulence patterns in various riverine infrastructure intended to aid in fish population restoration, and develop and test conceptual frameworks, methodologies, and novel instrumentation to support conservation goals. This work contributes to fluvial conservation research through encouraging future researchers and practitioners in the river restoration space to consider the effects of turbulence in their work, and provides them tools to do so.

6.1 Implications of Work

The wide extent to which rivers globally have been dammed presents a major challenge to freshwater fish populations, as these structures disconnect their habitat. While dam removal is an option for habitat reconnection, the process is extremely costly (Hepler, 2013), time-consuming due to its highly regulated nature (Wildman, 2013), and potentially carries short-term but serious hazards to downstream communities and the river biota (Bednarek, 2001). Therefore, alternatives that reconnect habitat without dam removal are often sought, the solution commonly being fishways.

Fishways do not currently meet ideal passage standards, and thus means to improve

success of these designs are consistently investigated. *Chapter 2* provides a design framework for engineers and conservationists to apply during the process of planning new or retrofitting existing fishways. The impact of environmental turbulence on fishes cannot be overstated (e.g. Jones et al., 2022), and moving forward, must be considered when designing hydraulic structures specifically meant to accommodate them. However, predicting turbulent characteristics in large-scale fishways prior to construction is challenging, since computational fluid dynamics (CFD) models are unreliable in these designs (Duguay et al., 2017). Therefore, the simple-to-apply equations developed in this chapter are a first step towards considering the interactions of fishes and turbulence in the fishway design process.

Another major challenge to restoration work is the lack of adequate instrumentation for effectively capturing environmental turbulence data at a scale relevant to fishes. Many instruments take point velocity measurements, requiring interpolation and simplifying assumptions to create a multi-dimensional picture of the flow. In laboratory settings, robust two-dimensional data has long been possible through use of Particle Image Velocimetry (PIV), a common method in experimental fluid mechanics investigations. The logical solution to the issue of environmental turbulence data is therefore to bring this technology to the field, and while several systems have been developed for this purpose (Jin, 2019; Katija & Dabiri, 2008; Morgan, 2013; Tritico et al., 2007), their limitations have restricted widespread adoption by the conservation world. *Chapter 3* describes a new field PIV system that addresses many of the limitations of its predecessors. It is also financially and logistically accessible to those it may be of interest to, such as NGOs and conservation groups with limited resources. This tool offers a means for future conservationists and researchers to better measure, understand, and consider turbulence in the environment.

Chapter 4 examines flow patterns in a common but inefficient fishway type, the Denil fishway. Recent design recommendations suggest milder slopes as a means of improving success of these designs (Mallen-Cooper & Stuart, 2007); to quantify the turbulence fishes face under these updated suggestions, flows were measured experimentally at 0%, 5%, and 10% grades. This study demonstrated that passage in these fishways can be challenging due to two flow phenomena that intensify with increasing slope: 1) low-speed refuges are lost, and 2) high-vorticity areas similar in size to fishes develop directly in the pathway fishes must take through the structure. Therefore, in addition to slope reduction, two new design guidelines follow from these results: 1) flowrates should be managed such that fishes are still able to effectively navigate the fishway without experiencing fatigue despite the absence of low-speed refuges, and 2) baffle design should be altered in a way that disperses the high-vorticity regions. Dispersal would be successful through either a reduction in vorticity values, or a reduction in diameter of the eddies produced in these regions, since smaller eddies have less potential to destabilize swimming and require less energy to navigate.

As with all environmental issues, the ecological impacts of dams are complex and not exclusively negative. A benefit provided by dams is their ability to act as barriers, preventing invasive species from moving farther into watersheds. At such dams, traps may be placed to monitor and remove these animals. An example of such a benefit being used is for sea lamprey control in the Laurentian Great Lakes, where several barriers alone are blocking their proliferation into the entire Great Lakes watershed (Jensen, 2017; Lavis et al., 2003). A current major goal for the sea lamprey control program is improving trapping rates at barriers to enhance removal by physical means. *Chapter 5* explores the flow patterns induced by these traps and sea lamprey response to these patterns, with the goal of increasing trap entrance rates by leveraging

the influence of hydrodynamics on entry behavior. Two common trap face types (mesh and solid) were compared to analyze their performance, and the results of this study offer four main insights into trapping rates: 1) downstream from the traps, there is no significant difference between the trap types in attraction performance, 2) near the trap face, solid face traps induce a more attractive flow, 3) despite the attractive nature of solid face trap flows at close range, the flow patterns impede trap entry, negating any positive effect the increased attraction may have on increasing trapping rates, and 4) mesh face traps under higher flow conditions are the most successful due to their balance of attracting lampreys near the trap and inducing flow that is easily navigable for trap entrance. This contradicts previous theory suggesting solid face traps should be used due to their attractive capability; instead, this study recommends using trap faces that more closely resemble those of the mesh face trap—ones that induce flows whose turbulent footprints are relatively steady and predictable, with manageable velocity gradients.

Summarily, this dissertation provides the following scientific advances to the field of environmental fluid mechanics:

1) A new design framework to consider turbulence in fishways prior to their initial construction or retrofit design

2) An accessible novel instrument to enhance environmental turbulence measurements

3) The first detailed experimental insight into flow patterns in Denil fishways under updated slope recommendations, and additional design recommendations for future fishways

4) The first experimental characterization of entrance flows at sea lamprey traps, coupled with observations of sea lamprey behavior to offer insight into trapping efficacy

The above four advances contribute to riverine fish conservation through offering a body of knowledge and methodologies future work may use to leverage hydrodynamics as a means of enhancing fluvial infrastructure.

6.2 Limitations of Work

The work presented in *Chapter 2* provides estimates of turbulent metrics significant to fishes within fishways. This framework is based in theory and has not yet been validated with field data and observations.

The field PIV system presented in *Chapter 3* is designed to be accessible, and therefore uses non-specialized and low-cost equipment. As a result, the data captured by this system is at a lower resolution and lower frequency than laboratory-based PIV data. While the system is able to capture adequate information in many environments of interest, the coarser raw data quality is a limitation. Additionally, the validation of the various flow characteristics explored in this chapter were limited through the methodology used. Velocity and TKE were validated through comparison to point measurements. The field validation of vorticity and eddy dynamics was performed through comparison to previous field measurements; as this environment is dynamic, comparison of datasets over a long time period is challenging.

The highly turbulent flow with significant air entrainment explored in Denil fishways in *Chapter 4* reduced raw data quality. While the PIV analysis excluded regions of air pockets to enhance robustness of results, it limited the study's scope and may have introduced minor errors.

The study in *Chapter 5* is limited by the methodology's inability to decouple sea lamprey responses to hydrodynamics and other biological possibilities. The bulk behavioral differences examined here are assumed to be induced by interaction with flow structures, but the behavior

may be additionally influenced by other confounding factors, e.g. visual stimulus, in a natural environment.

6.3 Future Work

This dissertation can serve as a foundation for future researchers to build upon and continue expanding knowledge of environmental turbulence through an ecohydraulic lens. To enhance *Chapter 2*, the proposed framework can be expanded to include methods for estimating other parameters significant to fishes, e.g. velocity gradient, turbulent kinetic energy (Li et al., 2021), or pressure differentials (Boys et al., 2016). Further, ways to estimate these parameters in other dam infrastructure fishes face, such as spillways or turbines, would enable future designs to more holistically consider conditions faced by fishes during upstream and downstream dam passage. The PIV system presented in *Chapter 3* is purposefully designed to be highly modifiable, leaving room for improvement and any alterations that may be necessary depending on the flows of interest. These changes could include for example increasing system stability, capturing a larger field of view, or using a higher framerate camera to characterize faster flows. The work in *Chapter 4* is limited by the facility used, and examining a longer model with more baffle sections would further understanding of turbulence development in these fishways. More PIV measurement locations in the baffle sections, both perpendicular to and parallel to the flow direction, would also create a larger picture of the hydrodynamics in this infrastructure. Additionally, studying more slopes and flowrates would offer greater insight into what flow conditions induce the hydraulic structures observed in this chapter. The results presented in *Chapter 5* could be expanded by examining more trap designs and flowrates. Further biological analysis examining statistically significant behavioral changes in regions relative to the traps, mapped to hydrodynamic patterns in these regions, would ensure the responses being examined

are due to the flow and not other variables, e.g. sight as mentioned in *6.2 Limitations of Work*. Future work on this chapter currently includes developing accurate CFD models for sea lamprey traps to extend the range of flows studied. Additionally, trap entry rates will be investigated in a natural river system, with hydrodynamics and lamprey behavior examined in-situ to verify and expand upon the laboratory results.

6.4 References

Bednarek, A. T. (2001). Undamming Rivers: A Review of the Ecological Impacts of Dam Removal. Environmental Management, 27(6), 803–814. https://doi.org/10.1007/s002670010189

Boys, C. A., Robinson, W., Miller, B., Pflugrath, B., Baumgartner, L. J., Navarro, A., Brown, R., & Deng, Z. (2016). How low can they go when going with the flow? Tolerance of egg and larval fishes to rapid decompression. Biology Open, 5(6), 786–793. https://doi.org/10.1242/bio.017491

Duguay, J. M., Lacey, R. W. J., & Gaucher, J. (2017). A case study of a pool and weir fishway modeled with OpenFOAM and FLOW-3D. Ecological Enginering, 103. https://doi.org/10.1016/j.ecoleng.2017.01.042

Hepler, T. E. (2013). Engineering considerations for large dam removals. In J. V. D. Graff & J. E. Evans (Eds.), The Challenges of Dam Removal and River Restoration (Vol. 21, p. 0). Geological Society of America. https://doi.org/10.1130/2013.4121(02)

Jensen, A. J. (2017). Modeling the impacts of barrier removal on Great Lakes sea lamprey [Thesis]. https://d.lib.msu.edu/etd/4592

Jin, T. (2019). Underwater Particle Image Velocimetry (PIV) Measurement of Turbulence Over Mussel Bed in a Deepsite of Lake Michigan [Thesis]. https://dc.uwm.edu/etd/2313

Jones, K., Cotel, A. J., & Webb, P. W. (2022). Stability and turbulence. In Reference Module in Life Sciences. Elsevier. https://doi.org/10.1016/B978-0-323-90801-6.00018-5

Katija, K., & Dabiri, J. O. (2008). In situ field measurements of aquatic animal-fluid interactions using a Self-Contained Underwater Velocimetry Apparatus (SCUVA). Limnology and Oceanography Methods, 6(4), 162–171. https://doi.org/10.4319/lom.2008.6.162

Lavis, D.S., Hallett, A., Koon, E.M., McAuley, T.C. (2003). History of and Advances in Barriers as an Alternative Method to Suppress Sea Lampreys in the Great Lakes. International Association of Great Lakes Research, 29, 362–372. https://doi.org/10.1016/S0380-1330(03)70500-0

Li, M., Shi, X., Jin, Z., Ke, S., Lin, C., An, R., Li, J., & Katopodis, C. (2021). Behaviour and ability of a cyprinid (Schizopygopsis younghusbandi) to cope with accelerating flows when migrating downstream. River Research and Applications, 37(8), 1168–1179. https://doi.org/10.1002/rra.3686

Mallen-Cooper, M., & Stuart, I. G. (2007). Optimising Denil fishways for passage of small and large fishes. Fisheries Management and Ecology, 14(1), 61–71. https://doi.org/10.1111/j.1365-2400.2006.00524.x

Morgan, J. (2013). Flow Characterization in a Vegetated Marsh Environment [Thesis]. https://deepblue.lib.umich.edu/handle/2027.42/99882

Tritico, H. M., Cotel, A. J., & Clarke, J. N. (2007). Development, testing and demonstration of a portable submersible miniature particle imaging velocimetry device. Measurement Science and Technology, 18(8), 2555. https://doi.org/10.1088/0957-0233/18/8/031

Wildman, L. (2013). Dam removal: A history of decision points. In J. V. D. Graff & J. E. Evans (Eds.), The Challenges of Dam Removal and River Restoration (Vol. 21, p. 0). Geological Society of America. https://doi.org/10.1130/2013.4121(01)